UNIVERSITY OF CALIFORNIA SAN DIEGO

Decellularized Extracellular Matrix Hydrogel Therapy for the Prevention and Treatment of Pathological Alterations Following Birth Injuries

A dissertation submitted in partial satisfaction of the

requirements for the degree Doctor of Philosophy

in

Bioengineering

by

Pamela Duran

Committee in charge

Professor Karen L. Christman, Chair
Professor Marianna Alperin, Co-Chair
Professor Adam Engler
Professor Jeffrey Omens
Professor Sameer B. Shah

2022

Copyright

Pamela Duran, 2022

All rights reserved.

The Dissertation of Pamela Duran is approved, and it is acceptable in quality and form for publication on microfilm and electronically.

University of California San Diego

2022

DEDICATION

To my parents, my brother, Aldo and “Miss Eva”.

TABLE OF CONTENTS

LIST OF ABBREVIATIONS

∝-SMA: alpha smooth muscle actin

ADSCs: Adipose derived mesenchymal stem cells

ANOVA: Analysis of Variance Test

BMSCs: Bone marrow derived mesenchymal stem cells

CTGF: Connective tissue growth factor

DMMB: 1,9-dimethylmethylene blue dye

ECM: Extracellular Matrix

EMG: Electromyography

FAPs: Fibroadipogenic progenitors

FGF: Fibroblast growth factor

H&E: Hematoxylin and eosin

HCl: Hydrochloric acid

HGF: Hepatocyte growth factor

IFN-γ: Interferon gamma

IGF-1: Insulin growth factor 1

LAM: Levator ani muscle

LC-MS/MS: Liquid chromatography tandem mass spectrometry

L_f: Fiber length

L_o: Optimal muscle length

Ls: Sarcomere length

MMPs: Matrix metalloproteinases

MRI: Magnetic resonance imaging

MuSCs: Muscle stem cells

NGF: Nerve growth factor

PC: Principal component

PCa: Pubocaudalis

PCL: Polycaprolactone

PCSA: Physiological cross-sectional area

PFDs: Pelvic floor disorders

PFM: Pelvic floor muscle tissue

PGA: Poly (glycolic acid)

PLGA: Poly (lactic-co-glycolic acid)

POP: Pelvic organ prolapse

SBI: Simulated birth injury

SDS: Sodium dodecyl sulfate

SEM: Scanning electron microscopy

sGAGs: Sulfated glycosaminoglycans

SIS: Small intestinal submucosa

SKM: Skeletal muscle-extracellular matrix

TIMPs: Tissue inhibitor of matrix metalloproteinases

TnBP: Tri(n-butyl) phosphate

TNF-∝: Tumor necrosis factor alpha

Tregs: Regulatory T cells

UBM: Urinary bladder matrix

VEGF: Vascular endothelial growth factor

VTI: Vaginal tactile imaging

LIST OF FIGURES

LIST OF TABLES

ACKNOWLEDGEMENTS

I would like to thank everyone would help me throughout this journey, my advisors, colleagues, friends, and, of course, my family.

First of all, I would like to thank my advisors Dr. Karen Christman and Dr. Marianna Alperin for their invaluable support. Dr. Christman for allowing me the opportunity to join her lab, and to transition to the PhD program. She provided mentorship, guidance, and motivated me to think independently, and to grow as a scientist through our scientific discussions. Dr. Alperin also provided outstanding mentorship. She continuously trained me to thoroughly critique scientific data, transmitted her passion towards women's health research, and has given me several opportunities and guidance to be involved in the field of female pelvic medicine. I see both of them as role models, and I will apply the skills and knowledge gained through them in my professional career. I would also like to acknowledge my remaining committee members Professor Adam Engler, Sameer Shah and Jeffrey Omens for their suggestions and support with my projects.

I would like to thank all the members of the Christman and Alperin labs, who I met over the past six years. Their guidance, support and helpful discussions were always highly appreciative. I am especially thankful to Dr. Jessica Ungerleider for being my first graduate student research mentor, Dr. Raymond Wang for introducing me to a variety of techniques in the lab, and always providing guidance and support, and Dr. Francesca Boscolo and Dr. Lindsey Burnett for their invaluable and critical discussions on my projects. Furthermore, I am incredibly thankful to Emma Zelus, she was my first undergraduate student and is now a graduate student in both labs. She was highly patience during my first time as a mentor and has since then provided me both research and emotional support. I will never forget our long days in lab optimizing mechanics experiments. In addition, current and past lab members provided me with continuous emotional support and research discussions, including Dr. Melissa Hernandez, Dr. Martin Spang, Holly Sullivan, Miranda Diaz, Jervaughn Hunter, Joshua Mesfin, and Rebecca Braden. I am also

thankful for my undergraduate students throughout the years, who helped me in my research projects and allowed me to grow as a mentor: Emmy Do, Neil Aid, Manali Shah, Saya French, in addition to undergraduate sectioners and summer students.

My family has always provided me endless support. I would like to thank my parents, Antonio Duran and Socorro Heredia, my brother, sister-in-law, and grandmother ("Miss Eva") for believing in me and for their incredible support and personal guidance, and Aldo, for his endless love, patience, and support throughout this journey.

Chapter 1, in part, is currently being prepared for submission for publication of the material, Pamela Duran, Karen L. Christman, and Marianna Alperin. "What do we really know about the anatomy and physiology of the pelvic floor muscles?". Other sections are a reprint of the material as it is published in: Raymond Wang, Pamela Duran, and Karen L. Christman. "Processed Tissues". Biomaterials Science, 4th edition (2020), and Pamela Duran, Marianna Alperin, and Karen L. Christman. "Decellularized Extracellular Matrix Hydrogels: Fabrication, Properties, Characterization, and Current Applications". Decellularized Extracellular Matrix: Characterization, Fabrication and Applications (2019). The dissertation author was the co-first and first author of these papers, respectively.

Chapter 2 and 3, in part, are currently being prepared for re-submission for publication of the material, Pamela Duran, Francesca Boscolo Sesillo, Lindsey Burnett, Shawn A. Menefee, Mark Cook, Gisselle Zazueta-Damian, Monika Dzieciatkowska, Emmy Do, Saya French, Manali M. Shah, Clyde Sanvictores, Kirk C. Hansen, Matthew Shtrahman, Karen L. Christman, Marianna Alperin. "Pro-regenerative Extracellular Matrix Hydrogel Prevents and Mitigates Pathological Alterations of Pelvic Muscles Following Birth Injury". The dissertation author was the first author of this paper.

Chapter 4 is currently being prepared for submission for publication of the material, Pamela Duran, Emma Zelus, Saya French, Lindsey Brunett, Karen L. Christman, and Marianna

Alperin. “Repeated birth injuries lead to pelvic floor muscle dysfunction and impairment in regeneration”. The dissertation author was the primary author of this paper.

VITA

2014 Bachelor of Science in Bioengineering at “Universidad Autónoma de Baja California”, Tijuana, Mexico

2022 Doctor of Philosophy in Bioengineering at University of California San Diego

PUBLICATIONS

Duran P, Boscolo Sesillo F, Burnett L, Menefee S, Cook M, Zazueta-Damian G, Dzieciatkowska M, Do E, French S, Shah M, Sanvictores C, Hansen K, Shtrahman M, Christman KL, Alperin M. Pro-regenerative Extracellular Matrix Hydrogel Prevents and Mitigates Pathological Alterations of Pelvic Muscles Following Birth Injury. Preprint. bioRxiv 2021.05.28.446170

Rieger M*, **Duran P***, Cook M*, Schenk S, Shah M, Jacobs M, Christman KL, Kado D, Alperin M. Quantifying the Effects of Aging on Morphological and Cellular Properties of Human Female Pelvic Floor Muscles. Ann Biomed Eng. 2021. *Shared first author

Wang R. *, **Duran P***, Christman KL. Processed Tissues. Biomaterials Science: An Introduction to Materials in Medicine. Elsevier, 4th edition. 2020. pg 377-400. *Shared first author

Duran P, Alperin M, Christman KL. Chapter 7: Decellularized Extracellular Matrix Hydrogels: Fabrication, Properties, Characterization, and Current Applications. Biomaterials Science Series No.6. Royal Society of Chemistry. 2019. pg 116-138.

Duran P, Ward S, Christman KL, Alperin M. Mechanical Impact of Parturition-Related Strains on Rat Pelvic Striated Sphincters. Neurourol Urodyn. 2019; 38(3).

Sheth V, **Duran P**, Wong J, Shah S, Du J, Christman KL, Chang E, Alperin M. Multimodal Imaging Assessment and Histologic Correlation of the Female Rat Pelvic Floor Muscles’ Anatomy. J Anat. 2019; 234(4).

ABSTRACT OF THE DISSERTATION

Decellularized Extracellular Matrix Hydrogel Therapy for the Prevention and Treatment of Pathological Alterations Following Birth Injuries

by

Pamela Duran

Doctor of Philosophy in Bioengineering

University of California San Diego, 2022

Professor Karen L. Christman, Chair
Professor Marianna Alperin, Co-Chair

Pelvic floor disorders, which include pelvic organ prolapse, and urinary and fecal incontinence, affect millions of women globally and represent a major public health concern. Pelvic floor muscle (PFM) dysfunction has been identified as one of the leading risk factors for the development of these morbid conditions. Even though childbirth, specifically vaginal delivery, has been long recognized as the most important potentially modifiable risk factor for PFM injury, the precise mechanisms of PFM dysfunction following childbirth remain elusive. In addition, treatments for PFM dysfunction are urgently needed as the current therapeutic approaches are delayed and mainly compensatory. Using a pre-clinical rat model, we first demonstrated that PFM undergoes atrophy and fibrosis following birth injury. The transcriptional signature of PFM post-

injury indicated a sustained inflammatory response, impairment in muscle anabolism, and persistent expression of extracellular matrix (ECM) remodeling genes. We then evaluated the administration of an injectable skeletal muscle ECM hydrogel to prevent and mitigate the pathological alterations following simulated birth injury. Treatment of PFMs with the biomaterial either at the time of birth injury or 4 weeks post-injury reduced muscle atrophy and mitigated fibrotic degeneration. Through gene expression analyses, we show that improvement in PFM phenotype is potentially associated with the hydrogel-induced modulation of the immune response and intramuscular fibrosis and the enhancement of endogenous myogenesis. Lastly, we investigated the PFM response following repeated simulated birth injuries (SBIs), as multiparity further exacerbates the risk for pelvic floor disorders. We demonstrated that repeated SBIs increase pathological alterations and muscle dysfunction compared to a single injury. Gene expression analyses indicated a prolonged inflammatory response compared to a single SBI. Delayed administration of the acellular biomaterial following repeated injuries improved PFM histological changes and modulated the immune response. Overall, this thesis contributes to the understanding of the mechanisms behind PFM birth injury and demonstrates proof-of-concept for utilizing the pro-regenerative biomaterial for treating injured PFMs.

Chapter 1: Dysfunction of pelvic floor muscles after childbirth and potential application of ECM-derived hydrogels

1.1 Evolution of human pelvis to aid in vaginal delivery

Evolution of human bipedalism consisted in adaptation of the pelvis to facilitate bipedal locomotion. Compared to non-human primates, a narrower pelvis allowed for a more energy-efficient movement processes, with enhancement of locomotion performance.[1] In relation to men, women pelvis are larger and wider to facilitate fetal delivery. The female pelvis sustains increases in encephalization by changing shape and alignment to facilitate fetal rotation during birth.[1] The horizontal pelvic floor supports the weight of a large fetus as well as the pelvic organs, resist increases in intra-abdominal pressure and maintain continence.

Although pelvis adaptation facilitated birth, the pelvic floor can undergo damage during delivery. Vaginal delivery is known as the most modifiable risk factor for the development of a series of conditions known as pelvic floor disorders (PFDs), which include urinary and fecal incontinence and pelvic organ prolapse. These conditions affect approximately 20% of the US and China women to ~50% of Australia and Japan female population. [2-5] Within the components of the pelvic floor, dysfunction of the pelvic floor muscle tissue (PFM) is the leading risk factor for PFDs. [6, 7]

1.2 Anatomy and morphological properties of the pelvic floor muscles

The PFMs, which include the levator ani muscle (LAM) complex and the coccygeus, provide support to the pelvic organs, keep the urogenital hiatus closed during baseline activity, and close the vagina, urethra and rectum by compressing them against the pubis.[8] They stabilize the upper vagina and cervix in a horizontal plane and prevent the downward descendent of the organs onto the perineal body.

The LAM includes the iliococcygeus and pubovisceralis, which is divided into pubococcygeus and puborectalis. The iliococcygeus forms a horizontal sheet that spans the opening within the pelvis and is attached to the pelvic bones ventrally and dorsally.[9, 10] It arises from a fibrous band on the pelvic wall (arcus tendinous of the levator ani) and inserts into the last two segments of the coccyx and midline anococcygeal raphe. The origin of the pubococcygeus is at the superior ramus of the pubis at the lower border of the pubic symphysis, is attached to the pelvic wall by the arcus tendinous levator ani and inserts at the lateral parts of the coccyx. The puborectalis arises from the superior and inferior rami of the pubis, the muscles from both sides form a sling around the rectal wall, where fiber bundles of each muscle cross the opposite side forming a muscular raphe. The coccygeus rises from the margins of the spine of the ischium and inserts into the lowest part of the sacrum and lateral side of the coccyx.[9-12]

PFMs are skeletal muscles, which are composed of contractile and extracellular matrix (ECM) components, that aid in overall muscle function and force transmission, respectively. Muscle force production can be indirectly assessed by its structure-function relationship. Therefore, to further delineate morphological properties of PFMs besides their anatomical landmarks, muscle architecture is widely used in the skeletal muscle field to understand such structure-function relationship.[13, 14] In general, the concept is based on the arrangement of muscle fibers relative to the axis of force generation and includes different parameters that influence muscle force production. These parameters include muscle fiber length, sarcomere length, and physiological cross-sectional area (PCSA). Fiber length is proportional to fiber excursion or velocity, sarcomere length (L_s) determines the length-tension relationship of the muscle under isometric force, and PCSA is the predictor of force generation that directly influences muscle tension. Muscle architecture has been widely used in the orthopedics field to predict muscle performance after therapeutic interventions.[13]

Tuttle, et al., analyzed muscle architecture of the PFMs in cadaveric human samples. The PCSA of all PFMs was lower compared to other skeletal muscles indicating that these muscles produce relatively small forces. Within the PFMs, the coccygeus had the largest PCSA and the shortest fiber length. The puboviscerali had the largest fiber length suggesting that this muscle undergoes the largest elongation and contraction. The design of these muscles corresponds to their functional needs—a larger excursion is needed for the puboviscerali to aid in defecation and pelvic floor distention, while a shorter fiber length and large PCSA is needed for the coccygeus which makes it a good stabilizer of the coccyx.[15] In addition, the L_s of all PFMs was shorter than the optimal human L_s of 2.7 μm—the in vivo L_s is known as the operational L_s and usually differs from the optimal one. A shorter L_s indicates that the muscle operates on the ascending limb of the length-tension curve, and after a muscle contraction, the L_s will increase towards the plateu of the curve where the maximum force is obtained.[14] As another example, another skeletal muscle of the pelvic floor—the external anal sphincter—also operates on the ascending limb of the length-tension curve with shorter L_s than the optimal one, this indicates that as the muscle contracts, the fibers elongate increasing the tension towards the plateu of the curve.[16]

Knowledge of the structure-function relationship is key for the development of scientifically rationale improvements of therapeutic approaches. For example, sphincteroplasty technique used to repair the external anal sphincter laceration, can be improved by placing the muscle to a L_s at which an increase in active tension can be achieved during muscle contraction.

Some of the muscle architectural parameters have been measured by non-invasive measurements such as ultrasound or magnetic resonance imaging (MRI); however, these techniques do not fully assess the morphological properties. MRI has a better resolution than ultrasound but does not provide measurement of sarcomere or fiber length. For assessment of L_s measurements, laser diffraction or second harmonic generation are used in the skeletal muscle

field. Although these techniques require exposure of the muscle together with a laser or microscope, portable equipments are being investigated that could be used in a clinical setting before a therapeutic intervention. Other sophisticated techniques, such as diffusor tensor imaging, are used to assess muscle fiber lengths and orientation (crucial to predict muscle function) by using directions of water diffusion to provide information about tissue architecture. A previous study used this technique on the female pelvic floor to demonstrate feasibility; however, using it as a clinical tool has limitations associated with long scan times, costs, and complex image post-processing routines.[17] Diffusor tensor imaging can be validated by photogrammetry, where 2D images are obtained, overlapped, and reconstructed to obtain a 3D image. Routzong, et al., used cadaveric pelves to visualize surface muscle fascicles and assess fascicle orientation. Authors observed that fascicle orientations of the PFMs represent lateral tension. Pubovisceralis had the most superior-inferior fascicle orientation, while coccygeus was the least superior-inferiorly oriented. This fascicle orientation indicates that pubovisceralis contributes mainly to the superior-inferior motion of the pelvic floor, and coccygeus contributes to pelvic floor and coccyx motion but also provides stabilization within the axial plane.[18] Overall, although each of the mentioned techniques provide valuable approaches for the assessment of PFM architecture, a standardized technique should be optimized and implanted in the clinical setting.

1.3 Function of the pelvic floor muscles

The PFMs provide support to the pelvic viscera and act as a constrictor mechanism for the urethra, vagina, and anal orifices. Aside from knowing the general function of the muscles, it is also important to investigate the mechanical properties (i.e., stresses and strain) during physiological activities to detect changes of these parameters under the presence of PFDs. Different computational models have included several material parameters to understand the mechanical behavior of PFMs. As an example, one study used data from an old female cadaver

to simulate the passive behavior of the muscles and identified that the regions of maximum stress occur at the enthesial region of the LAM.[19] Another study determined the LAM deformation during a bear down maneuver of a female live subject MRI and observed that the maximum compression in the superior to inferior direction occurs at the bottom of the LAM and around the bottom coccyx region.[20] Through MRI, Lee, et al., identified that under stress (sitting and squatting) the angle of the LAM changes and the thickness increases, which is an indicator of increased muscle contraction.[21] The same group analyzed the structural changes of the LAM during different simulated physiological loadings and observed that the areas with highest stress distribution corresponded to the anterior pubococcygeus and anterior and posterior puborectalis, which are known to represent the most significant movement during PFM exercise.[22]

The previous examples have included healthy females, which can be used as a baseline to detect further changes under the presence of PFDs. In this context, Saleme, et al., simulated the passive behavior of the pubovisceralis muscle from a woman with stress urinary incontinence.[23] Different degrees of muscular activation demonstrated that a 50% contraction would produce enough resistance to increase the pelvic pressure avoiding possible urine loss. Results from the model correlated with displacements obtained from MRI images. The model also correlated with clinical studies indicating that during valsalva maneuver, the puborectalis is the main constrictor of the urogenital hiatus and counteracts pelvic organ descendent during the intra-abdominal pressure.

In general, the mentioned computational models do not include all the tissue properties necessary to simulate PFM function. Addition of anisotropic behavior (different mechanical properties depending on the muscle direction analyzed), muscle fiber orientation, contractile behavior, and incorporation of surrounding structures (i.e., ligaments) are crucial to better represent PFMs mechanical properties. Some studies have analyzed each of these components

separately [24, 25], but addition of them to previous models will greatly enhance studies investigating changes in PFM function.

1.4 Clinical evaluations of pelvic floor muscle function

The standard method in clinical practice for evaluating the function of the PFMs is through a digital vaginal exam wherein the examiner places 1 or 2 of his or her fingers into the vagina approximately mid-way and then instructs the subject to contract her PFMs. Numerical scales, including the modified Oxford scale (numbered 0 to 6) and Brinks scale (numbered 0 to 4), have been used to attempt to quantify the examiner's subjective assessment of the strength and duration of the contraction.[26-29] Subjective assessments like these are clinically useful because they do not require additional equipment, however they are limited by their subjective nature despite reporting results on a quantitative scale.

Perineometry is a non-subjective measure for the assessment of the LAM function through intravaginal assessment. This method consists of using an intravaginal probe connected to a pressure transducer that gives a measurement of the vaginal pressure in cmH_2O during a PFM contraction.[6, 30] The Brink scale assessment for maximum squeeze pressure was found to correlate moderately well with perineometry.[28] Despite the advantage of perineometry in providing an objective measurement for vaginal pressure during pelvic floor contraction, a limitation of this technique is that it cannot differentiate between an increase in vaginal pressure due to PFM contraction and an increase in intra-abdominal pressure due to another cause.[26, 28] Another method to assess PFM function is through electromyography, which can be performed with electrodes placed on the perineum or intravaginally.[31, 32] Devreese et al found that there was good correlation between perineal and vaginal surface electrodes for assessing voluntary PFM contraction.[33] A dynamometer was developed to target contraction of the PFMs more specifically. This method uses an intravaginal dynamometer to directly measure muscle strength as opposed

to the pressure transducer used with the perineometer. The probe needs to be placed in a dorsal lithotomy position with an anterior-posterior orientation with only 10 degrees of error.[34]

Vaginal tactile imaging (VTI) was recently used to develop a biomechanical mapping of the pelvic floor by using an intravaginal probe that translated touch into a digital image. This method, still in its first stages of implementation, allows to measure passive properties of the PFMs as well as other biomechanical parameters of the muscle and surrounding structures. [35]

Radiological imaging modalities, such as ultrasound and MRI, may also be used to indirectly assess PFM function by assessing the changes in muscle appearance with movement. Ultrasound is used to assess PFM function during rest, contraction, and valsalva maneuver through measurement of bladder neck descent, change in anorectal angle, and changes in levator hiatus measurement.[36] Elevation of the bladder neck occurs with PFM contraction, with greater elevation indicating a greater strength of contraction. In addition, changes in anorectal angle and increase in muscle thickness, are indicators of increased PFM contraction.[37] MRI consists of better resolution images of the PFMs and surrounding structures; this technique also assesses PFM function by measuring their configuration and position with movements. MRI is not widely used in everyday clinical practice, due to the high cost and complexity of examination.

Altogether, from a muscle physiology point of view, the ideal assessment of PFM function includes evaluation of both active and passive mechanical properties, which mostly indicate changes in contractile and ECM components, respectively. Therefore, EMG assessment in combination with VTI are the most promising techniques. However, intersession reliability needs to be investigated for EMG, together with implementation of VTI in clinic.

1.5 Pelvic floor muscles during vaginal delivery

Multiple epidemiological studies have unequivocally identified vaginal childbirth as the leading risk factor for the PFM injury. [7] Several computational models of human parturition have investigated the stresses and strain imposed on the PFMs during delivery. The first studies considered the PFMs attachments and the fetal head size as a sphere, demonstrating that the highest stretch ratio occurs at the pubovisceralis muscle, either the pubococcygeus or puborectalis.[38, 39] However, these models did not consider variations in pelvic shape, fetal head shape and orientation, fetal head molding, and muscle fiber orientation, indicating that those previous models did not represent physiological conditions. Throughout the years, studies have incorporated one of these parameters separately into their models.

Jing, et al., used in vivo MRI data of fetal head and maternal pelvis to develop a computational model that better represents the structures of the pelvic floor components. Authors incorporated skeletal muscle parameters such as anisotropy and viscoelasticity.[40] The study confirmed that the highest levator stress occurred at the enthesis of the pubovisceralis muscle with an overall levator stretch of 3.55 and of 4.64 at the enthesial region, which is above the physiological limit at which appendicular skeletal muscle injury occurs.[41] Addition of fetal head molding is relevant since during delivery the fetal head has an elongated shape due to the elevated pressure during its passage through the birth canal. The incorporation of this parameter together with the skull, sutures and fontanelles, and the fetus head movements demonstrated a reduction on the forces exerted on the PFMs compared to a rigid model.[42] In addition, a decrease in stretch was identified with a deformable fetus head. Later, other authors included the fetal head molding in their computational analysis derived from serial MRI of a live childbirth and identified that the highest stretch was found at the posterior-medial portion of the LAM.[43] Besides confirming that pubovisceralis undergoes the largest stretch during parturition, Oliveira et al., identified that

~10% of muscle fibers are damaged during delivery by incorporating a structural damage model to the simulation of childbirth.[44]

In summary, the mentioned computational models demonstrate that the puboviscerali s muscle undergoes the largest stretch during parturition. Even though these models include different components of the pelvic floor such as ligaments and attachments, as well as changes during delivery (i.e., fetal head molding), other parameters need to be included to better represent the stresses and strains imposed on the PFMs during delivery. These can include incorporation of changes in pelvic shape, and fibers orientation of each PFM.[18, 45]

1.6 Function of the pelvic floor muscles after childbirth

The function of the PFMs after vaginal delivery has been evaluated with different objective techniques. Peschers, et al., used a perioneometer to identify that PFM strength was reduced 3 days post-delivery and continued to be decreased 10 weeks later in primiparous women.[46] By also using a perineometer, another study identified that the squeeze and resting pressures were lower at 14 weeks after vaginal delivery compared to a cesarean section, with prolonged decreased resting pressure at 1-year post-partum.[47] Besides perineometry, EMG has demonstrated a reduced PFM strength 8 weeks after delivery. In addition, while some women recovered the muscle function 1 year post-delivery, others did not.[48] In a recent paper from Davidson, et al., muscle force and stiffness, assessed by elastometry, were reduced 12 weeks after delivery.[49] As elastometry can include stiffness from other components of the pelvic floor, such as vagina walls and fascia, other non-invasive measurements are needed to effectively measure this parameter in the PFMs. Blomquist, et al., identified that a reduced PFM strength analyzed 5-10 years after delivery, was associated with an increased incidence of PFDs.[6] In agreement with the authors, assessment of muscle strength shortly after childbirth would be ideal to demonstrate a temporal relationship with future development of PFDs.

1.7 Clinically accepted phenotype of levator ani muscle after vaginal delivery

In the last two decades, several studies have demonstrated changes in the appearance of the PFMs, giving insights into the pathophysiology of the skeletal muscles. DeLancey, et al., identified unilateral and bilateral defects in the puboviscerali muscle 1 year after delivery through MRI.[50] These avulsions were also observed by ultrasound at the same time point, and at shorter time points, which were identified mainly by the presence of darker areas.[51-55]

Although the presence of avulsions through imaging modalities has been well established, several studies have shown resolution of this defect. Chan, et al., did not observed the presence of avulsions 3-5 years later after being identified 8 weeks post-partum.[56] In addition, Garcia-Mejido, et al., classified the avulsions based on their appearance and observed that type II defects (complete detachment of puboviscerali from its insertion) were present 1 year after delivery while type I avulsions (lateral fibers of puboviscerali were still observed at the insertion) were not identified.[57] A cadaveric study demonstrated that avulsions present with ultrasound were not visualized after dissection, indicating that defects observed with ultrasound might not represent a true anatomical avulsion. In general, the avulsion phenotype is not present in all women with pelvic floor dysfunction or decreased pelvic floor muscle strength.[58] Thus, there is a necessity to study other potential phenotypes of PFMs after birth injury.

1.8 Currently available treatments for pelvic floor muscle dysfunction

There are currently minimal strategies to treat PFM dysfunction after childbirth. Pelvic floor physical therapy or PFM training has been the first option to strengthen the PFMs by manual therapy, electrical stimulation, or home exercises in women with symptomatic PFDs. Although the therapy has shown short-term effectiveness (~12 months), long-term clinical trials are needed. In addition, PFM exercises are associated with poor adherence.[59, 60] Other treatments for PFM dysfunction and the associated PFDs include midurethral slings to prevent the leakage of urine,

nerve stimulation for fecal incontinence, or pessaries and surgeries to accommodate the pelvic organs in place.[61, 62] These options are related to high failure rates and are compensatory as they do not address the underlying pathophysiology of PFM weakness. In terms of prevention of PFM dysfunction, Cesarean section is the only available option which is associated with a higher prevalence of maternal mortality and morbidity compared to vaginal delivery.[63]

Although the pathophysiology behind PFM dysfunction consequent to vaginal delivery is not completely understood, capitalizing on the established endogenous repair after skeletal muscle injuries[64] is a promising approach for the prevention of PFM weakness and the later development of PFDs. Within this context, regenerative strategies have shown to promote a healing environment after several muscle-related conditions.[65] To investigate a potential therapeutic approach that will enhance muscle regeneration, it is essential to first understand the established skeletal muscle response after an injury.

1.9 Skeletal muscle regeneration after an acute injury

Skeletal muscle is known to have a high regenerative capacity. Following muscle injury, a population of muscle stem cells (MuSCs) lead the regeneration process that is influenced by intrinsic and extrinsic factors.[66] Muscle regeneration or myogenesis is divided by different stages identified by expression markers of MuSCs, defined as myogenic regulatory factors. Quiescent or inactive satellite cells are identified by Pax7. After muscle injury, MuSCs are influenced by changes in their niche and migrate towards the site of injury and re-enter the cell cycle to proliferate. During proliferation, a population of MuSCs continue towards myogenesis while another portion self-renew to replenish the stem cell pool. Committed satellite cells are named myoblasts (Pax7, MyoD, Myf5). After proliferation, myoblasts exit the cell cycle and begging to differentiate (Myog, Mrf4) into mature myocytes. At last, myocytes fuse together to form de novo myofibers or fuse to pre-existing ones. At this stage, embryonic myosin heavy chain is expressed

together with contractile proteins.[66, 67] Regenerated myofibers are also identified by the presence of centralized nuclei; thus, completion of regeneration is analyzed by the return of this parameter to baseline levels.

Efficient communication between satellite cells and other cell types is crucial factor for muscle regeneration. After a muscle injury, a complex inflammatory process initiate. This process can be divided into initiation, development and resolution. First, damaged myofibers secrete molecules named damaged-associated molecular pattern, such as DNA, RNA, metabolites, that will be identified by resident leukocytes (macrophages).[66] Macrophages release cytokines such as TNF-α, and IL-6, which are known to simulate satellite cell activation. The beginning of the inflammatory process is associated with the activation of satellite cells.[64, 68]

The next phase in the immune response continues with the recruitment of blood-circulating leukocytes—influenced by cytokines released by resident leukocytes. Neutrophils infiltration peaks at approximately 12 to 24 hours post injury, cleaning muscle debris during this period. The pro-inflammatory cytokines (e.g., IFNγ, TNF-α) released by neutrophils encourage the recruitment of monocytes, which will differentiate and mature into macrophages. The local microenvironment polarizes this cellular population into two subpopulations—pro-inflammatory macrophages (M1) and anti-inflammatory macrophages (M2). Pro-inflammatory macrophages recruit T helper type 1 cells and together secrete cytokines such TNF-α and IL-1β, which are known to promote satellite cell proliferation. This period peaks 2-3 days post-injury with dampening by 4 days.[64, 66]

The resolution of inflammation is represented by the polarization of macrophages towards an anti-inflammatory phenotype which coincides with T helper type 2 cells. These two cell populations secrete molecules (IL-4, IL-10, IGF-1, TGF-β) that are necessary for the dampening of inflammation, leading to a pro-remodeling environment. This phase, which peaks around 5

days post-injury, is associated with the differentiation of satellite cells and fusion of myoblasts. The polarization of immune response towards the anti-inflammatory phase is mainly regulated by a subpopulation of T helper type 2 cells, known as regulatory T cells (Tregs). These cells peak around the same time frame as M2-associated macrophages.[64] Previous studies identified that depletion of Tregs slowed muscle regeneration and prolonged inflammation.[69]

Besides the communication between immune cells, MuSCs function is also influenced by other cellular populations such as fibroadipogenic progenitors (FAPs). This mesenchymal cell population aids during the last stages of myogenesis by supporting MuSCs differentiation. In addition, FAPs are greatly involved in the temporal increase in extracellular matrix (ECM) deposition—which serves as a scaffold for myofiber formation—by differentiating into fibroblasts. This population together with macrophages secrete a variety of ECM-related proteins and growth factors (e.g., TGF-β, CTGF) to synthesize the temporal scaffold. ECM remodeling is also influenced by the balance between MMPs (matrix metalloproteinases) and TIMPs (tissue inhibitors of matrix metalloproteinases) which promote or inhibit ECM degradation, respectively.[70,71]

Even though skeletal muscle follows a regeneration process in a timely manner, muscle injuries can lead to an insufficient regeneration identified by a prolonged inflammatory response, impairment in MuSCs function, and imbalance in ECM remodeling—all leading to the presence of pathological alterations, such as muscle atrophy and fibrosis. In this manner, the rapidly evolving field of biomaterials can be applied to induce a pro-remodeling environment, with the overall goal of augmenting the established muscle regeneration process.

1.10 Tissue engineering approaches for skeletal muscle regeneration

Two approaches for tissue regeneration include in vivo and in vitro regenerative strategies. In vivo strategies rely on the delivery of cells, bioactive molecules, or biomaterials alone or in combination with these components, while in vitro approaches include the growth and maintenance of cells on a biomaterial substrate to develop a mature and functional muscle construct that can be implanted into the defect site.

1.10.1 Cell-based therapies

Several studies have investigated the efficacy of direct injection of MuSCs in muscle injuries and demonstrated promotion of muscle fiber repair and improved contractile function.[72] Mesenchymal stem cells have also been studied for muscle regeneration approaches.[73] These cells can contribute to myogenic differentiation giving rise to myotubes and contributing to muscle repair and contraction (Figure 1.1). Although benefits have been observed in small animal models, poor cell survival and expansion are challenges that interfere with clinical translation of cell-based therapies. Cells undergo apoptosis within hours of transplantation leading to low survival rates. One solution can be the ex vivo expansion of MuSCs, however, this can limit its proliferative capacity and regenerative capabilities.[74] Cell-based therapies also have challenges associated with potential tumorigenicity, and high costs for development.

Cell-based therapies are widely investigated for the treatment of PFDs. These therapies focus on the treatment of the sphincteric skeletal muscles, which include the external urethral and anal sphincters—injury to these muscles is involved in the development of urinary and fecal incontinence. Several pre-clinical studies have focused on investigating the efficacy of mesenchymal stem cells derived from different sources. Adipose derived mesenchymal stem cells (ADSCs) were injected into the urethra after a vaginal distention injury model to simulate childbirth injury. Four weeks after treatment, cystometry measurements indicated normal voiding pattern in

57% of the animals.[75] Several studies have focused on the isolation of mesenchymal stem cells from the bone marrow. In a previous study, rats underwent bilateral pudendal nerve transection as another model to induce childbirth injury. Periurethral injection of bone marrow derived mesenchymal stem cells (BMSCs) demonstrated increased leak point pressure 4 weeks after treatment—this measurement is an indirect assessment of urethral function and urinary continence.[76] BMSCs have also been investigated after an anal sphincter injury model demonstrating that the anal pressure started to increase at 10 days post-injection with reduced fibrosis by 5 weeks compared to experimental control.[77] Another cellular source that has been explored includes myoblasts. These cells were injected into the urethra after a sciatic nerve transection injury model to simulate urinary incontinence, ex vivo mechanical testing demonstrated increased muscle contraction and muscle fiber formation in relation to saline injection.[78]

Although efficiency of cell-based therapies has been observed in animal models, beneficial impact of stem cell treatment in clinical trials is not clearly defined. For example, myoblasts were injected into the external anal sphincter via ultrasound guidance in patients with fecal incontinence. Subjective assessments indicated patient satisfaction up to 12 months post-injection, however, quantitative assessment by anal pressure was not improved.[79] In another study, injection of umbilical cord blood stem cells demonstrated mild to no improvement based on 24hr pad test to assess involuntary leakage of urine.[80] ADSCs and BMSCs have also been investigated in clinical trials. In general, the majority of the few trials include improvements by objective measurements in ~50% or less of the patients, while other studies showed no improvements.[81-84] In all the clinical trials, efficacy was assessed in small patient population (5-40 patients) and at short-term periods after injection with the longest one being a 2 year follow up. Thus, studies with larger sample size and longer time points are needed. In addition, a concise

source and method for the isolation of stem cells, and dosing is also needed, together with the possible investigation of multiple injections.

1.10.2 Bioactive molecules-based therapies

Another option to potentiate muscle repair is through delivery of growth factors that enhance a specific process in endogenous tissue regeneration (Figure 1.1). For example, since vascularization is a key component in MuSCs survival, revascularization after an injury is essential for successful repair and regeneration. Pro-angiogenic growth factors, such as vascular endothelial growth factor (VEGF), have been delivered systemically, stimulating blood vessel formation in vivo after muscle injury.[85] Other growth factors, such as insulin growth factor-1 (IGF-1), fibroblast growth factor (FGF), and nerve growth factor (NGF), have shown to improve muscle regeneration by promoting protein synthesis, MuSCs activation and differentiation, and reinnervation, respectively.[85, 86] Despite the improvements observed after the delivery alone of such biomolecules, the short half-life of growth factors requires frequent administration of high dosage injections.

Alternative biologics for cell-free therapies include exosomes which are small membrane vesicles secreted in a variety of cells (Figure 1.1). These biological products are involved in cell-to-cell communication and contain messenger RNA, microRNA (miRNA), proteins, and nucleic acids, which reflect their original cell sources. The delivery of the bioactive content of exosomes aids in several tissue processes such as angiogenesis, immune response, and regeneration. Choi, et al., investigated the efficacy of exosomes (secreted from myoblasts) after a laceration injury model. The exosomes, which contained growth factors that aid in muscle regeneration, reduced muscle fibrosis and increased the number of regenerated fibers.[87] In another study, exosomes derived from mesenchymal stem cells, promoted angiogenesis, decreased fibrosis and improved muscle regeneration in a chemically induced injury model.[88] Within the components of

exosomes, delivery alone of miRNAs has also been explored as a therapy for promoting muscle repair.[89] These bioactive molecules are noncoding RNAs that regulate post-transcriptional gene expression. A previous study showed that administration of synthetic skeletal muscle specific miR-206, known to promote myoblast proliferation and differentiation, hinder muscle fibrosis and aid in muscle regeneration.[90] Although these options for cell-free therapies demonstrated efficacy in pre-clinical animal studies, clinical translation of these therapies has challenges associated with rapid diffusion and degradation after injection.

Mesenchymal stem cells secrete several bioactive molecules such as growth factors, chemokines, and cytokines, either alone or in extracellular vesicles.[91] Together these molecules are known as the secretome of stem cells, which have been tested in animal models as a treatment for urinary and fecal incontinence. Previous studies showed improvement in leak point pressure at 1 and 3 weeks after delivery of the therapeutic in a pudendal nerve crush and vagina distention model, however, direct assessment of external urethral sphincter function by electromyography did not demonstrated improvement in muscle contraction.[92, 93] These studies suggest that secretome might not directly influence skeletal muscle regeneration but seems to have an effect on other components of the urethra. Exosomes derived from ADSCs were investigated in the previous animal model, demonstrating increased bladder capacity and leak point pressure at 2, 4, an 8 weeks post-injection together with higher proportion of skeletal muscle fiber area in relation to no treatment group.[94] Another study investigated the efficacy of exosomes derived from urine-derived stem cells. The exosomes were injected into the pubococcygeus muscle after vaginal distention, the treatment group demonstrated increased leak point pressure and bladder capacity at 4- and 8-weeks post-injection, together with number of regenerated fibers and percent of collagen content similar to uninjured group at the long-term time point.[95] Although these few animal studies have demonstrated functional improvements after exosomes delivery,

the application of these cell-derived vesicles as a therapeutic approach for urinary incontinence is still in its preliminary stage.

1.10.3 Scaffold-based therapies

To address issues associated with scaffold-free therapies, biomaterials are used in tissue engineering as a guide for tissue regeneration to increase cell viability and retention and deliver bioactive molecules in a controlled manner.[85, 96, 97] These biomaterials simulate or mimic the native microenvironment and aid in cellular adhesion, migration and proliferation. Synthetic materials allow for the control of mechanical properties, degradation rate and biomaterial composition. Examples of synthetic materials commonly used after skeletal muscle injuries include polyester materials, such as poly(glyocolic acid) (PGA) and poly(lactic-co-glycolic acid) (PLGA), and elastomeric materials like polyurethane.[96] A disadvantage of these materials is that they do not have cell attachment sites but can be coated with a protein layer to improve cell adhesion. On the other hand, natural biomaterials provide the biochemical cues or native signaling cues important for a successful muscle regeneration. These materials usually consist of a component of the ECM, or the whole matrix isolated from decellularization protocols (Figure 1.1). [85, 96-98]

Scaffolds should mimic the architecture and morphology of the native tissue for an efficient muscle healing and regeneration, which could be achieved by providing biophysical and biochemical cues. The former one includes topographical characteristics to provide contact guidance that promotes myoblast alignment, and ultimately maturation of myotubes organized into the characteristic unidirectional orientation of muscle fibers. [85, 96, 97] Others biophysical cues include scaffold stiffness that resemble that of the native tissue to influence cellular behavior, and guidance of electrical impulses which is critical for muscle function. Biochemical properties further influence cellular behavior by promoting cell adhesion and proliferation, these properties tend to be intrinsic to the scaffold as it is the case for natural biomaterials (Figure 1.1). [85, 96, 97]

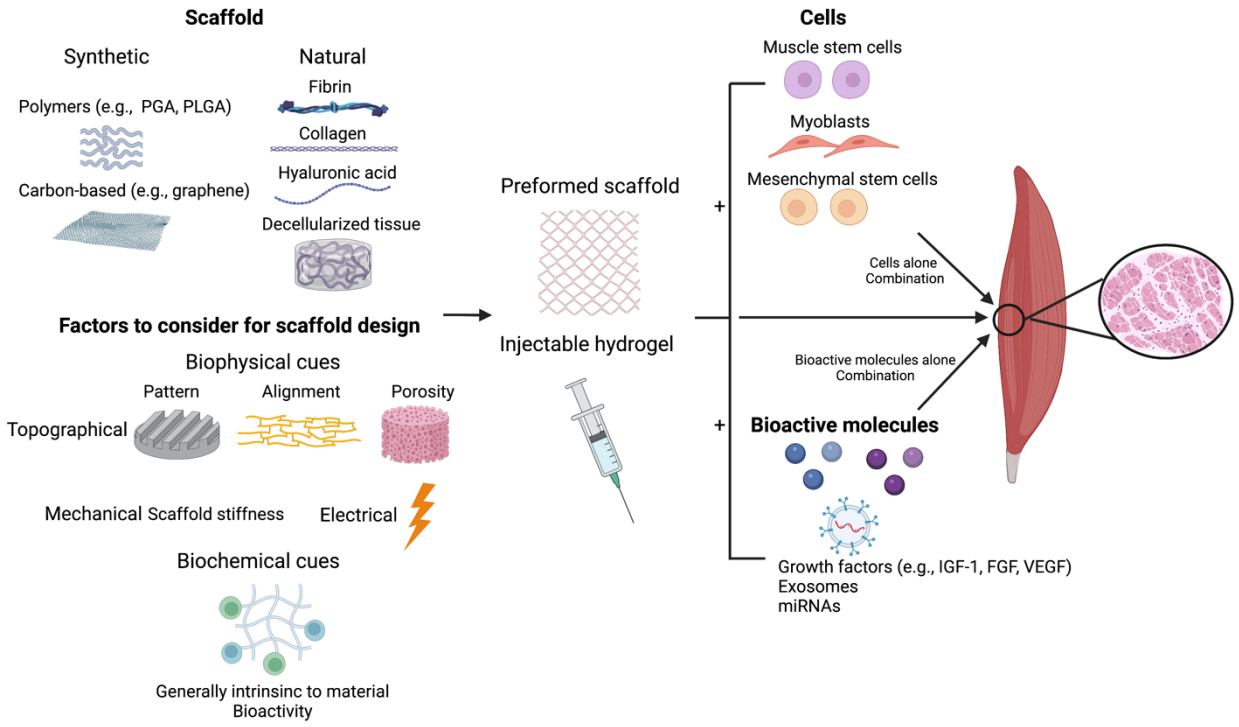

Figure 1.1 Tissue engineering approaches for skeletal muscle regeneration.
Cells, bioactive molecules and scaffolds can be delivered alone or in combination to the injured muscle. Examples of types of materials and factors to consider for scaffold design, as well as examples of cells and biomolecules are included.

1.10.3.1 Factors to consider for the design of a scaffold-based therapy for skeletal muscle regeneration

1.10.3.1.1 Biophysical cues

Topographical cues: These cues can be achieved by using materials that can be used to create micropatterned substrates, such as wavelengths, grooves/channels, and posts or holes, usually used in combination with cells to build a multi-layered cell-scaffold construct.[96] Most of the research done on these substrates has been in vitro studies to characterize myoblast response under the presence of topographical cues that promote myogenic differentiation. A previous study

demonstrated that myoblasts cultured on a laminin-coated micropatterned polymer substrate with a continuous wavy pattern led to alignment of myotubes after 6 days compared to the random orientation of cells cultured on flat substrate.[99] Other in vitro studies have also showed influence of channels and grooves, as well as evenly spaced posts on myoblast alignment and myotube formation through contact guidance.[100, 101] Despite the abundant in vitro experiments, few studies have focused on in vivo efficacy. Yang, et al., investigated the potency of nanopatterned substrates composed of PLGA with aligned nanogrooves seeded with myoblasts. The patch was transplanted over quadriceps muscles in a dystrophin-deficient mouse model and demonstrated higher number of dystrophin-positive fibers compared to a patch with flat surface.[102]

Contact guidance to stimulate myotube formation can also be achieved through aligned fibers in the nanometer and micrometer scale. Studies have suggested that influence of myoblast alignment on nanofiber topography may be due to direct cytoskeletal reorganization to orient cells along the axis of fibers.[96] The most common method for production of these fibers is electrospinning where a polymer solution is charged and ejected through a spinner under a high-voltage electric field to form fibers as the solvent evaporates.[96, 97] This method allows for the control over fiber diameter and alignment, formation of composite nanofibers with and without cells. A previous study showed that electrospinned PLGA fibers with the larger fiber diameter (~3000 nm) led to enhancement of myoblasts alignment, growth, and differentiation in vitro. When the fiber scaffold was seeded with myoblasts, dystrophin-positive myofibers in a limb muscle were observed in a dystrophin-deficient mouse model.[103]

Two-dimensional topographical cues include the alignment of fibers and micropatterned surfaces as previously explained. Although these cues influence cell behavior through contact guidance, cells are unable to infiltrate the fiber mesh due limited thickness and close packing density of fibers. Cellular infiltration and improved diffusion of oxygen and nutrients to cells depends on the three-dimensional topographical cues which include porous structure. Freeze

drying and phase separation techniques have been used to fabricate three-dimensional scaffolds with elongated pores to guide muscle fiber formation.[97] These scaffolds allow for the delivery of large number of cells in a small mesh volume, as opposed to two-dimensional substrates. Synthetic materials used for the fabrication of scaffold with aligned pore structures include polycaprolactone (PCL) and PLGA, while natural materials usually consist of collagen-based scaffolds. [85, 96, 97] As an example, a previous study fabricated collagen scaffolds with parallel oriented pores (20-50 μm) allowing cells to migrate into the scaffold. The scaffold with myoblasts suspensions were transplanted into the bed of an excised tibialis anterior muscle. Fifty days after transplantation, muscle fibers formed at the defect site, and force generation was obtained by direct stimulation.[104]

Mechanical and electrical cues: Besides topographical characteristics, it is important to consider the mechanical cues of the tissue-engineered construct to mimic native muscle tissue. When mesenchymal stem cells were seeded on collagen-coated polyacrylamide gels of different stiffness, the cells had a neural lineage when cultured on soft gels, an osteoblastic lineage with stiff gels, but underwent myogenic differentiation with an intermediate stiffness that resembles that of muscle tissue (1-10 kPa). Several variables can be modified to influence substrate stiffness, including composition of polymers, molecular weights, and crosslinking agents.[105]

Aside from mechanical and topographical properties, electrical cues can further aid in myogenesis, and potentially restore neuromuscular junctions which are critical for contractile force.[106] Polyaniline is one of the most common conductive polymers that combined with aligned polycaprolactone fibers, led to myotube maturation, and increased expression of early and late markers of myogenesis in vitro.[106] Another example of composite materials that combine electrical with topographic cues include elastomeric polymers with graphene, a carbon-based conductive material.[107] An in vivo study demonstrated that implantation of such nanocomposite in a muscle defect model resulted in the formation of regenerated myofibers.

1.10.3.1.2 Biochemical cues

While synthetic and natural materials can be tunable to achieve a desired biophysical cue, natural biomaterials can also provide the biochemical cues that aid in muscle regeneration. These materials are also generally biocompatible, are primed for enzymatic degradation and can enhance the delivery of bioactive molecules. Naturally derived materials, such as alginate, chitosan, and silk fibroin improve biocompatibility and are used to sustain the delivery of growth factors and to increase the viability of cells. Components of ECM are also used as biomaterial platforms, including fibrin, collagen, and hyaluronic acid, among others.[96] These components influence the myogenesis process; for instance, fibrin is associated with the proliferation and differentiation of muscle stem cells,[108] and collagen and hyaluronic acid influence the migration of myoblasts and promote the release of cytokines that have an effect on myogenesis.[109, 110] Although individual components of ECM aid in muscle regeneration, a scaffold that includes the complex ECM composition most closely resembles the muscle environment. A body of research has focused on the development and efficacy of decellularized tissues (see section 1.10.5) demonstrating that the isolated natural scaffold influences myogenesis and shifts the immune response towards a pro-regenerative/anti-inflammatory stage.

1.10.4 Forms of delivery for scaffold-based therapies

Biomaterials can have different forms based on the intended application. They can be delivered as preformed scaffolds (Figure 1.1), such as patches, to repair a muscle defect that may result from acute trauma (i.e., battlefield injuries) or muscle wasting diseases with the purpose of providing structural support and rigidity as well as cell attachment, and proliferation. The previous studies mostly included preformed scaffold with a defined geometry to fill in the void space.

Preformed scaffolds are used as a treatment for pelvic organ prolapse to provide support to the weakened organs. The mesh, made by synthetic or natural materials, is implanted through

the abdomen or through the vagina and held in place by sutures or tissue fixation devices. Since this approach does not target regeneration of the pelvic skeletal muscles, examples of this treatment can be found in other reviews.[111, 112]

Scaffolds can also be delivered as injectable biomaterials which are used for skeletal muscle regeneration in conditions where a minimally invasive approach is required (Figure 1.1). The hydrogel is formed after the material has been injected in vivo, filling in and adopting the shape of the defect and forming a three-dimensional scaffold that allows for cellular migration and proliferation. Hydrogels can be formed due to changes in their external environment, such as temperature, pH, ions, electric and magnetic field, and light.[113] Temperature-sensitive hydrogels are the ones widely investigated for tissue engineering approaches since this factor has physiological significance in the human body. Some synthetic hydrogels have been investigated but most of the research has been made on natural hydrogels due to their native bioactivity and increase biocompatibility. Synthetic hydrogels are usually used as carriers for cells or bioactive molecules; for example, a previous study encapsulated adipose derived stem cells and VEGF in a synthetic polymer demonstrating differentiation of such cellular population into mature muscle fibers together with enhancement of vascularization.[114]

Naturally derived materials and individual components of the ECM are also used as delivery vehicles for cells and bioactive molecules. Borselli, et al., investigated the efficacy of an injectable alginate hydrogel with IGF-1 and VEGF in an ischemic mouse model and demonstrated that delivery of both growth factors aids in angiogenesis, myogenesis and reinnervation, as opposed to bolus delivery of each biomolecule.[115] Moreover, natural hydrogels have been modified to adjust their biophysical cues. For instance, Liu, et al., added degradable microbeads to fibrin hydrogel to create microporous scaffold and enhance cell viability and migration. Myogenic differentiation of mesenchymal stem cells with formation of myotubes was observed in vitro.[116] Hyaluronic acid and collagen hydrogels have also been studied for skeletal muscle

regeneration.[117, 118] In addition, hydrogels derived from decellularized tissues (see section 1.10.6) are highly investigated due to their immunomodulatory properties and resemblance to native ECM.

1.10.5 Extracellular matrix scaffolds

Over the past two decades, tissue decellularization, by isolating the ECM scaffold, has shown promise for tissue engineering and regenerative medicine approaches. Decellularized scaffolds retain noncellular components representative of native tissue. These characteristics promote cell growth, survival and development. [119, 120] An effective decellularization process depends on the type and age of tissue, and the method used. A summary of decellularization methods (Figure 1.2) is presented below while in-depth review on methods, and effects on composition and structure of decellularized scaffolds have been previously published. [121, 122]

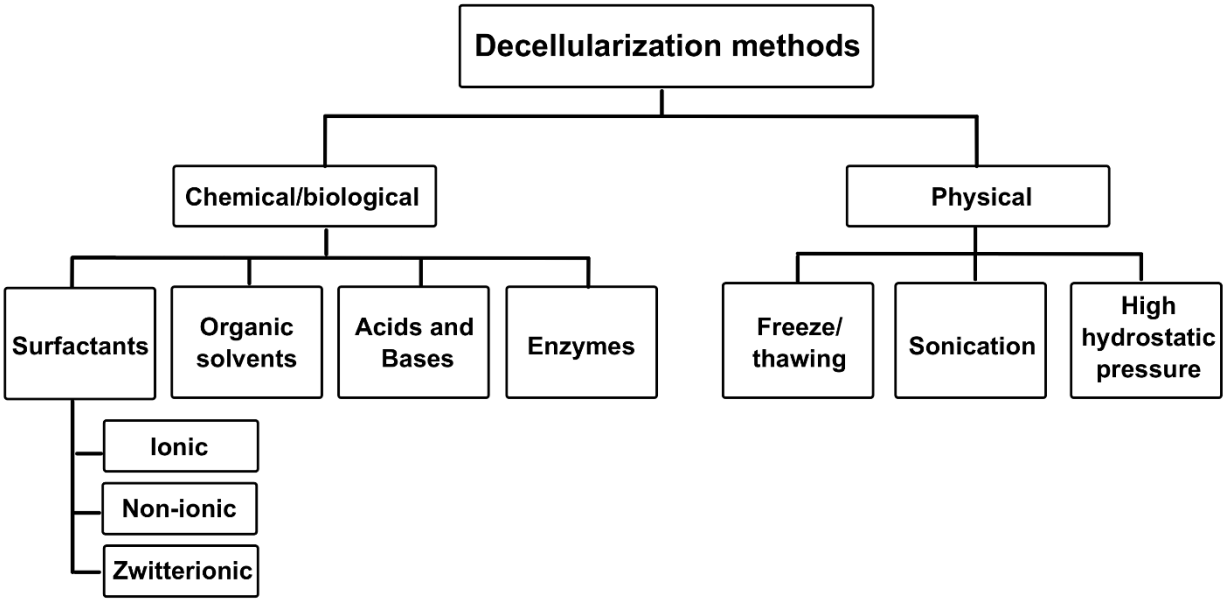

Figure 1.2. Schematic of decellularization methods

1.10.5.1 Decellularization Methods

Chemical/Biological methods: Different chemical agents are commonly used as the main agent of the decellularization process; these include surfactants, organic solvents, acids and bases. Enzymes are used in combination with these chemical agents to enhance removal of DNA (e.g., DNAse, RNAse, trypsin). Surfactants are classified as ionic, nonionic or zwitterionic. They disorganize the phospholipid cellular membrane leading to cell lysing. Examples include sodium dodecyl sulfate (SDS), Triton X-100, and sodium deoxycholate. SDS, an ionic detergent, has been widely used in the decellularization process for diverse tissue types, from tissues to whole organ decellularization. SDS has been associated with efficient cellular removal, though loss of ECM components and structure to varying degrees is expected due to the strength of this agent. For additional preservation of the organ structure, perfusion of the surfactant through the native vasculature allows for whole organ decellularization as was first demonstrated with a rat heart. [123] Isolation of a whole decellularized organ initiated an entirely new field of study for recellularization of whole decellularized tissue as a potential alternative source of transplant tissue. Similar methods for SDS perfusion have since been applied for numerous tissues including rabbit bladder [124], liver [125, 126], rat lung [127], rat uterus [124], porcine urethra [128], porcine kidneys [119] and rat spleen [129]. Alternatively, thin or minced tissue under agitation allows for diffusion of SDS throughout.

Triton X-100 is another surfactant that is used for the fabrication of acellular scaffolds. This nonionic agent has been mainly used in combination with other surfactants or enzymes. As an example, for whole organ decellularization, such as rat kidneys, triton X-100 alone led to incomplete cellular removal, and disruption of basement membrane. However, triton combined with SDS resulted in efficient absence of nuclei, preservation of growth factors and underlying vasculature, with a small loss of collagen IV. [130]

Tri(n-butyl) phosphate (TnBP) is an organic solvent that disrupts protein-protein interactions. [131] TnBP has been used in soft tissues, especially in tendon decellularization, due to

high protein content. TnBP alone maintained ECM composition, and mechanical properties of porcine diaphragm tendon. [132] However, TnBP treatment alone can cause a decreased degree of collagen crosslinking, which may affect the long-term biomechanical properties of the tissue. Thus, surfactants can be used in combination with this organic solvent to stabilize it.

Physical methods: Mechanical processes decellularize ECM by eliminating cell-matrix interactions and lysis of cells. These methods include freeze and thawing, sonication by ultrasound, and high hydrostatic pressure. Alternating between freezing (at -80°C or immersion in liquid nitrogen) and thawing (37°C) cycles have been demonstrated to preserve ECM composition and biomechanical properties. [133] However, the freezing and thawing method is often not efficient for all tissue types.

Exposure of tissue to ultrasound at high frequencies can increase the effectiveness of the decellularization process. Sonication alone has been inefficient for cellular removal as demonstrated in human cornea processing. [134] However, in skeletal muscle, combination of this method with enzymes efficiently removed cellular nuclei, retained sulfate glycosaminoglycans, and preserved biomechanical properties similar to native tissue. [135]

Pressures around 1000 MPa with an onset temperature set at 10°C or 30°C have also been applied to tissues as a decellularization method. After the applied pressure porcine corneas were efficiently decellularized, with preservation of glycosaminoglycan content. [120] In another study of porcine aortic blood vessels, the mechanical properties were also similar to native tissue. [136] A further *in vitro* study with endothelial and smooth muscle cells, demonstrated that a pressure of 200 MPa for only 10 minutes, was enough to cause cellular disruption. [137]

1.10.6 ECM-derived hydrogels

After decellularization, the isolated ECM scaffold is lyophilized by uniformly milling the material to form ECM particulate. For some applications, the ECM can be simply mixed with a liquid carrier for injection, such as the use of micronized acellular dermis for soft tissue augmentation.[138] However, to form a self-assembling hydrogel, partial enzymatic digestion is necessary. The most common method, developed by Freytes et al., involves the use of pepsin diluted in hydrochloric acid (HCl).[139] This enzyme cleaves the telopeptide bonds of collagen and the peptide bond on the N-terminal side of hydrophobic amino acids (e.g. phenylalanine and leucine).[140, 141] The digestion consist of 48 hours of stirring at room temperature (25°C). Modifications of this protocol, which may be necessary depending on the tissue source, involve changing the acid strength, digestion period and temperature. Another method developed by Voytik-Harbin et al. uses acetic acid instead of HCl with 70 hours of stirring at 4°C.[142] In general, digestion times of 24-96 hours have been used. The digested ECM is then neutralized to physiologic pH and salt concentrations at 4°C. Incubation of ECM at 37°C or injection *in vivo* will lead to self-assembly and hydrogel formation. The process for the formation of ECM hydrogels is indicated in Figure 1.3.

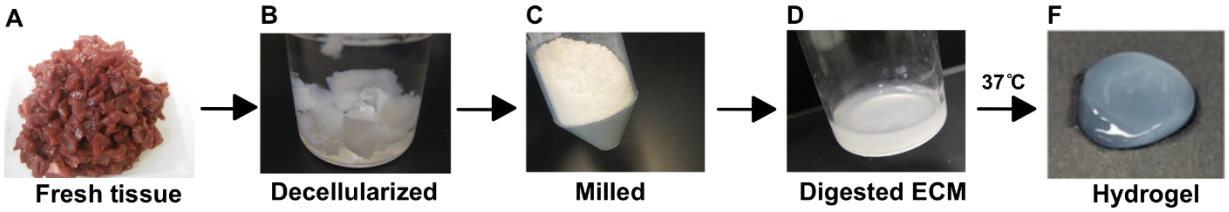

Figure 1.3. Process for decellularized extracellular matrix (ECM) hydrogel formation. Fresh tissue is minced (A), decellularized (B), lyophilized and milled (C), and partially enzymatically digested (D). When temperature is increased to 37°C, the material self-assembles (E) leading to hydrogel formation (F). Reproduced from Ref. 47 with permission from Elsevier, Copyright 2012, 2018.

1.10.6.1 Biochemical composition

The ECM is composed of a range of structural and functional proteins that influence cellular adhesion, survival, and signaling. It is important to characterize the biochemical composition before and after solubilization to ensure retention of ECM components as well as proper digestion conditions. Pre-digestion, liquid chromatography tandem mass spectrometry (LC-MS/MS) can be performed to obtain the protein composition of the decellularized ECM. Global analysis of protein composition can be performed by comparing the fragments to a protein data bank;[143, 144] however, this method is only semi-quantitative. ECM targeted mass spectrometry using stable isotype protein labeled standards is a more quantitative method to determine exact biochemical composition of the decellularized ECM and can also be used to assess effective decellularization.[144]

While structural collagens are the most abundant proteins, many other proteins have been identified in decellularized ECM including basement membrane (e.g. laminin, collagen IV, nidogen) and matricellular proteins (e.g. collagen VI, periostin, fibulin-5), and these abundances are tissue specific.[143, 145-147] Proteoglycans, such as agrin, perlecan, biglycan, decorin, lumican and prolargin have also been identified.[144] Post-digestion, qualitative assessment of protein composition and extent of digestion is usually performed by gel electrophoresis.[148] In addition, quantification of sulfated glycosaminoglycans (sGAGs) is commonly performed by a dimethylmethylene blue assay. Ranges between 2 to 15 μg sGAGs/mg ECM have been reported.[146, 148-150] The concentration of sGAGs can influence the mechanical properties and gelation time. For example, high sGAG concentration in a porcine brain-derived ECM hydrogel led to a lower storage modulus and shorter gelation time compared to a spinal cord-derived hydrogel with a smaller sGAG concentration.[149]

Besides the intact ECM hydrogel composition, the degradation products are also important for the bioactivity of the material. They have been shown to have chemoattractant and mitogenic

properties.[151, 152] For example, small-molecular-weight peptides (5 to 16 kDa), derived from degradation of porcine small intestinal submucosa (SIS) acted as chemoattractants for endothelial cells *in vitro*, and enhanced vascularization *in vivo*.[153] This chemoattractant activity can be modulated by differences in age of ECM as evidenced by the degradation products of human fetal skin ECM having enhanced chemoattract activity compared to an adult source.[154]

1.10.6.2 Physical properties

Assessment of the physical properties of hydrogels is important to determine the feasibility of the material for a particular tissue engineering or regenerative medicine application. While mechanical stiffness regulates cell adhesion, migration, phenotype, and gene expression, adequate fluid properties are crucial for injectable delivery of the material. A viscosity range of 0.01 to 100 Pa·s at 0.1-100 Hz has been reported for the liquid form (pre-gelation) of ECM hydrogels.[139, 148, 155] The liquid form also exhibits shear thinning behavior, which is characterized by a decrease in viscosity under increasing shear strain.[156] This property aids in material injectability, especially for catheter delivery. The viscoelastic properties of hydrogels are typically measured by rheology. Typical ranges of storage moduli for ECM hydrogels are 5 to 800 Pa.[139, 148, 149, 155-157] Studies have shown that increasing the material concentration leads to an increase in the rate of gelation and storage modulus.[156] Moreover, adjusting the salt concentration after the digestion process affects the mechanical properties of the hydrogel. An increase in this parameter led to a decrease in storage moduli.[156] Overall, decellularized ECM hydrogels are very weak hydrogels. While differences in stiffness are known to affect cell differentiation,[105] lower stiffness environment have been associated with increased regeneration.[158, 159]

Aside from viscosity and hydrogel stiffness, gelation kinetics is an important property to ensure retention of the biomaterial at the site of interest. First, in order to confirm appropriate gel

formation after decellularization and enzymatic digestion, a gelation test can be performed. The digested ECM is placed in a vial and incubated for 1 hour or overnight at 37°C. Gelation is evaluated by observing minimal displacement when the vial is turned upside down. However, to provide a detailed characterization of the gelation kinetics, a turbidimetric assay can be performed. This consists of acquiring the absorbance of the ECM hydrogel at specific time points while gelation occurs, which causes an increase in turbidity. Since collagen hydrogels demonstrate a sigmoidal curve, ECM-derived hydrogels also experience this pattern as observed with pancreatic, urinary bladder and dermal hydrogels.[149] However, porcine brain ECM hydrogels demonstrated an exponential shape, which might be due to the abundance of other ECM components (i.e. sGAGs). Porcine umbilical cord ECM hydrogels also demonstrated an exponential shape due to the high presence of sGAGs contained in fetal and newborn tissues.[160] Previous studies have shown that sGAGs can alter the mechanical properties and gelation kinetics of collagen-based hydrogels.[161]

Besides viscoelastic properties, the ultrastructure of ECM hydrogels can influence cellular behavior.[162] Different techniques are used to visualize the ultrastructure of the hydrogel, such as scanning electron microscopy (SEM). SEM is widely used since it enables a three-dimensional visualization of hydrogel morphology. This technique also provides a quantitative assessment of pore size, fiber diameter and alignment, although these can be impacted by differences in sample preparation. The average fiber diameter of various ECM tissue sources has been reported to range from 70 to 100 nm.[155-157, 163] Adjustments to the pH, salt, and material concentration did not modify this parameter with a porcine myocardial ECM hydrogel.[156] For porcine urinary bladder matrix (UBM)-derived hydrogel, material concentration was also independent of fiber diameter or pore size. However, for porcine dermal-derived hydrogels, an increase in the material concentration led to a decrease in fiber diameter and pore size, evident on SEM.[155]

1.10.6.3 Applications

ECM hydrogels have been used for a wide variety of *in vivo* and *in vitro* applications. *In vivo*, they have been applied for numerous tissue engineering and regenerative medicine applications. *In vitro* applications involve the development of 3D constructs for drug screening studies or disease models.

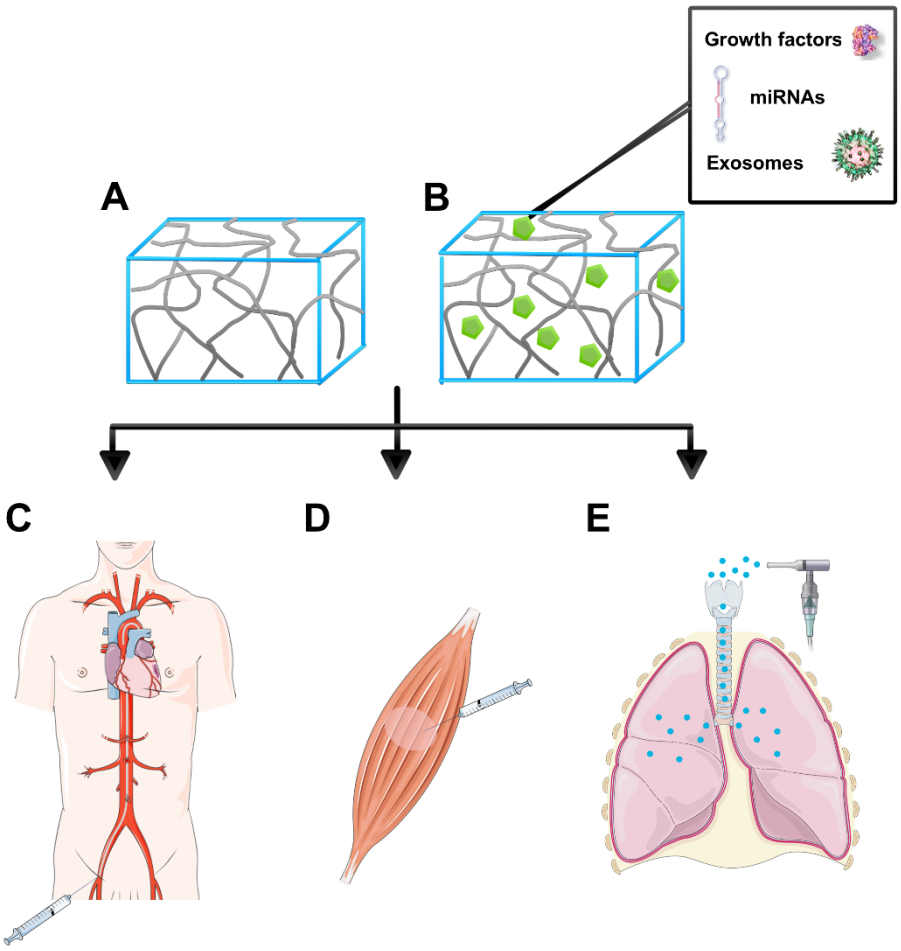

Figure 1.4. *In vivo* applications of decellularized ECM hydrogels.
The materials can be delivered alone (A) or used as delivery vehicles (B) for biomolecules such as growth factors, miRNAs, and exosomes. These biomaterials can be administered by minimally invasive techniques such as catheterization (C), intramuscular injection (D), or nebulization (E).

1.10.6.3.1 In vivo applications

Use of ECM hydrogels for *in vivo* applications (Figure 1.4) has increased over the last decade. Delivery of these biomaterials to prevent or treat a clinical condition is a promising approach to enhance tissue remodeling. Examples of muscle-related conditions that were treated with an ECM hydrogel are described below.

Heart: Tissue engineering approaches could aid in the treatment of myocardial infarction and associated heart failure given the limit regenerative capacity of the heart. A decellularized porcine left ventricular myocardial hydrogel has been investigated in small and large animal models of myocardial infarction and is currently in clinical trials. This myocardial matrix is biocompatible, hemocompatible and non-arrhythmogenic.[164, 165] Initial *in vitro* experiments demonstrated endothelial and smooth muscle cell migration towards the matrix.[166] In an ischemia-reperfusion rat myocardial infarction model, the ECM hydrogel led to increased number of cardiomyocytes in the infarct area with long-term preservation of cardiac function compared to the saline group.[164] Furthermore, a whole transcriptome microarray analysis indicated that the material increased arteriogenesis, immune cell infiltration, and also decreased cardiomyocyte apoptosis and cardiac hypertrophy and fibrosis.[167] Studies have shown that this biomaterial led to the transition of macrophages towards M2 pro-remodeling phenotype.[168] When the myocardial matrix was further tested in a pig model, a larger zone of cardiac muscle was observed at the endocardium together with a reduction in the percentage of collagen content in the infarct compared to the controls.[165] Also, negative left ventricular remodeling was decreased as indicated by reduced left ventricular volumes, and cardiac function was improved three months after injection compared to non-treated and saline controls.[165] A Phase I clinical trial demonstrated safety and feasibility of the myocardial matrix (VentriGel) delivery after myocardial infarction.[169]

Non-tissue specific ECM hydrogels have also been investigated for cardiac tissue engineering.[170-172] Delivery of porcine-derived SIS ECM hydrogel after acute myocardial

infarction, led to improve cardiac function, evidenced from increase in ejection fraction compared to saline group.[172] Histological analysis demonstrated increase in left ventricular wall thickness and arteriole density, together with decrease in infarct size in the hydrogel group.[172] Furthermore, another tissue ECM source was tested in a rat myocardial infarction model. Human placenta-derived hydrogel reduced scar size with normal patterns of electrical activity 8 weeks post-injection compared to saline.[170]

ECM hydrogels have also been used as a delivery vehicle in the heart to increase the stability and activity of different molecules, such as growth factors.[173] Delivery of these molecules alone has limitations due to their rapid diffusion and degradation. Retention of basic fibroblast growth factor in a porcine pericardium ECM hydrogel led to acute neovascularization in a myocardial infarction model, compared to delivery of growth factor in saline or collagen alone.[174] In addition, retention of a hepatocyte growth factor (HGF) fragment in the porcine pericardium ECM hydrogel was assessed also in the rat myocardial infarction model.[175] A significant increase in a measurement of cardiac function was observed in the HGF in ECM hydrogel group compared to HGF or biomaterial alone. Moreover, increase in neovasculature, indicated by higher arteriole density, was observed in HGF in ECM hydrogel. In terms of cross-sectional area of cardiomyocytes, only this group and hydrogel alone were similar to healthy hearts.[175] In addition, a myocardial ECM hydrogel has been tested to enhance the delivery of other biomolecules, such as miRNAs and exosomes, involved in key cellular processes.[176] In the *in vitro* studies, the bioactivity of these biologic products was maintained with the prolonged release from the hydrogel. The combination of these therapeutic molecules with ECM hydrogels is a promising option for *in vivo* applications in cardiovascular diseases.

Skeletal muscle: Non-tissue specific ECM hydrogels have been tested in a muscle defect model as a potential therapy for conditions where muscle is lost with the idea that an injectable material could more easily fill in a void compared to a patch form of ECM. Decellularized porcine

dermis and UBM hydrogels were implanted in a rat model of abdominal wall defect.[155] Dermis hydrogel led to decreased degradation and less cellular infiltration *in vivo* possibly due to smaller pore size compared to UBM.[155] The former resulted in greater muscle regeneration than dermis material, as indicated by fusing myoblasts with centrally located nuclei.

Tissue-specific ECM hydrogels have been tested in skeletal muscle for their potential to treat the ischemic muscle associated with periphery artery disease. In a hindlimb ischemia rat model, injection of a porcine skeletal muscle ECM hydrogel resulted in increased arteriole and endothelial cell density within one week after material injection compared to collagen.[177] Recruitment of proliferating muscle cells were increased in the ECM hydrogel group.[177] Another study was performed to provide insight into the efficacy of tissue-specific hydrogels by comparing porcine skeletal muscle ECM and human umbilical cord ECM hydrogels in a rat hindlimb ischemia model. Perfusion down the foot was improved in both hydrogels 35 days post-injection.[178] At this time point, the arteriole diameter was increased for the skeletal muscle hydrogel group in the gracilis muscle. Differences between both materials were more pronounced when muscle remodeling was evaluated, where fiber cross-sectional area of only the tissue-specific hydrogel group was similar to healthy tissue. A whole transcriptome analysis demonstrated that the skeletal muscle ECM hydrogel led to upregulation of pathways associated with muscle and blood vessel development and cell survival, together with downregulation of cell death and response to hypoxia.[178]

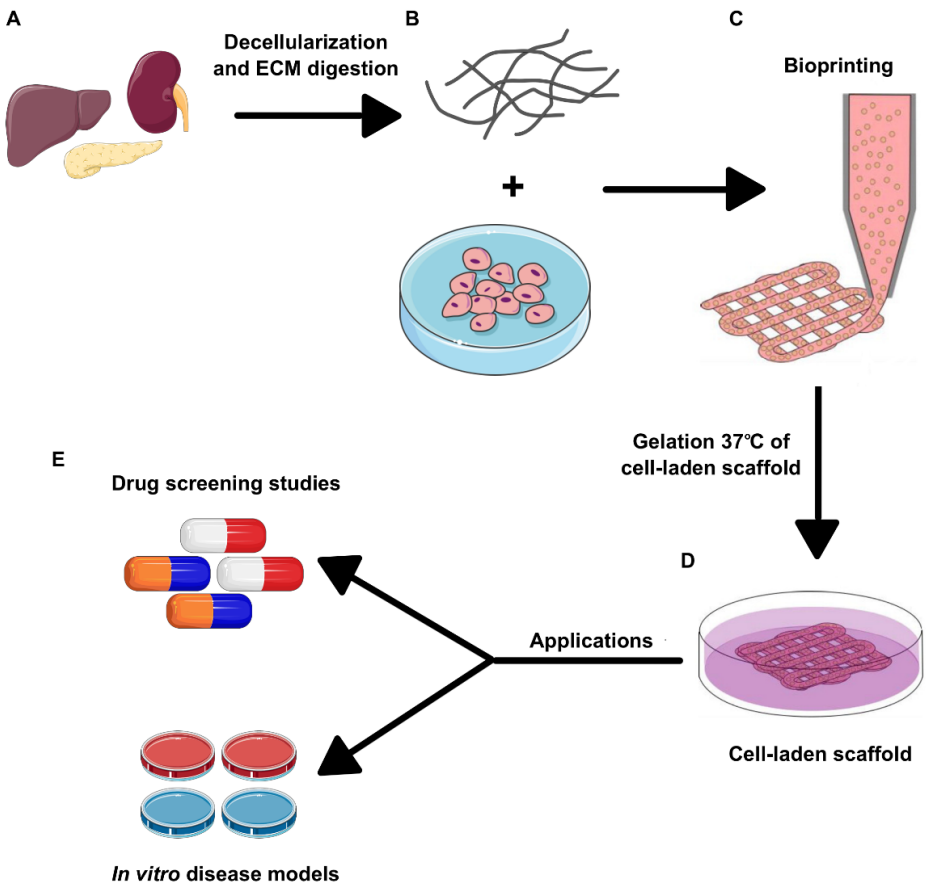

Figure 1.5. *In vitro* applications for ECM hydrogels.
Fresh tissue (A) goes through decellularization and ECM digestion process. Cells are encapsulated in the biomaterial (B) to create a construct by 3D bioprinting (C), which forms a gel at 37°C. The cell-laden scaffold (D) can be used for drug screening studies or in vitro disease models (E).

1.10.6.3.2 In vitro applications

Besides delivery of ECM hydrogels to prevent or treat different clinical conditions, the use of these biomaterials has expanded towards the development of in vitro models to imitate the complex tissue microenvironment. Studies include the development of 3D cultures for organ-on-a-chip or 3D bioprinted constructs that can be used for drug screening, toxicology studies or in vitro disease models (Figure 1.5).

Organ-on-a-chip applications: Recent examples recapitulated the liver or pancreas by using the ECM hydrogels. A 3D encapsulation of primary rat hepatocytes in rat liver ECM hydrogel led to enhanced albumin secretion and urea production compared to collagen I alone.[179] A decellularized porcine pancreas ECM hydrogel was used for 3D encapsulation of rat pancreatic beta cells leading to maintained cell viability and functionality until 10 days in culture.[146] Another study assessed the development of islets on a chip based on three different ECM hydrogels generated from porcine pancreas and bladder.[180] Rat and human islets were encapsulated within the 3D matrix, increasing islet variability and insulin secretion compared to standard culture conditions. Between the different hydrogels analyzed, pancreas ECM hydrogel led to favorable insulin secretion profiles as opposed to bladder ECM—giving insights into the importance of tissue specificity.[180] This study demonstrated that ECM hydrogels provide a 3D supportive microenvironment for *in vitro* culture and can be used for islet-on-a-chip devices.

Bio-printing: Decellularized ECM hydrogels have been used as bioinks for 3D cell printing, providing environmental cues that modulate cellular processes (e.g., migration and differentiation). The shear-thinning behavior of ECM hydrogels allows them to be extruded through a printing nozzle; however, because of their weak mechanical properties, they require another material to provide physical support. Recently, biodegradable polymers have been combined with the ECM material. As an example, porcine skeletal muscle ECM hydrogel was used for the fabrication of functional muscle constructs.[181] The muscle ECM combined with polycaprolactone was compared with collagen alone printed constructs, demonstrating higher cell viability, increased cellular proliferation, and greater expression of transcription factors involved in the muscle regeneration process in the tissue-specific ECM environment. Myotubes in the muscle construct were structurally and functionally mature compared to collagen only with multinucleated and aligned muscle fibers. Moreover, increase in mechanical properties (i.e., ultimate tensile strength and elastic modulus) were higher in muscle ECM construct.[181]

1.10.7 Future of ECM-derived biomaterials

Despite several decellularized tissues are commercially available, there are still challenges involving optimization and variability of the decellularization process. The need for a standard technique is required, especially for scaling-up production for clinical translation. Along with optimizing methods, elevating mechanistic understanding of material properties supporting pro-regenerative cellular responses will aid future improvements in decellularized tissue-based therapies. Despite the needed optimization and mechanistic studies, decellularized ECM hydrogels are a potential option for numerous tissue engineering and regenerative medicine applications. The preservation of ECM composition, together with the bioactivity of the hydrogel degradation products make them suitable to recapitulate the native tissue microenvironment. These biomaterials offer potential for clinical translation due to minimally invasive delivery with one cardiac ECM hydrogel already in clinical trials. With the development of 3D constructs or organ-on-a-chip, disease models or drug testing is also a promising opportunity.

1.11 Thesis outline

This thesis is divided into 4 subsequent chapters.

Chapter 2 investigates the early and delayed responses of PFMs following birth injury using a rat pre-clinical model. We hypothesized that simulated birth injury leads to PFM atrophy and fibrosis associated with an inflammatory response—as observed after excessive mechanical strains in limb skeletal muscles. The chapter shows that the rat model of simulated birth injury replicates the PFM atrophic and fibrotic phenotype observed in women with pelvic organ prolapse. Further investigation through histology and gene expression analyses demonstrates that potential mechanisms behind the identified pathological alterations. Following birth injury, the PFM undergoes a sustained inflammatory response, impairment in muscle anabolism and persistent ECM remodeling.

Chapter 3 continues based on the results of Chapter 2, which provides the rationale for the application of an ECM-based therapy to counteract pathological alterations of PFMs after birth injury. We specifically hypothesized that delivery of skeletal muscle-ECM (SKM) hydrogel prevents and treats PFM atrophy and the associated fibrosis. The chapter investigates the efficacy of SKM either immediately after parturition or at delayed time point, to prevent and mitigate PFM atrophy and fibrosis. Gene expression analyses further showed that the hydrogel modulates the immune response, native ECM remodeling and enhances myogenesis pathway.

Chapter 4 expands on previous chapters by investigating the impact of repeated birth injuries on PFM regeneration and function. Based on repeated limb skeletal muscle injuries, our hypothesis was that repeated SBIs further overwhelm PFM regenerative capacity, leading to more substantial pathological alterations than a single birth injury. The chapter demonstrates that subsequent vaginal distentions lead to muscle dysfunction, impairment in regeneration, and prolonged inflammatory response via ex vivo mechanics, histology, and gene expression analyses, respectively. In addition, the skeletal muscle-ECM hydrogel improved PFM phenotype, as observed after a single injury in Chapter 3.

The final chapter describes a summary of the results of this dissertation and significance of the presented work in women's health research. Finally, the chapter suggests future studies for a deeper understanding of the mechanisms behind birth injury as well as evaluation of ECM hydrogels for the treatment of pelvic skeletal muscles.

1.12 Acknowledgements

Chapter 1, in part, is currently being prepared for submission for publication of the material, Pamela Duran, Karen L. Christman, and Marianna Alperin. "What do we really know about the anatomy and physiology of the pelvic floor muscles?". Other sections are a reprint of the material as it is published in: Raymond Wang, Pamela Duran, and Karen L. Christman. "Processed

Tissues". Biomaterials Science, 4th edition (2020), and Pamela Duran, Marianna Alperin, and Karen L. Christman. "Decellularized Extracellular Matrix Hydrogels: Fabrication, Properties, Characterization, and Current Applications". Decellularized Extracellular Matrix: Characterization, Fabrication and Applications (2019). The dissertation author was the co-first and first author of these papers.

1.13 References

1. Gruss, L.T. and D. Schmitt, The evolution of the human pelvis: changing adaptations to bipedalism, obstetrics and thermoregulation. *Philos Trans R Soc Lond B Biol Sci*. 2015; 370(1663): p. 20140063.

2. Shen, L., Yang, J., Bai, X., Sun, Z., Analysis of the current status of pelvic floor dysfunction in urban women in Xi'an City. *Ann Palliat Med*. 2020; 9(3): p. 979-984.

3. J. M. Wu, C.P.V., P. S. Goode, D. T. Redden, K. L. Burgio, H. E. Richter, A. D. Markland, Prevalence and trends of symptomatic pelvic floor disorders in U.S. women. . *Obstet Gynecol* 2014; 123: p. 141-148.

4. Zeleke, B.M., R.J. Bell, B. Billah, and S.R. Davis, Symptomatic pelvic floor disorders in community-dwelling older Australian women. *Maturitas*. 2016; 85: p. 34-41.

5. Hasuda, T., A. Ueda, and C. Nian Wei, Prevalence of Symptomatic Pelvic Floor Disorders among Japanese Women. *Journal of Womens Health Care*. 2017; 06(04).

6. Blomquist, J.L., M. Carroll, A. Munoz, and V.L. Handa, Pelvic floor muscle strength and the incidence of pelvic floor disorders after vaginal and cesarean delivery. *Am J Obstet Gynecol*. 2020; 222(1): p. 62 e1-62 e8.

7. Hallock, J.L. and V.L. Handa, The Epidemiology of Pelvic Floor Disorders and Childbirth: An Update. *Obstet Gynecol Clin North Am*. 2016; 43(1): p. 1-13.

8. Ashton-Miller, J., DeLancey, J., *Functional anatomy of the female pelvic floor*, in *Evidence-based physical therapy of the pelvic floor*, K. Bo, Berghmans, B., Morkved, S., Van Kampen, M., Editor. 2014, ElSevier: China. p. 19-31.

9. Frölich, B., Hötzinger, H., Fritsch, H., Tomographical Anatomy of the Pelvis, Pelvic Floor, and Related Structures. *Clinical Anatomy*. 1997; 10: p. 223-230.

10. Stoker, J., Wallner, C., *The Anatomy of the Pelvic Floor and Sphincters*, in *Imaging of the Pelvic Floor Disorders*, B. Leuven, Göttingen, K., Editor. 2008, Springer: Berlin. p. 1-30.

11. Chin, H.-Y., C.-W. Peng, M.-P. Wu, C.-H. Chen, Y.-T. Feng, and T.-H. Fong, Attachment of the levator ani muscle extends to the superior ramus of the pubic bone through electrophysiological and anatomical examinations. *Scientific Reports*. 2021; 11(1).

12. Flusberg, M., M. Kobi, S. Bahrami, P. Glanc, S. Palmer, V. Chernyak, D. Kanmaniraja, and R.F. El Sayed, Multimodality imaging of pelvic floor anatomy. *Abdom Radiol (NY)*. 2021; 46(4): p. 1302-1311.

13. Lieber, R.L., Friden, J., Functional and clinical significance of skeletal muscle architecture. *Muscle and nerve*. 2000: p. 1647-1665.

14. Lieber, R.L. and S.R. Ward, Skeletal muscle design to meet functional demands. *Philos Trans R Soc Lond B Biol Sci*. 2011; 366(1570): p. 1466-76.

15. Tuttle, L.J., O.T. Nguyen, M.S. Cook, M. Alperin, S.B. Shah, S.R. Ward, and R.L. Lieber, Architectural design of the pelvic floor is consistent with muscle functional subspecialization. *Int Urogynecol J*. 2014; 25(2): p. 205-12.

16. Stewart, A.M., M.S. Cook, K.Y. Dyer, and M. Alperin, Structure-function relationship of the human external anal sphincter. *Int Urogynecol J*. 2018; 29(5): p. 673-678.

17. Brandao, S., M. Parente, E. Silva, T. Da Roza, T. Mascarenhas, J. Leitao, J. Cunha, R. Natal Jorge, and R.G. Nunes, Pubovisceralis Muscle Fiber Architecture Determination: Comparison Between Biomechanical Modeling and Diffusion Tensor Imaging. *Ann Biomed Eng*. 2017; 45(5): p. 1255-1265.

18. Routzong, M.R., M.S. Cook, W. Barone, S.D. Abramowitch, and M. Alperin, Novel Application of Photogrammetry to Quantify Fascicle Orientations of Female Cadaveric Pelvic Floor Muscles. *Ann Biomed Eng*. 2021; 49(8): p. 1888-1899.

19. d'Aulignac, D., J.A. Martins, E.B. Pires, T. Mascarenhas, and R.M. Jorge, A shell finite element model of the pelvic floor muscles. *Comput Methods Biomech Biomed Engin*. 2005; 8(5): p. 339-47.

20. Noakes, K.F., A.J. Pullan, I.P. Bissett, and L.K. Cheng, Subject specific finite elasticity simulations of the pelvic floor. *J Biomech*. 2008; 41(14): p. 3060-5.

21. Lee, S.L., Horkaew, P., Darzi, A., Yang, G. , Statistical shape modelling of the levator ani with thickness variation. 2004: p. 258-265.

22. Lee, S.L., E. Tan, V. Khullar, W. Gedroyc, A. Darzi, and G.Z. Yang, Physical-based statistical shape modeling of the levator ani. *IEEE Trans Med Imaging*. 2009; 28(6): p. 926-36.

23. Saleme, C.S., M.P. Parente, R.M. Natal Jorge, M. Pinotti, A.L. Silva-Filho, T. Roza, T. Mascarenhas, and J.M. Tavares, An approach on determining the displacements of the pelvic floor during voluntary contraction using numerical simulation and MRI. *Comput Methods Biomech Biomed Engin*. 2011; 14(4): p. 365-70.

24. Brandao, S., T. Da Roza, M. Parente, I. Ramos, T. Mascarenhas, and R.M. Natal Jorge, Magnetic resonance imaging of the pelvic floor: from clinical to biomechanical imaging. *Proc Inst Mech Eng H*. 2013; 227(12): p. 1324-32.

25. Pato, M.P.M. and P. Areias, Active and passive behaviors of soft tissues: Pelvic floor muscles. *International Journal for Numerical Methods in Biomedical Engineering*. 2010: p. n/a-n/a.

26. Peschers, U.M., G.N. Schaer, J.O. DeLancey, and B. Schuessler, Levator ani function before and after childbirth. *Br J Obstet Gynaecol*. 1997; 104(9): p. 1004-8.

27. Sapsford, R.R. and P.W. Hodges, Contraction of the pelvic floor muscles during abdominal maneuvers. *Arch Phys Med Rehabil*. 2001; 82(8): p. 1081-8.

28. Hundley, A.F., J.M. Wu, and A.G. Visco, A comparison of perineometer to brink score for assessment of pelvic floor muscle strength. *Am J Obstet Gynecol*. 2005; 192(5): p. 1583-91.

29. Talasz, H., G. Himmer-Perschak, E. Marth, J. Fischer-Colbrie, E. Hoefner, and M. Lechleitner, Evaluation of pelvic floor muscle function in a random group of adult women in Austria. *Int Urogynecol J Pelvic Floor Dysfunct*. 2008; 19(1): p. 131-5.

30. Braekken, I.H., M. Majida, M. Ellstrom Engh, I.M. Holme, and K. Bo, Pelvic floor function is independently associated with pelvic organ prolapse. *BJOG*. 2009; 116(13): p. 1706-14.

31. Deffieux, X., K. Hubeaux, R. Porcher, S.S. Ismael, P. Raibaut, and G. Amarenco, Abnormal pelvic response to cough in women with stress urinary incontinence. *Neurourol Urodyn*. 2008; 27(4): p. 291-6.

32. South, M.M., S.S. Stinnett, D.B. Sanders, and A.C. Weidner, Levator ani denervation and reinnervation 6 months after childbirth. *Am J Obstet Gynecol*. 2009; 200(5): p. 519 e1-7.

33. Devreese, A., F. Staes, L. Janssens, F. Penninckx, R. Vereecken, and W. De Weerdt, Incontinent women have altered pelvic floor muscle contraction patterns. *J Urol*. 2007; 178(2): p. 558-62.

34. Dumoulin, C., D. Gravel, D. Bourbonnais, M.C. Lemieux, and M. Morin, Reliability of dynamometric measurements of the pelvic floor musculature. *Neurourol Urodyn*. 2004; 23(2): p. 134-42.

35. Egorov, V., V. Lucente, V.A.N.R. H, M. Murphy, S. Ephrain, N. Bhatia, and N. Sarvazyan, Biomechanical mapping of the female pelvic floor: changes with age, parity and weight. *Pelviperineology*. 2019; 38(1): p. 3-11.

36. Kruger, J.A., H.P. Dietz, and B.A. Murphy, Pelvic floor function in elite nulliparous athletes. *Ultrasound Obstet Gynecol*. 2007; 30(1): p. 81-5.

37. Peng, Q., R. Jones, K. Shishido, and C.E. Constantinou, Ultrasound evaluation of dynamic responses of female pelvic floor muscles. *Ultrasound Med Biol*. 2007; 33(3): p. 342-52.

38. Hoyte, L., M.S. Damaser, S.K. Warfield, G. Chukkapalli, A. Majumdar, D.J. Choi, A. Trivedi, and P. Krysl, Quantity and distribution of levator ani stretch during simulated vaginal childbirth. *Am J Obstet Gynecol*. 2008; 199(2): p. 198 e1-5.

39. Lien, K., Mooney, B., DeLancey, J., Ashton-Miller, J., Levator ani muscle stretch induced by simulated vaginal birth. *Obstetrics and Gynecology*. 2004; 103(1): p. 31-40.

40. Jing, D., J.A. Ashton-Miller, and J.O. DeLancey, A subject-specific anisotropic visco-hyperelastic finite element model of female pelvic floor stress and strain during the second stage of labor. *J Biomech*. 2012; 45(3): p. 455-60.

41. Brooks, S.V., E. Zerba, and J.A. Faulkner, Injury to muscle fibres after single stretches of passive and maximally stimulated muscles in mice. *J Physiol*. 1995; 488 (Pt 2): p. 459-69.

42. Silva, M.E., D.A. Oliveira, T.H. Roza, S. Brandao, M.P. Parente, T. Mascarenhas, and R.M. Natal Jorge, Study on the influence of the fetus head molding on the biomechanical behavior of the pelvic floor muscles, during vaginal delivery. *J Biomech*. 2015; 48(9): p. 1600-5.

43. Sindhwani, N., C. Bamberg, N. Famaey, G. Callewaert, J.W. Dudenhausen, U. Teichgraber, and J. Deprest, In vivo evidence of significant levator ani muscle stretch on MR images of a live childbirth. *Am J Obstet Gynecol*. 2017; 217(2): p. 194 e1-194 e8.

44. Oliveira, D.A., M.P. Parente, B. Calvo, T. Mascarenhas, and R.M. Natal Jorge, Numerical simulation of the damage evolution in the pelvic floor muscles during childbirth. *J Biomech*. 2016; 49(4): p. 594-601.

45. Routzong, M.R., G. Rostaminia, P.A. Moalli, and S.D. Abramowitch, Pelvic floor shape variations during pregnancy and after vaginal delivery. *Comput Methods Programs Biomed*. 2020; 194: p. 105516.

46. Peschers, U., Schaer, G., DeLancey, J., Schuessler., Levator ani function before and after childbirth. *British Journal of Obstetrics and Gynecology*. 1997: p. 1004-1008.

47. Elenskaia, K., Thakar, R., Sultan, A., Scheer, I., Beggs, A., The effect of pregnancy and childbirth on pelvic floor muscle function. *Int Urogynecol J*. 2011; 22: p. 1421-1427.

48. Van Geelen, H., D. Ostergard, and P. Sand, A review of the impact of pregnancy and childbirth on pelvic floor function as assessed by objective measurement techniques. *Int Urogynecol J*. 2018; 29(3): p. 327-338.

49. Davidson, M.J., P.M.F. Nielsen, A.J. Taberner, and J.A. Kruger, Change in levator ani muscle stiffness and active force during pregnancy and post-partum. *Int Urogynecol J*. 2020; 31(11): p. 2345-2351.

50. DeLancey, J.O., R. Kearney, Q. Chou, S. Speights, and S. Binno, The appearance of levator ani muscle abnormalities in magnetic resonance images after vaginal delivery. *Obstet Gynecol*. 2003; 101(1): p. 46-53.

51. Araujo, C.C., S.S.A. Coelho, N. Martinho, M. Tanaka, R.M. Jales, and C.R.T. Juliato, Clinical and ultrasonographic evaluation of the pelvic floor in primiparous women: a cross-sectional study. *Int Urogynecol J*. 2018; 29(10): p. 1543-1549.

52. Cassado, J., M. Simo, N. Rodriguez, O. Porta, E. Huguet, I. Mora, M. Girvent, R. Fernandez, and I. Gich, Prevalence of levator ani avulsion in a multicenter study (PAMELA study). *Arch Gynecol Obstet*. 2020; 302(1): p. 273-280.

53. Chan, S.S., R.Y. Cheung, K.W. Yiu, L.L. Lee, and T.K. Chung, Effect of levator ani muscle injury on primiparous women during the first year after childbirth. *Int Urogynecol J*. 2014; 25(10): p. 1381-8.

54. Grob, A.T., M.I. Withagen, M.K. van de Waarsenburg, K.J. Schweitzer, and C.H. van der Vaart, Changes in the mean echogenicity and area of the puborectalis muscle during pregnancy and postpartum. *Int Urogynecol J*. 2016; 27(6): p. 895-901.

55. Nishibayashi, M. and R. Okagaki, Ultrasonographic evaluation of pelvic floor structure at antepartum and postpartum periods using three-dimensional transperineal ultrasound. *J Med Ultrason (2001)*. 2021; 48(3): p. 345-351.

56. Chan, S.S.C., R.Y.K. Cheung, L.L. Lee, R.K.W. Choy, and T.K.H. Chung, Longitudinal follow-up of levator ani muscle avulsion: does a second delivery affect it? *Ultrasound Obstet Gynecol*. 2017; 50(1): p. 110-115.

57. Garcia-Mejido, J.A. and J.A. Sainz, Type of levator ani muscle avulsion as predictor for the disappearance of avulsion. *Neurourol Urodyn*. 2020; 39(8): p. 2293-2300.

58. Da Silva, A.S., G.A. Digesu, C. Dell'Utri, H. Fritsch, P. Piffarotti, and V. Khullar, Do ultrasound findings of levator ani "avulsion" correlate with anatomical findings: A multicenter cadaveric study. *Neurourol Urodyn*. 2016; 35(6): p. 683-8.

59. Wallace, S.L., L.D. Miller, and K. Mishra, Pelvic floor physical therapy in the treatment of pelvic floor dysfunction in women. *Curr Opin Obstet Gynecol*. 2019; 31(6): p. 485-493.

60. Dumoulin, C., L.P. Cacciari, and E.J.C. Hay-Smith, Pelvic floor muscle training versus no treatment, or inactive control treatments, for urinary incontinence in women. *Cochrane Database Syst Rev*. 2018; 10: p. CD005654.

61. Gormley, E.A., Evaluation and management of the patient with a failed midurethral synthetic sling. *Can Urol Assoc J*. 2012; 6(5 Suppl 2): p. S123-4.

62. George, A.T., K. Kalmar, A. Panarese, T.C. Dudding, R.J. Nicholls, and C.J. Vaizey, Long-term outcomes of sacral nerve stimulation for fecal incontinence. *Dis Colon Rectum*. 2012; 55(3): p. 302-6.

63. Sandall, J., R.M. Tribe, L. Avery, G. Mola, G.H. Visser, C.S. Homer, D. Gibbons, N.M. Kelly, H.P. Kennedy, H. Kidanto, P. Taylor, and M. Temmerman, Short-term and long-term effects of caesarean section on the health of women and children. *Lancet*. 2018; 392(10155): p. 1349-1357.

64. Tidball, J.G., Regulation of muscle growth and regeneration by the immune system. *Nat Rev Immunol*. 2017; 17(3): p. 165-178.

65. Kwee, B.J. and D.J. Mooney, Biomaterials for skeletal muscle tissue engineering. *Curr Opin Biotechnol*. 2017; 47: p. 16-22.

66. Dumont, N.A., C.F. Bentzinger, M.C. Sincennes, and M.A. Rudnicki, Satellite Cells and Skeletal Muscle Regeneration. *Compr Physiol*. 2015; 5(3): p. 1027-59.

67. Ciciliot, S. and S. Schiaffino, Regeneration of mammalian skeletal muscle. Basic mechanisms and clinical implications. *Curr Pharm Des*. 2010; 16(8): p. 906-14.

68. Tidball, J.G. and S.A. Villalta, Regulatory interactions between muscle and the immune system during muscle regeneration. *Am J Physiol Regul Integr Comp Physiol*. 2010; 298(5): p. R1173-87.

69. Burzyn, D., W. Kuswanto, D. Kolodin, J.L. Shadrach, M. Cerletti, Y. Jang, E. Sefik, T.G. Tan, A.J. Wagers, C. Benoist, and D. Mathis, A special population of regulatory T cells potentiates muscle repair. *Cell*. 2013; 155(6): p. 1282-95.

70. Biferali, B., D. Proietti, C. Mozzetta, and L. Madaro, Fibro-Adipogenic Progenitors Cross-Talk in Skeletal Muscle: The Social Network. *Front Physiol*. 2019; 10: p. 1074.

71. Mann, C.J., E. Perdiguero, Y. Kharraz, S. Aguilar, P. Pessina, A.L. Serrano, and P. Munoz-Canoves, Aberrant repair and fibrosis development in skeletal muscle. *Skelet Muscle*. 2011; 1(1): p. 21.

72. Montarras, D., J. Morgan, C. Collins, F. Relaix, S. Zaffran, A. Cumano, T. Partridge, and M. Buckingham, Direct isolation of satellite cells for skeletal muscle regeneration. *Science*. 2005; 309(5743): p. 2064-7.

73. Pittenger, M.F., A.M. Mackay, S.C. Beck, R.K. Jaiswal, R. Douglas, J.D. Mosca, M.A. Moorman, D.W. Simonetti, S. Craig, and D.R. Marshak, Multilineage potential of adult human mesenchymal stem cells. *Science*. 1999; 284(5411): p. 143-7.

74. Shadrach, J.L. and A.J. Wagers, Stem cells for skeletal muscle repair. *Philos. Trans. R. Soc. Lond. B Biol. Sci.* 2011; 366(1575): p. 2297-306.

75. Lin, G., G. Wang, L. Banie, H. Ning, A.W. Shindel, T.M. Fandel, T.F. Lue, and C.S. Lin, Treatment of stress urinary incontinence with adipose tissue-derived stem cells. *Cytotherapy*. 2010; 12(1): p. 88-95.

76. Corcos, J., O. Loutochin, L. Campeau, N. Eliopoulos, M. Bouchentouf, B. Blok, and J. Galipeau, Bone marrow mesenchymal stromal cell therapy for external urethral sphincter restoration in a rat model of stress urinary incontinence. *Neurourol Urodyn*. 2011; 30(3): p. 447-55.

77. Salcedo, L., M. Penn, M. Damaser, B. Balog, and M. Zutshi, Functional outcome after anal sphincter injury and treatment with mesenchymal stem cells. *Stem Cells Transl Med*. 2014; 3(6): p. 760-7.

78. Cannon, T., Lee, J., Somogyi, G., Pruchnic, R., Smith, C., Huard, J., Chancellor, M., Improved sphincter contractility after allogenic muscle-derived progenitor cell injection into the denervated rat urethra. *Urology*. 2003; 62(5): p. 958-963.

79. Frudinger, A., R. Marksteiner, J. Pfeifer, E. Margreiter, J. Paede, and M. Thurner, Skeletal muscle-derived cell implantation for the treatment of sphincter-related faecal incontinence. *Stem Cell Res Ther*. 2018; 9(1): p. 233.

80. Lee, C.N., J.B. Jang, J.Y. Kim, C. Koh, J.Y. Baek, and K.J. Lee, Human cord blood stem cell therapy for treatment of stress urinary incontinence. *J Korean Med Sci*. 2010; 25(6): p. 813-6.

81. Kuismanen, K., R. Sartoneva, S. Haimi, B. Mannerstrom, E. Tomas, S. Miettinen, and K. Nieminen, Autologous adipose stem cells in treatment of female stress urinary incontinence: results of a pilot study. *Stem Cells Transl Med*. 2014; 3(8): p. 936-41.

82. Sharifiaghdas, F., F. Tajalli, M. Taheri, M. Naji, R. Moghadasali, N. Aghdami, H. Baharvand, V. Azimian, and N. Jaroughi, Effect of autologous muscle-derived cells in the treatment of urinary incontinence in female patients with intrinsic sphincter deficiency and epispadias: A prospective study. *Int J Urol*. 2016; 23(7): p. 581-6.

83. Sharifiaghdas, F., Zohrabi, F., Moghadasali, R., Shekarchian, S., Jaroughi, N., Bolurieh, T., Baharvand, H., Aghdami, N., Autologous Muscle-derived Cell Injection for Treatment of Female Stress Urinary Incontinence: A Single- Arm Clinical Trial with 24-months Follow-Up. *Urology*. 2019; 16(5): p. 482-487.

84. de la Portilla, F., J.L. Guerrero, M.V. Maestre, L. Leyva, S. Mera, D. Garcia-Olmo, A. Rodriguez, R. Mata, and F. Lora, Treatment of faecal incontinence with autologous expanded mesenchymal stem cells: results of a pilot study. *Colorectal Dis*. 2021; 23(3): p. 698-709.

85. Reid, G., F. Magarotto, A. Marsano, and M. Pozzobon, Next Stage Approach to Tissue Engineering Skeletal Muscle. *Bioengineering (Basel)*. 2020; 7(4).

86. Song, Y.H., J.L. Song, P. Delafontaine, and M.P. Godard, The therapeutic potential of IGF-I in skeletal muscle repair. *Trends Endocrinol Metab*. 2013; 24(6): p. 310-9.

87. Choi, J.S., H.I. Yoon, K.S. Lee, Y.C. Choi, S.H. Yang, I.S. Kim, and Y.W. Cho, Exosomes from differentiating human skeletal muscle cells trigger myogenesis of stem cells and provide biochemical cues for skeletal muscle regeneration. *J Control Release*. 2016; 222: p. 107-15.

88. Nakamura, Y., S. Miyaki, H. Ishitobi, S. Matsuyama, T. Nakasa, N. Kamei, T. Akimoto, Y. Higashi, and M. Ochi, Mesenchymal-stem-cell-derived exosomes accelerate skeletal muscle regeneration. *FEBS Lett*. 2015; 589(11): p. 1257-65.

89. Yao, X., W. Wei, X. Wang, L. Chenglin, M. Bjorklund, and H. Ouyang, Stem cell derived exosomes: microRNA therapy for age-related musculoskeletal disorders. *Biomaterials*. 2019; 224: p. 119492.

90. Liu, N., A.H. Williams, J.M. Maxeiner, S. Bezprozvannaya, J.M. Shelton, J.A. Richardson, R. Bassel-Duby, and E.N. Olson, microRNA-206 promotes skeletal muscle regeneration and delays progression of Duchenne muscular dystrophy in mice. *J Clin Invest*. 2012; 122(6): p. 2054-65.

91. Sandona, M., L. Di Pietro, F. Esposito, A. Ventura, A.R. Silini, O. Parolini, and V. Saccone, Mesenchymal Stromal Cells and Their Secretome: New Therapeutic Perspectives for Skeletal Muscle Regeneration. *Front Bioeng Biotechnol*. 2021; 9: p. 652970.

92. Dissaranan, C., M.A. Cruz, M.J. Kiedrowski, B.M. Balog, B.C. Gill, M.S. Penn, H.B. Goldman, and M.S. Damaser, Rat mesenchymal stem cell secretome promotes elastogenesis and facilitates recovery from simulated childbirth injury. *Cell Transplant*. 2014; 23(11): p. 1395-406.

93. Deng, K., D.L. Lin, B. Hanzlicek, B. Balog, M.S. Penn, M.J. Kiedrowski, Z. Hu, Z. Ye, H. Zhu, and M.S. Damaser, Mesenchymal stem cells and their secretome partially restore nerve and urethral function in a dual muscle and nerve injury stress urinary incontinence model. *Am J Physiol Renal Physiol*. 2015; 308(2): p. F92-F100.

94. Ni, J., H. Li, Y. Zhou, B. Gu, Y. Xu, Q. Fu, X. Peng, N. Cao, Q. Fu, M. Jin, G. Sun, J. Wang, Y. Jin, and F. Liu, Therapeutic Potential of Human Adipose-Derived Stem Cell Exosomes in Stress Urinary Incontinence - An in Vitro and in Vivo Study. *Cell Physiol Biochem*. 2018; 48(4): p. 1710-1722.

95. Wu, R., C. Huang, Q. Wu, X. Jia, M. Liu, Z. Xue, Y. Qiu, X. Niu, and Y. Wang, Exosomes secreted by urine-derived stem cells improve stress urinary incontinence by promoting repair of pubococcygeus muscle injury in rats. *Stem Cell Res Ther*. 2019; 10(1): p. 80.

96. Qazi, T.H., D.J. Mooney, M. Pumberger, S. Geissler, and G.N. Duda, Biomaterials based strategies for skeletal muscle tissue engineering: existing technologies and future trends. *Biomaterials*. 2015; 53: p. 502-21.

97. Jana, S., S.K. Levengood, and M. Zhang, Anisotropic Materials for Skeletal-Muscle-Tissue Engineering. *Adv Mater*. 2016; 28(48): p. 10588-10612.

98. Quigley, A., C. Ngan, K. Firipis, C.D. O'Connell, E. Pirogova, S.E. Moulton, R.J. Williams, and R.M.I. Kapsa, Towards bioengineered skeletal muscle: recent developments in vitro and in vivo. *Essays Biochem*. 2021; 65(3): p. 555-567.

99. Lam, M.T., S. Sim, X. Zhu, and S. Takayama, The effect of continuous wavy micropatterns on silicone substrates on the alignment of skeletal muscle myoblasts and myotubes. *Biomaterials*. 2006; 27(24): p. 4340-7.

100. Gingras, J., R.M. Rioux, D. Cuvelier, N.A. Geisse, J.W. Lichtman, G.M. Whitesides, L. Mahadevan, and J.R. Sanes, Controlling the orientation and synaptic differentiation of myotubes with micropatterned substrates. *Biophys J*. 2009; 97(10): p. 2771-9.

101. Zhao, Y., H. Zeng, J. Nam, and S. Agarwal, Fabrication of skeletal muscle constructs by topographic activation of cell alignment. *Biotechnol Bioeng*. 2009; 102(2): p. 624-31.

102. Yang, H.S., N. Ieronimakis, J.H. Tsui, H.N. Kim, K.Y. Suh, M. Reyes, and D.H. Kim, Nanopatterned muscle cell patches for enhanced myogenesis and dystrophin expression in a mouse model of muscular dystrophy. *Biomaterials*. 2014; 35(5): p. 1478-86.

103. Narayanan, N., C. Jiang, C. Wang, G. Uzunalli, N. Whittern, D. Chen, O.G. Jones, S. Kuang, and M. Deng, Harnessing Fiber Diameter-Dependent Effects of Myoblasts Toward Biomimetic Scaffold-Based Skeletal Muscle Regeneration. *Front Bioeng Biotechnol*. 2020; 8: p. 203.

104. Kroehne, V., I. Heschel, F. Schugner, D. Lasrich, J.W. Bartsch, and H. Jockusch, Use of a novel collagen matrix with oriented pore structure for muscle cell differentiation in cell culture and in grafts. *J Cell Mol Med*. 2008; 12(5A): p. 1640-8.

105. Engler, A.J., S. Sen, H.L. Sweeney, and D.E. Discher, Matrix elasticity directs stem cell lineage specification. *Cell*. 2006; 126(4): p. 677-89.

106. Chen, M.C., Y.C. Sun, and Y.H. Chen, Electrically conductive nanofibers with highly oriented structures and their potential application in skeletal muscle tissue engineering. *Acta Biomater*. 2013; 9(3): p. 5562-72.

107. Palmieri, V., F. Sciandra, M. Bozzi, M. De Spirito, and M. Papi, 3D Graphene Scaffolds for Skeletal Muscle Regeneration: Future Perspectives. *Front Bioeng Biotechnol*. 2020; 8: p. 383.

108. Zhu, P., Y. Zhou, F. Wu, Y. Hong, X. Wang, G. Shekhawat, J. Mosenson, and W.S. Wu, Selective Expansion of Skeletal Muscle Stem Cells from Bulk Muscle Cells in Soft Three-Dimensional Fibrin Gel. *Stem Cells Transl Med*. 2017; 6(5): p. 1412-1423.

109. Liu, X., Y. Gao, X. Long, T. Hayashi, K. Mizuno, S. Hattori, H. Fujisaki, T. Ogura, D.O. Wang, and T. Ikejima, Type I collagen promotes the migration and myogenic differentiation of C2C12 myoblasts via the release of interleukin-6 mediated by FAK/NF-kappaB p65 activation. *Food Funct*. 2020; 11(1): p. 328-338.

110. Leng, Y., A. Abdullah, M.K. Wendt, and S. Calve, Hyaluronic acid, CD44 and RHAMM regulate myoblast behavior during embryogenesis. *Matrix Biol*. 2019; 78-79: p. 236-254.

111. Wu, X., Y. Jia, X. Sun, and J. Wang, Tissue engineering in female pelvic floor reconstruction. *Eng Life Sci*. 2020; 20(7): p. 275-286.

112. Mironska, E., C. Chapple, and S. MacNeil, Recent advances in pelvic floor repair. *F1000Res*. 2019; 8.

113. Mantha, S., S. Pillai, P. Khayambashi, A. Upadhyay, Y. Zhang, O. Tao, H.M. Pham, and S.D. Tran, Smart Hydrogels in Tissue Engineering and Regenerative Medicine. *Materials (Basel)*. 2019; 12(20).

114. Kim, M.H., H.N. Hong, J.P. Hong, C.J. Park, S.W. Kwon, S.H. Kim, G. Kang, and M. Kim, The effect of VEGF on the myogenic differentiation of adipose tissue derived stem cells within thermosensitive hydrogel matrices. *Biomaterials*. 2010; 31(6): p. 1213-8.

115. Borselli, C., H. Storrie, F. Benesch-Lee, D. Shvartsman, C. Cezar, J.W. Lichtman, H.H. Vandenburgh, and D.J. Mooney, Functional muscle regeneration with combined delivery of angiogenesis and myogenesis factors. *Proc. Natl. Acad. Sci. U. S. A.* 2010; 107(8): p. 3287-92.

116. Liu, J., H.H. Xu, H. Zhou, M.D. Weir, Q. Chen, and C.A. Trotman, Human umbilical cord stem cell encapsulation in novel macroporous and injectable fibrin for muscle tissue engineering. *Acta Biomater*. 2013; 9(1): p. 4688-97.

117. Okano, T. and T. Matsuda, Muscular tissue engineering: capillary-incorporated hybrid muscular tissues in vivo tissue culture. *Cell Transplant*. 1998; 7(5): p. 435-42.

118. Rossi, C.A., M. Flaibani, B. Blaauw, M. Pozzobon, E. Figallo, C. Reggiani, L. Vitiello, N. Elvassore, and P. De Coppi, In vivo tissue engineering of functional skeletal muscle by freshly isolated satellite cells embedded in a photopolymerizable hydrogel. *FASEB J*. 2011; 25(7): p. 2296-304.

119. Hussein, K.H., T. Saleh, E. Ahmed, H.H. Kwak, K.M. Park, S.R. Yang, B.J. Kang, K.Y. Choi, K.S. Kang, and H.M. Woo, Biocompatibility and hemocompatibility of efficiently decellularized whole porcine kidney for tissue engineering. *J Biomed Mater Res A*. 2018; 106(7): p. 2034-2047.

120. Sasaki, S., Funamoto, S., Hashimoto, Y., Kimura, T., Honda, T., Hattori, S., Kobayashi, H., Kishida, A., Mochizuki, In vivo evaluation of a novel scaffold for artificial corneas prepared by using ultrahigh hydrostatic pressure to decellularize porcine corneas. *Molecular Vision*. 2009; 15: p. 2022-2028.

121. Crapo, P.M., T.W. Gilbert, and S.F. Badylak, An overview of tissue and whole organ decellularization processes. *Biomaterials*. 2011; 32(12): p. 3233-43.

122. Keane, T.J., I.T. Swinehart, and S.F. Badylak, Methods of tissue decellularization used for preparation of biologic scaffolds and in vivo relevance. *Methods*. 2015; 84: p. 25-34.

123. Ott, H.C., T.S. Matthiesen, S.K. Goh, L.D. Black, S.M. Kren, T.I. Netoff, and D.A. Taylor, Perfusion-decellularized matrix: using nature's platform to engineer a bioartificial heart. *Nat Med*. 2008; 14(2): p. 213-21.

124. Miyazaki, K. and T. Maruyama, Partial regeneration and reconstruction of the rat uterus through recellularization of a decellularized uterine matrix. *Biomaterials*. 2014; 35(31): p. 8791-8800.

125. Shupe, T., M. Williams, A. Brown, B. Willenberg, and B.E. Petersen, Method for the decellularization of intact rat liver. *Organogenesis*. 2010; 6(2): p. 134-6.

126. Baptista, P.M., M.M. Siddiqui, G. Lozier, S.R. Rodriguez, A. Atala, and S. Soker, The use of whole organ decellularization for the generation of a vascularized liver organoid. *Hepatology*. 2011; 53(2): p. 604-17.

127. Petersen, T.H., E.A. Calle, L. Zhao, E.J. Lee, L. Gui, M.B. Raredon, K. Gavrilov, T. Yi, Z.W. Zhuang, C. Breuer, E. Herzog, and L.E. Niklason, Tissue-engineered lungs for in vivo implantation. *Science*. 2010; 329(5991): p. 538-41.

128. Simoes, I.N., P. Vale, S. Soker, A. Atala, D. Keller, R. Noiva, S. Carvalho, C. Peleteiro, J.M. Cabral, D. Eberli, C.L. da Silva, and P.M. Baptista, Acellular Urethra Bioscaffold: Decellularization of Whole Urethras for Tissue Engineering Applications. *Sci Rep*. 2017; 7: p. 41934.

129. Zheng, X.L., J.X. Xiang, W.Q. Wu, B. Wang, W.Y. Liu, R. Gao, D.H. Dong, and Y. Lv, Using a decellularized splenic matrix as a 3D scaffold for hepatocyte cultivation in vitro: a preliminary trial. *Biomed Mater*. 2015; 10(4): p. 045023.

130. Caralt, M., J.S. Uzarski, S. Iacob, K.P. Obergfell, N. Berg, B.M. Bijonowski, K.M. Kiefer, H.H. Ward, A. Wandinger-Ness, W.M. Miller, Z.J. Zhang, M.M. Abecassis, and J.A. Wertheim, Optimization and critical evaluation of decellularization strategies to develop renal extracellular matrix scaffolds as biological templates for organ engineering and transplantation. *Am J Transplant*. 2015; 15(1): p. 64-75.

131. Keane, T.J., L.T. Saldin, and S.F. Badylak, *Decellularization of mammalian tissues*, in *Characterisation and Design of Tissue Scaffolds*. 2016. p. 75-103.

132. Deeken, C.R., A.K. White, S.L. Bachman, B.J. Ramshaw, D.S. Cleveland, T.S. Loy, and S.A. Grant, Method of preparing a decellularized porcine tendon using tributyl phosphate. *J Biomed Mater Res B Appl Biomater*. 2011; 96(2): p. 199-206.

133. Ning, L.J., Y.L. Jiang, C.H. Zhang, Y. Zhang, J.L. Yang, J. Cui, Y.J. Zhang, X. Yao, J.C. Luo, and T.W. Qin, Fabrication and characterization of a decellularized bovine tendon sheet for tendon reconstruction. *J Biomed Mater Res A*. 2017; 105(8): p. 2299-2311.

134. He, Z., Forest, F., Bernard, A., Gauthier, A., Montard, R., Peoc'h, M., Jumelle, C., Courrier, E., Perrache, C., Gain, P., Thuret, G., Cutting and Decellularization of Multiple Corneal Stromal Lamellae for the Bioengineering of Endothelial Grafts. *Investigative Opthalmology and Visual Science*. 2016; 57(15).

135. Lin, C.H., J.R. Yang, N.J. Chiang, H. Ma, and R.Y. Tsay, Evaluation of decellularized extracellular matrix of skeletal muscle for tissue engineering. *Int J Artif Organs*. 2014; 37(7): p. 546-55.

136. Funamoto, S., K. Nam, T. Kimura, A. Murakoshi, Y. Hashimoto, K. Niwaya, S. Kitamura, T. Fujisato, and A. Kishida, The use of high-hydrostatic pressure treatment to decellularize blood vessels. *Biomaterials*. 2010; 31(13): p. 3590-5.

137. Mahara, A., N. Morimoto, T. Sakuma, T. Fujisato, and T. Yamaoka, Complete cell killing by applying high hydrostatic pressure for acellular vascular graft preparation. *Biomed Res Int*. 2014; 2014: p. 379607.

138. Sclafani, A., Romo, T., Jacono, A., McCormick, S., Cocker, R., Parker, A., Evaluation of Acellular Dermal Graft in Sheet (AlloDerm) and Injectable (Micronized AlloDerm) Forms for Soft Tissue Augmentation. . *Arch Facial Plast Surg*. 2000; 2: p. 130-136.

139. Freytes, D.O., J. Martin, S.S. Velankar, A.S. Lee, and S.F. Badylak, Preparation and rheological characterization of a gel form of the porcine urinary bladder matrix. *Biomaterials*. 2008; 29(11): p. 1630-7.

140. DJS., H., *Collagen Diversity, Synthesis, and Assembly.* . 2008: Springer.
141. López-Ferrer, D., Petritis, K., Robinson, E., Hixson, K., Tian, Z., Lee, J., Lee, S., Tolić, N., Weitz, K., Belov, M., Smith, R., Paša-Tolić, L., Pressurized Pepsin Digestion in Proteomics. *Molecular and Cellular Proteomics*. 2011; 10(2).
142. Voytik-Harbin, S., Brightman, A., Waisnet, B., Robinson, J., Lamar, C., Small Intestinal Submucosa: A Tissue-Derived Extracellular Matrix That Promotes Tissue-Specific Growth and Differentiation of Cells in Vitro. *Tissue Engineering*. 1998; 4(2): p. 157-174.

143. Johnson, T.D., R.C. Hill, M. Dzieciatkowska, V. Nigam, A. Behfar, K.L. Christman, and K.C. Hansen, Quantification of decellularized human myocardial matrix: A comparison of six patients. *PROTEOMICS - Clinical Applications*. 2016; 10(1): p. 75-83.

144. Hill, R.C., Calle, E., Dzieciatkowska, M., Niklason, L., Hansen, K., Quantification of Extracellular Matrix Proteins from a Rat Lung Scaffold to Provide a Molecular Readout for Tissue Engineering. *Molecular and Cellular Proteomics*. 2015; 14: p. 961-973.

145. Goddard, E.T., R.C. Hill, A. Barrett, C. Betts, Q. Guo, O. Maller, V.F. Borges, K.C. Hansen, and P. Schedin, Quantitative extracellular matrix proteomics to study mammary and liver tissue microenvironments. *Int J Biochem Cell Biol*. 2016; 81(Pt A): p. 223-232.

146. Gaetani, R., S. Aouad, L.L. Demaddalena, H. Straessle, M. Dzieciatkowska, M. Wortham, H.R. Bender, K.V. Nguyen-Ngoc, G.W. Schmid-Schoenbein, S.C. George, C.C.W. Hughes, M. Sander, K.C. Hansen, and K.L. Christman, Evaluation of different decellularization protocols on the generation of pancreas-derived hydrogels. *Tissue Eng Part C Methods*. 2018.

147. Calle, E.A., R.C. Hill, K.L. Leiby, A.V. Le, A.L. Gard, J.A. Madri, K.C. Hansen, and L.E. Niklason, Targeted proteomics effectively quantifies differences between native lung and detergent-decellularized lung extracellular matrices. *Acta Biomater*. 2016; 46: p. 91-100.

148. Ungerleider, J.L., T.D. Johnson, N. Rao, and K.L. Christman, Fabrication and characterization of injectable hydrogels derived from decellularized skeletal and cardiac muscle. *Methods*. 2015; 84: p. 53-59.

149. Medberry, C.J., P.M. Crapo, B.F. Siu, C.A. Carruthers, M.T. Wolf, S.P. Nagarkar, V. Agrawal, K.E. Jones, J. Kelly, S.A. Johnson, S.S. Velankar, S.C. Watkins, M. Modo, and S.F. Badylak, Hydrogels derived from central nervous system extracellular matrix. *Biomaterials*. 2013; 34(4): p. 1033-40.

150. Johnson, T.D., J.A. Dequach, R. Gaetani, J. Ungerleider, D. Elhag, V. Nigam, A. Behfar, and K.L. Christman, Human versus porcine tissue sourcing for an injectable myocardial matrix hydrogel. *Biomater Sci*. 2014; 2014: p. 60283D.

151. Reing, J.E.Z., L., Myers-Irvin, J., Corder, K., Freytes, D., Heber-Katz, E., Bedelbaeva, K., McIntosh, D., Dewilde, A., Braunhut, S., Badylak, S., Degradation Products of

Extracellular Matrix Affect Cell Migration and Proliferation. . *Tissue Eng Part A*. 2009; 15: p. 605-613.

152. Beattie, A., Gilbert, T., Guyot, J.P., Yates, A., Badylak, S., Chemoattraction of Progenitor Cells by Remodeling Extracellular Matrix Scaffolds. *Tissue Eng Part A*. 2009; 15(5).

153. Li, F., W. Li, S. Johnson, D. Ingram, M. Yoder, and S. Badylak, Low-molecular-weight peptides derived from extracellular matrix as chemoattractants for primary endothelial cells. *Endothelium*. 2004; 11(3-4): p. 199-206.

154. Brennan, E.P., X.H. Tang, A.M. Stewart-Akers, L.J. Gudas, and S.F. Badylak, Chemoattractant activity of degradation products of fetal and adult skin extracellular matrix for keratinocyte progenitor cells. *J Tissue Eng Regen Med*. 2008; 2(8): p. 491-8.

155. Wolf, M.T., K.A. Daly, E.P. Brennan-Pierce, S.A. Johnson, C.A. Carruthers, A. D'Amore, S.P. Nagarkar, S.S. Velankar, and S.F. Badylak, A hydrogel derived from decellularized dermal extracellular matrix. *Biomaterials*. 2012; 33(29): p. 7028-38.

156. Johnson, T.D., S.Y. Lin, and K.L. Christman, Tailoring material properties of a nanofibrous extracellular matrix derived hydrogel. *Nanotechnology*. 2011; 22(49): p. 494015.

157. Pouliot, R.A., P.A. Link, N.S. Mikhaiel, M.B. Schneck, M.S. Valentine, F.J. Kamga Gninzeko, J.A. Herbert, M. Sakagami, and R.L. Heise, Development and characterization of a naturally derived lung extracellular matrix hydrogel. *J Biomed Mater Res A*. 2016; 104(8): p. 1922-35.

158. Williamson, A., Cheng, A., Sah, R., Compressive properties and function-composition relationship of developing bovine articular cartilage. *Journal of Orthipaedic Research*. 2001: p. 1113-1121.

159. Notari, M., Ventura-Rubio, A., Bedford-Guaus, S., Jorba, I., Mulero, L., Navajas, D., Martí, M., Raya, A., The local microenvironment limits the regenerative potential of the mouse neonatal heart. *Science Advances*. 2018; 4(5): p. 1-12.

160. Koci, Z., K. Vyborny, J. Dubisova, I. Vackova, A. Jager, O. Lunov, K. Jirakova, and S. Kubinova, Extracellular Matrix Hydrogel Derived from Human Umbilical Cord as a Scaffold for Neural Tissue Repair and Its Comparison with Extracellular Matrix from Porcine Tissues. *Tissue Eng Part C Methods*. 2017; 23(6): p. 333-345.

161. Stuart, K. and A. Panitch, Influence of chondroitin sulfate on collagen gel structure and mechanical properties at physiologically relevant levels. *Biopolymers*. 2008; 89(10): p. 841-51.

162. S, U., E, Labay., M, Francis-Sedlak., M, Moya., R, Weichselbaum, N., Ervin, Z, Cankova., Extraction and Assembly of Tissue-Derived Gels for Cell Culture and Tissue Engineering. *Tissue Eng Part C Methods*. 2009; 15(3): p. 309-321.

163. Young, D.A., D.O. Ibrahim, D. Hu, and K.L. Christman, Injectable hydrogel scaffold from decellularized human lipoaspirate. *Acta Biomater*. 2011; 7(3): p. 1040-9.

164. Singelyn, J.M., P. Sundaramurthy, T.D. Johnson, P.J. Schup-Magoffin, D.P. Hu, D.M. Faulk, J. Wang, K.M. Mayle, K. Bartels, M. Salvatore, A.M. Kinsey, A.N. Demaria, N. Dib, and K.L. Christman, Catheter-deliverable hydrogel derived from decellularized ventricular extracellular matrix increases endogenous cardiomyocytes and preserves cardiac function post-myocardial infarction. *J Am Coll Cardiol*. 2012; 59(8): p. 751-63.

165. Seif-Naraghi, S.B., J.M. Singelyn, M.A. Salvatore, K.G. Osborn, J.J. Wang, U. Sampat, O.L. Kwan, G.M. Strachan, J. Wong, P.J. Schup-Magoffin, R.L. Braden, K. Bartels, J.A. DeQuach, M. Preul, A.M. Kinsey, A.N. DeMaria, N. Dib, and K.L. Christman, Safety and efficacy of an injectable extracellular matrix hydrogel for treating myocardial infarction. *Sci Transl Med*. 2013; 5(173): p. 173ra25.

166. Singelyn, J.M., J.A. DeQuach, S.B. Seif-Naraghi, R.B. Littlefield, P.J. Schup-Magoffin, and K.L. Christman, Naturally derived myocardial matrix as an injectable scaffold for cardiac tissue engineering. *Biomaterials*. 2009; 30(29): p. 5409-16.

167. Wassenaar, J.W., R. Gaetani, J.J. Garcia, R.L. Braden, C.G. Luo, D. Huang, A.N. DeMaria, J.H. Omens, and K.L. Christman, Evidence for Mechanisms Underlying the Functional Benefits of a Myocardial Matrix Hydrogel for Post-MI Treatment. *J Am Coll Cardiol*. 2016; 67(9): p. 1074-86.

168. Wang, R.M., T.D. Johnson, J. He, Z. Rong, M. Wong, V. Nigam, A. Behfar, Y. Xu, and K.L. Christman, Humanized mouse model for assessing the human immune response to xenogeneic and allogeneic decellularized biomaterials. *Biomaterials*. 2017; 129: p. 98-110.

169. Traverse, J.H., T.D. Henry, N. Dib, A.N. Patel, C. Pepine, G.L. Schaer, J.A. DeQuach, A.M. Kinsey, P. Chamberlin, and K.L. Christman, First-in-Man Study of a Cardiac Extracellular Matrix Hydrogel in Early and Late Myocardial Infarction Patients. *JACC Basic Transl Sci*. 2019; 4(6): p. 659-669.

170. Francis, M.P., E. Breathwaite, A.A. Bulysheva, F. Varghese, R.U. Rodriguez, S. Dutta, I. Semenov, R. Ogle, A. Huber, A.M. Tichy, S. Chen, and C. Zemlin, Human placenta hydrogel reduces scarring in a rat model of cardiac ischemia and enhances cardiomyocyte and stem cell cultures. *Acta Biomater*. 2017; 52: p. 92-104.

171. Okada, M., T.R. Payne, H. Oshima, N. Momoi, K. Tobita, and J. Huard, Differential efficacy of gels derived from small intestinal submucosa as an injectable biomaterial for myocardial infarct repair. *Biomaterials*. 2010; 31(30): p. 7678-83.

172. Toeg, H.D., R. Tiwari-Pandey, R. Seymour, A. Ahmadi, S. Crowe, B. Vulesevic, E.J. Suuronen, and M. Ruel, Injectable Small Intestine Submucosal Extracellular Matrix in an Acute Myocardial Infarction Model. *The Annals of Thoracic Surgery*. 2013; 96(5): p. 1686-1694.

173. Zisch, A.H., M.P. Lutolf, and J.A. Hubbell, Biopolymeric delivery matrices for angiogenic growth factors. *Cardiovascular Pathology*. 2003; 12(6): p. 295-310.

174. Seif-Naraghi, S.B., D. Horn, P.J. Schup-Magoffin, and K.L. Christman, Injectable extracellular matrix derived hydrogel provides a platform for enhanced retention and delivery of a heparin-binding growth factor. *Acta Biomater*. 2012; 8(10): p. 3695-703.

175. Sonnenberg, S.B., A.A. Rane, C.J. Liu, N. Rao, G. Agmon, S. Suarez, R. Wang, A. Munoz, V. Bajaj, S. Zhang, R. Braden, P.J. Schup-Magoffin, O.L. Kwan, A.N. DeMaria, J.R. Cochran, and K.L. Christman, Delivery of an engineered HGF fragment in an extracellular matrix-derived hydrogel prevents negative LV remodeling post-myocardial infarction. *Biomaterials*. 2015; 45: p. 56-63.

176. Hernandez, M.J., R. Gaetani, V.M. Pieters, N.W. Ng, A.E. Chang, T.R. Martin, E. van Ingen, E.A. Mol, M. Dzieciatkowska, K.C. Hansen, J.P.G. Sluijter, and K.L. Christman, Decellularized Extracellular Matrix Hydrogels as a Delivery Platform for MicroRNA and Extracellular Vesicle Therapeutics. *Advanced Therapeutics*. 2018; 1(3).

177. DeQuach, J.A., Lin, J.E., Cam, C., Hu, D., Salvatore, M., Sheikh, F., Christman, K. L., Injectable skeletal muscle matrix hydrogel promote neovascularization and muscle cell infiltration in a hindlimb ischemia model. *Eur Cell Mater*. 2013; 23: p. 400-412.

178. Ungerleider, J.L., T.D. Johnson, M.J. Hernandez, D.I. Elhag, R.L. Braden, M. Dzieciatkowska, K.G. Osborn, K.C. Hansen, E. Mahmud, and K.L. Christman, Extracellular Matrix Hydrogel Promotes Tissue Remodeling, Arteriogenesis, and Perfusion in a Rat Hindlimb Ischemia Model. *JACC Basic Transl Sci*. 2016; 1(1-2): p. 32-44.

179. Lee, J.S., J. Shin, H.M. Park, Y.G. Kim, B.G. Kim, J.W. Oh, and S.W. Cho, Liver extracellular matrix providing dual functions of two-dimensional substrate coating and three-dimensional injectable hydrogel platform for liver tissue engineering. *Biomacromolecules*. 2014; 15(1): p. 206-18.

180. Jiang, K., D. Chaimov, S.N. Patel, J.P. Liang, S.C. Wiggins, M.M. Samojlik, A. Rubiano, C.S. Simmons, and C.L. Stabler, 3-D physiomimetic extracellular matrix hydrogels provide a supportive microenvironment for rodent and human islet culture. *Biomaterials*. 2018.

181. Choi, Y.J., T.G. Kim, J. Jeong, H.G. Yi, J.W. Park, W. Hwang, and D.W. Cho, 3D Cell Printing of Functional Skeletal Muscle Constructs Using Skeletal Muscle-Derived Bioink. *Adv Healthc Mater*. 2016; 5(20): p. 2636-2645.

Chapter 2: Pelvic floor muscles undergo atrophy and fibrosis following birth injury

2.1 Introduction

The previous chapter emphasized the lack of understanding behind the mechanisms leading to pelvic floor muscle (PFM) dysfunction after childbirth. Moreover, the alterations in the intrinsic PFM components have not been well characterized in women with pelvic floor disorders. Thus, we first sought to determine the morphological properties of PFMs procured from vaginally parous women with symptomatic pelvic organ prolapse and compare these to control specimens procured from nulliparous cadaveric donors without history of pelvic floor disorders.

As discussed in the first chapter, during vaginal delivery, PFMs are subjected to mechanical strains that significantly exceed the upper physiological limit (~60%) beyond which appendicular skeletal muscle injury ensues.[1] Based on computational models of human parturition, the enthesial region of the puboviscerali portion of the levator ani complex experiences the highest strains, up to 300%, during fetal delivery. [2, 3] These excessive strains have been presumed to cause radiologically detected avulsions; however, this phenotype is not present in all women with pelvic floor dysfunction or decreased PFM strength.[4, 5] Due to ethical and technical constraints associated with directly probing PFMs in postpartum women, animal models are essential to study other potential phenotypes of PFM birth injury that are not evident on the conventionally used imaging modalities. We previously validated the rat model for the study of the human PFMs [6] and observed that the rat pubocaudalis (PCa) muscle—analogous to the human puboviscerali—experiences stretch ratios similar to humans during vaginal distention that simulates fetal crowning and delivery.[7] These strains led to sarcomere hyperelongation and associated myofibrillar disruption of the rat PFMs [7], major causes of mechanical skeletal muscle injury [8]. Unlike studies of the limb muscles, which identify that an inflammatory cascade following acute injury negatively impacts muscle recovery [8, 9], the downstream events subsequent to PFM

birth injury have not been determined to date. Thus, in the current study we examined early and delayed PFM responses to simulated birth injury (SBI) using the rat model. We determined that the morphological alterations observed in the injured rat PFMs applicably modeled pathological changes observed in parous women with symptomatic pelvic floor disorders.

In this study, we observed substantial PFM atrophy and fibrosis in parous women with pelvic organ prolapse compared to PFMs procured from age-comparable nulliparous cadaveric donors without history of pelvic floor disorders. These pathological alterations, replicated in the simulated birth injury pre-clinical model, appear to be governed by the sustained inflammatory response that negatively effects muscle anabolism and potentiates fibrosis.

2.2 Results

2.2.1 Pelvic floor muscles in women with symptomatic pelvic organ prolapse demonstrate substantial muscle atrophy and fibrosis

We collected biopsies of the puboviscerali portion of levator ani from nulliparous cadaveric controls without history of pelvic floor disorders and from parous women, undergoing surgeries for symptomatic pelvic organ prolapse (POP). With respect to race/ethnicity, all cadaveric donors were White/Non-Hispanic; in the POP group - 73.9% of subjects were White/Non-Hispanic, 17.4% were White/Hispanic, and 8.7% were Asian. The two groups did not differ with respect to age (control: 72.0 $\pm$ 7.5 y; POP: 69.9 $\pm$ 3.1 y, P=0.6) or body mass index (control: 25.4 $\pm$ 2.4 kg/m^2; POP: 27.1 $\pm$ 1.1 kg/m^2, P=0.5). The median parity in the POP group was 3 (1-4). To compare the morphological properties of puboviscerali, we assessed fiber shape and packing, collagen content (fibrosis), fiber area (atrophy), centralization of nuclei (degeneration-regeneration), and intramuscular fat content (fatty degeneration).

In the POP group, 20% of biopsies contained no myofibers on histological examination. In the remaining biopsies, myofibers exhibited disrupted fiber packing, whereas in the control group - moderate fiber packing density was observed (Fig. 2.1A). A significant decrease in fiber cross-sectional area was found in the POP group relative to the controls (P<0.0001, Fig. 2.1B). The smaller fiber size was accompanied by the dramatically increased collagen content in the POP group compared to the controls (P=0.001, Fig. 2.1C). The proportion of centralized nuclei (P=0.2, Fig. 2.1D) or intramuscular fat content (P=0.7, Fig. 2.1E) did not differ between groups. Altogether, our results demonstrate atrophy (i.e., decrease in fiber size) and fibrotic degeneration (i.e., pathological increase in collagen content) of PFMs in parous women with symptomatic POP.

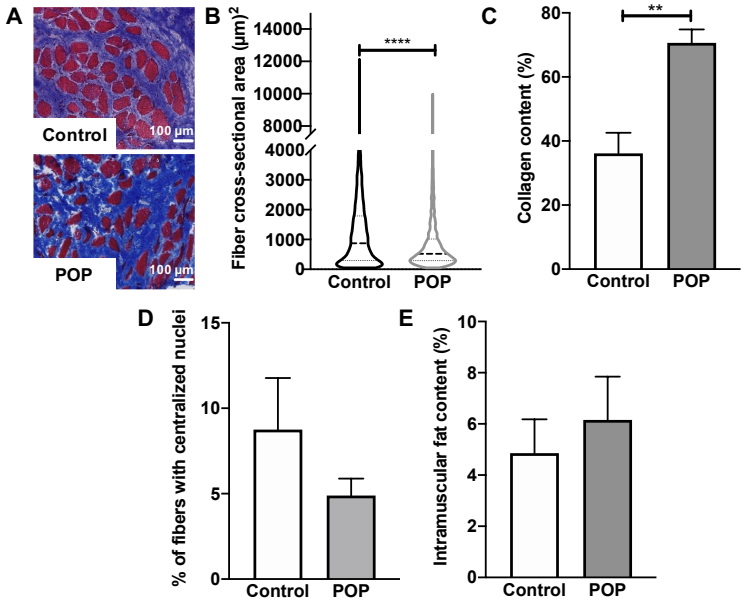

Figure 2.1. Pelvic floor muscles in women with symptomatic pelvic floor disorders demonstrate an atrophic and fibrotic phenotype.
(A) Gomori's trichrome stained cross-sections of the puboviscerales portion of the levator ani muscle procured from vaginally nulliparous cadaveric donors without history of pelvic floor disorders (control) and parous women undergoing surgical repair of pelvic organ prolapse (POP). (B) Violin plots of fiber cross-sectional area (marker of atrophy) quantified from the trichrome images. Shape of the plots demonstrates the distribution of the myofibers of various cross-sectional areas with a median indicated by the dash line. (C) Collagen content (marker of fibrosis) quantified from Gomori's trichrome stained muscle cross-sections. (D) Centralized nuclei quantification (marker of regeneration/degeneration). (E) Intramuscular fat content quantified from Oil-Red-O stained muscle cross-sections (not shown). N=4 (Control); N=20 (POP). *P*-values derived from Student's t-tests for parametric and Mann-Whitney tests for non-parametric data. **p<0.01, ****p<0.0001, mean±SEM.

2.2.2 Rat model of simulated birth injury replicates pathological alterations observed in parous women with pelvic organ prolapse

We previously identified that the PCa component of the rat levator ani muscle (analogous to the human puboviscerallis) undergoes the largest macro- and microscopic structural alteration acutely in response to SBI.[7] To assess the impact of SBI on the PCa morphological properties, we compared fiber size and collagen content at subacute (4 weeks post-SBI) and long-term (8 weeks post-SBI) timepoints. Given that revascularization has an important role in muscle regeneration [9], we also compared vessel density, specifically arterioles. We first compared 3- and 5-month-old uninjured controls to rule out possible age-related differences between rats at the time of SBI (3-month-old) and 8 weeks post-SBI (5-month-old). No significant differences were observed between these groups in either the PFM fiber area (P=0.1), collagen content (P=0.3), or arteriole density (P=0.4) (Fig. 2.2). Given the above, 3-month-old uninjured controls were used to assess changes in the morphological muscle parameters consequent to birth injury.

We observed a significant decrease in PFM fiber area 4 weeks after injury compared to uninjured controls (P<0.0001). Fiber area distribution (Fig. 2.3A-B) revealed that injured PCa was enriched with smaller fibers. To determine whether changes in fiber size at this sub-acute timepoint were due to muscle atrophy or ongoing muscle regeneration, we assessed the centralization of nuclei, a marker of regeneration.[9] The number of fibers with centralized nuclei was significantly increased 4 weeks post-SBI compared to controls (P=0.02), indicating ongoing regeneration (Fig. 2.3C). By 8 weeks post birth injury, percent centralized nuclei returned to baseline (P=0.7). Despite an increase in cross-sectional area at this longer-term timepoint compared to 4-weeks post SBI (P<0.0001, Fig. 2.3A-B), fiber size remained smaller than in uninjured controls (P<0.0001). The return of the centralized nuclei proportion to baseline levels with persistent smaller fiber size at 8 weeks post-SBI indicates that birth injury leads to PFM atrophy. Since myofiber atrophy is often accompanied by the pathological thickening of endo- and

perimysium [10], we investigated whether the total amount of collagen, the major constituent of the intramuscular ECM, is altered by birth injury. We observed a significant increase in the PCa collagen content 4 weeks post-SBI compared to controls (P=0.02), which persisted at 8 weeks (P=0.03, Fig. 2.3D-E). These results indicate that in addition to muscle atrophy, birth injury also leads to PFM fibrosis.

With respect to the intramuscular vasculature, we observed an increase in total arteriole density at 4 (P=0.01) and 8 weeks (P=0.02) post-SBI relative to controls (Fig. 2.3F-G). We then compared the distribution of arterioles of various diameters between groups.[11] The smaller arterioles (11-25 μm) were increased at 4 and 8 weeks post-SBI compared to controls (Fig. 2.3H), while no significant differences were observed in the density of larger arterioles (26-50 μm, 51-75 μm, 76-150 μm). The above indicates that birth injury alters PFM vascularization, consistent with the observations in fibrotic injured appendicular skeletal muscles.[12]

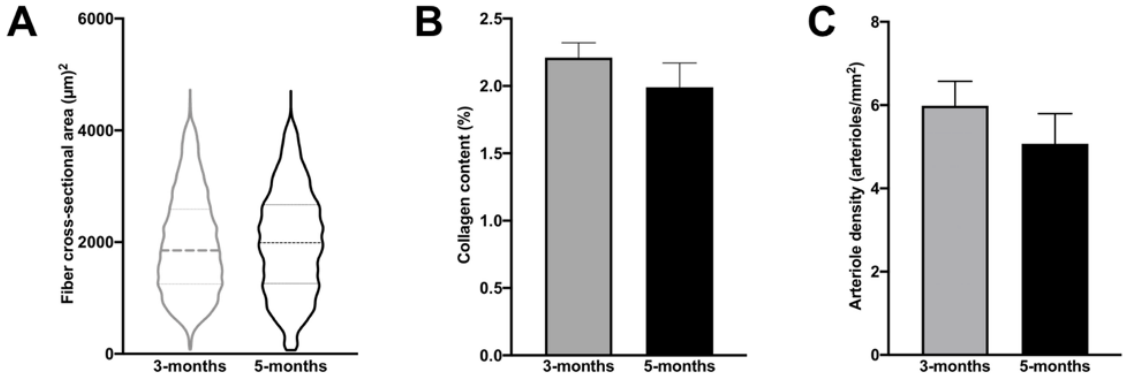

Figure 2.2. Pelvic floor muscle fiber cross-sectional area, total collagen content, and overall arteriole density do not differ between 3- vs 5-month-old rats.
(A) Violin plot for fiber cross-sectional area with median indicated by dash line. (B) Collagen content quantification. (C) Total vessel density. N=3/group. P-values derived from Student's t-tests for parametric and Mann-Whitney tests for non-parametric data, mean±SEM.

Figure 2.3. Pre-clinical rat model of simulated birth injury (SBI) recapitulating atrophic and fibrotic pelvic floor muscle phenotype observed in parous women with symptomatic pelvic floor disorders. (A) Laminin- and DAPI-stained cross-sections of the pubocaudalis portion of the levator ani muscle in uninjured controls, and 4- and 8-weeks post-SBI groups used for fiber cross-sectional area (B) and centralized nuclei (C) quantification. (D) Masson's trichrome staining of pubocaudalis from the same groups used for intramuscular collagen quantification (E). (F) Alpha smooth muscle staining of pubocaudalis from the same groups used for quantification of the total vessel (arteriole) density (G) and distribution of vessels by size (H). N=3-6/group. *P*-values derived from one-way ANOVA followed by pairwise comparisons with Tukey's range test for parametric data and Kruskal-Wallis followed by pairwise comparisons with Dun's test for non-parametrically distributed data. *p<0.05, ***p<0.001, ****p<0.0001, mean$\pm$SEM.

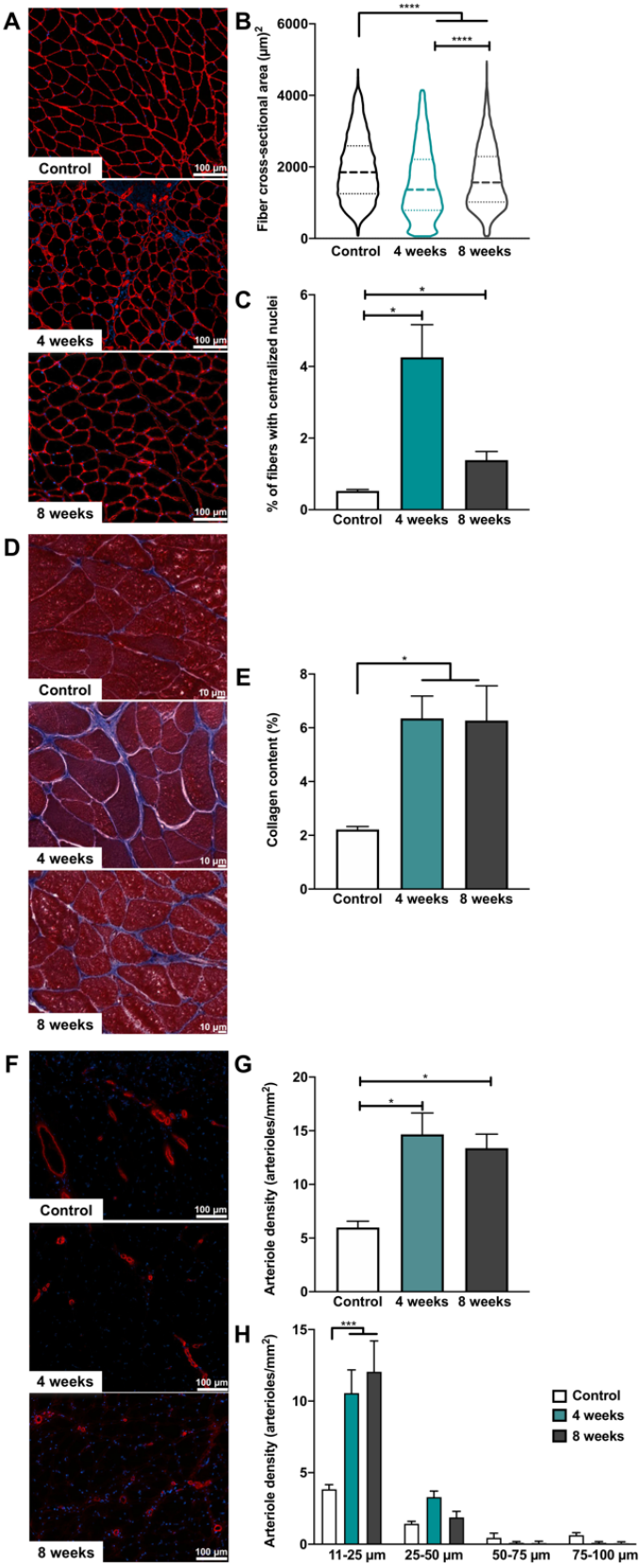
A
Control
4 weeks
8 weeks
100 µm
B
Fiber cross-sectional area (µm)²
6000
4000
2000
0
****
****
Control
4 weeks
8 weeks
C
% of fibers with centralized nuclei
6
4
2
0
*
*
Control
4 weeks
8 weeks
D
Control
4 weeks
8 weeks
10 µm
E
Collagen content (%)
8
6
4
2
0
*
Control
4 weeks
8 weeks
F
Control
4 weeks
8 weeks
100 µm
G
Arteriole density (arterioles/mm²)
20
15
10
5
0
*
*
Control
4 weeks
8 weeks
H
Arteriole density (arterioles/mm²)
15
10
5
0
***
Control
4 weeks
8 weeks
11-25 µm
25-50 µm
50-75 µm
75-100 µm

2.2.3 Myogenesis occurs within one week after simulated birth injury

To identify potential mechanisms accountable for the above long-term pathological alterations of PFMs, we elucidated, for the first time, cellular events following SBI. The unperturbed PCa demonstrated tightly packed myofibers (Fig. 2.4A). One day post-SBI, widespread myofiber death was observed, followed by accumulation of cellular infiltrate (mononuclear phagocytes (i.e., monocytes and macrophages) and neutrophils) 3 days post injury. Regenerating myofibers were observed at 7 days, identified by centralized nuclei, with endomysial thickening at 10 days post injury (Fig. 2.4A). Given that muscle stem cells (MuSCs) play a key role in muscle regeneration, we next investigated their differentiation and self-renewal capacities at 1, 3, 7, and 10 days after SBI. In injured appendicular muscles, MuSCs replace or repair the damaged muscle by differentiating into myoblasts and forming new myofibers (3-4 days post-injury) or fusing with pre-existing ones, while a portion of MuSCs self-renew to replenish the stem cell pool (5-7 days post-injury) [13, 14]. We used myogenin as a marker of differentiated MuSCs and Pax7 to identify quiescent and self-renewing cells. The peak density of differentiated MuSCs was observed 3 days post-SBI ($P=0.01$ vs control), with return to baseline at 7 days (Fig. 2.4B). The number of Pax7 expressing MuSCs increased substantially 7 days post-SBI relative to uninjured levels ($P<0.0001$), returning to baseline by 10 days after birth injury (Fig. 2.4C). The rapid differentiation of MuSCs following birth injury was confirmed by the presence of fibers positive for embryonic myosin heavy chain, a marker of de novo or fused myofibers, starting as early as 3 days post-SBI. Altogether, the above data indicate that after birth injury, PFM myogenesis followed the time-course expected from the findings in the models of chemical or mechanical [14, 15] appendicular skeletal muscle injury. Thus, disturbance in the early regenerative process is an unlikely mechanism behind the long-term atrophic and fibrotic phenotype of the PFMs consequent to birth injury.

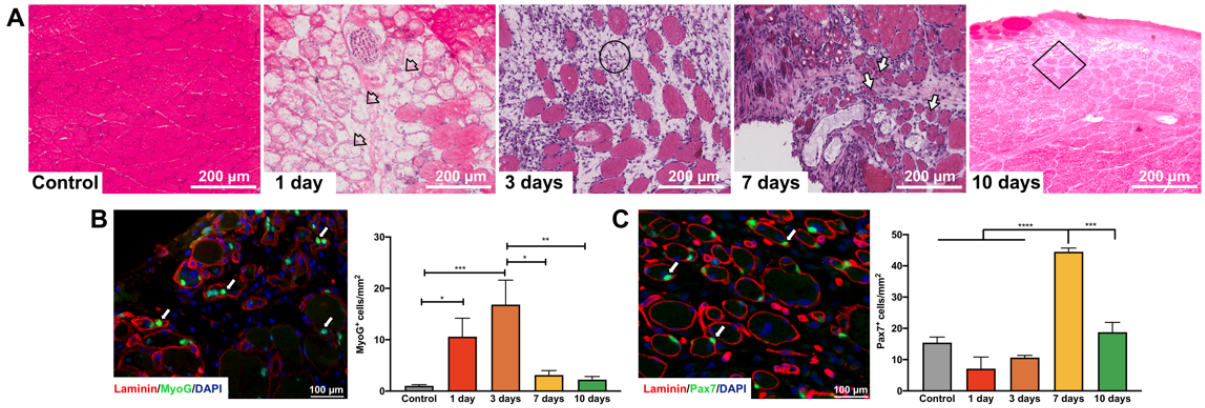

Figure 2.4. Myogenesis of the pelvic floor muscles takes place within one week after simulated birth injury (SBI).
(A) Hematoxylin and Eosin staining of pubocaudalis cross-sections along a 10-day continuum following SBI. Damaged myofibers with preservation of basal lamina (arrowheads) were observed 1 day post-SBI with separation of myofibers and cellular infiltration (circle) at 3 days. Regenerated myofibers, indicated by centralized nuclei (arrows) were identified 7 days post-SBI with endomysial thickening (square) at 10 days. Muscle cross-sections were incubated with anti-Myogenin (B) and anti-Pax7 (C) antibodies for *in situ* quantification of differentiated muscle stem cells and assessment of muscle stem pool, respectively. N=3-9/group. *P*-values derived from one-way ANOVA followed by pairwise comparisons with Tukey's range test. *p<0.05, **p<0.01, ***p<0.001, ****p<0.0001, mean±SEM.

2.2.4 Sustained inflammatory response of the pelvic floor muscles follows simulated birth injury

To further decipher the mechanisms underlying the observed muscle phenotype, we next examined gene expression changes associated with PFM injury and subsequent recovery. We composed a custom panel of 150 genes from physiologically relevant pathways known to regulate injury response of the appendicular skeletal muscles. These pathways include immune response, myogenesis, muscle anabolism and catabolism, extracellular matrix (ECM) remodeling, neovascularization, and neuromuscular junction development and maturation (Table 2.1). We assessed the transcriptional signature of PCa at 1, 3, 7, 10, 31, and 35 days following SBI. To determine patterns across the post-injury continuum, principal component (PC) analyses were performed for all assayed transcripts together (Fig. 2.5A) and separately for each individual

pathway (Fig. 2.6A-G). Unsurprisingly, PC1 that accounts for the highest variability was attributable to the pubocaudalis response to birth injury, with progressive return towards the uninjured state during the recovery period (Fig. 2.5A). The same pattern was observed for each individual pathway (Fig. 2.6A-G).

We then evaluated differentially expressed genes in each pathway to determine the longitudinal alterations in gene expression in relation to the uninjured state (Tables 2.2-7). Figure 2.7 demonstrates the gene expression profile across the samples per timepoint. Unsupervised clustered heat maps of the fold change with respect to uninjured controls are shown in Figure 2.5B-G. For the immune response pathway (Fig. 2.5B), pro-inflammatory genes increased dramatically following injury, with sustained upregulation of Il1b, Tbx21 (T helper cells type 1) and Irf5 (Macrophages type 1) until day 31 post-SBI. In contrast, genes associated with the pro-regenerative phase were upregulated until day 7. Notably, Foxp3, which encodes for regulatory T cells involved in the polarization of immune response towards the pro-regenerative phase, was downregulated. For myogenic pathway (Fig. 2.5C), expression of genes related to muscle structure predominantly decreased in response to injury, returning toward the uninjured state by 31 days. In contrast, genes coding for muscle transcription factors had variable expression. Myog, Myh3, and Pax7 expression decreased 1 day post injury. This initial decrease was followed by increased expression of Myog and Myh3 at 3 days and Pax7 at 7 days post-SBI, mimicking the differentiation/self-renewal pattern observed by immunostaining (Fig. 2.4B-C). For muscle anabolism pathways (Fig. 2.5D), we observed downregulation of all genes related to the AkT/mTOR signaling until day 10, with decreased expression of its downstream target until day 31. For muscle catabolism pathways, the majority of the genes were decreased at all time points, with the exception of Ctsl gene —involved in protein and lysosomal degradation— that increased at days 1 and 3 (Fig. 2.5D). For the ECM remodeling pathways (Fig. 2.5E), increased expression of an ECM remodeling gene, Pdgfra, was observed until day 7, while others continued

upregulated until 31 days post injury, particularly Tgfb1 and Timp1. In addition, increased expression of Col1a1 and Col3a1 occurred from 3 to 10 days post-injury. For vascularization pathways, genes that promote vascularization were decreased until day 31, while genes that inhibit vascularization were increased between 1 and 10 days (Fig. 2.5F). Genes related to neuromuscular junction development (Nrg1, Tnc) were increased from day 1 on, while the expression of genes associated with neuromuscular junction maturation (App) started to rise at day 7 (Fig. 2.5G). Overall, birth injury led to impairment in PFM anabolism, sustained upregulation of ECM remodeling genes, and a persistent inflammatory response.

Table 2.1 Customized Nanostring nCounter panel list

Category	**Gene**	**Accession**	**Classification**
Immune response Pro-inflammatory	Il1b	NM_031512.1	Cytokine
	Il6	NM_053836.1	Cytokine
	Tnf	NM_012675.2	Cytokine
	Ifng*	NM_138880.2	Cytokine
	Il12b	NM_022611.1	Cytokine
	Il2	NM_022611.1	Cytokine
	Tnfrsf1a	NM_013091.1	Receptor/growth factor
	Ccl2	NM_031530.1	Chemokine
	Ccl3	NM_013025.2	Chemokine
	Ccl4	NM_053858.1	Chemokine
	Ccr2	NM_021866.1	Chemokine
	Cxcl1	NM_053960.3	Chemokine
	Cxcl5	NM_053304.1	Chemokine
	Cxcr2	NM_017183.1	Chemokine
	Nos2	NM_012611.2	M1
	Tbx21	NM_001271120.1	Th1
	Il23a	NM_130410.2	Cytokine

Table 2.1 Customized Nanostring nCounter panel list, continued

Category	Gene	Accession	Classification
	Stat1	NM_032612.2	M1 transcription factor
	Irf5	NM_001106586.1	M1 transcription factor
	Adgre1	NM_001007557.1	Macrophages
	Myd88	NM_198130.1	Monocytes
	Nfkb1	XM_342346.3	Transcription factor
	Nkg7	NM_133540.1	T cells
	Mmp12	NM_053963.2	Metalloelastase
Immune response Pro-regenerative (Anti-inflammatory)	Il33	NM_001014166.1	Cytokine
	Il13*	NM_053828.1	Cytokine
	Il4*	NM_201270.1	Cytokine
	Il5*	NM_021834.1	Cytokine
	Il15*	XM_008772363.2	Cytokine
	Il17*	NM_001106897.1	Cytokine
	Il10	NM_012854.2	Cytokine
	Il10ra	NM_057193.2	Cytokine/Receptor
	Igf1	NM_001082477.2	Growth factor
	Igf1r	NM_052807.2	Growth factor/Receptor
	Ccr5	NM_053960.3	Chemokine
	Arg1	NM_017134.2	M2
	Gata3	NM_133293.1	Th2
	Foxp3	NM_001108250.1	T regulatory cells
	Stat6	NM_001044250.1	M2 transcription factor
	Irf4	NM_001106108.1	M2 transcription factor

Table 2.1 Customized Nanostring nCounter panel list, continued

Category	Gene	Accession	Classification
Myogenesis	Pax7	NM_001191984.1	Quiescent and activated muscle stem cells
	Myod1	NM_176079.1	Activated muscle stem cells
	Myf5	NM_001106783.1	Activated cells
	Myf6	NM_013172.1	Differentiated cells
	Myog	NM_017115.2	Differentiated muscle stem cells
	MyH3	NM_012604.1	Regenerated myofibers
	Hgf	NM_017017.2	Growth factor
	Adam12	XM_017590240.1	Metallopeptidase
	Actn2	NM_001170325.1	Muscle structure
	Des	NM_022531.1	Muscle structure
	Dmd	NM_001005244.1	Muscle structure
	Tpm3	NM_173111.1	Muscle structure
	Tpm4	NM_012678.2	Muscle structure
	Tcap	NM_001271277.1	Muscle structure
	Acta1	NM_019212.2	Muscle structure
	Mybpc1	NM_001100758.1	Muscle structure
	Mybpc2	NM_001106257.1	Muscle structure
	Tmod1	NM_013044.2	Muscle structure
	Ttn	XM_001065955.4	Muscle structure
	Jsrp1	NM_001109591.1	Muscle structure
	Tnnt1	NM_001277260.1	Muscle structure
	Tnnt3	NM_001270665.1	Muscle structure

Table 2.1 Customized Nanostring nCounter panel list, continued

Category	Gene	Accession	Classification
	MyH1	NM_001135158.1	Muscle structure
	MyH7	NM_017240.1	Muscle structure
	Mylk2	NM_057209.1	Muscle structure
	Sln	NM_001013247.1	Muscle structure
	Wnt7a*	NM_001100473.1	Muscle homeostasis
Extracellular matrix remodeling	Mmp1	NM_001134530.1	Metalloproteinase
	Mmp8	NM_053963.2	Metalloproteinase
	Mmp13*	NM_133530.1	Metalloproteinase
	Mmp2	NM_031054.2	Metalloproteinase
	Mmp9	NM_031055.1	Metalloproteinase
	Timp1	NM_053819.1	Tissue inhibitor of metalloproteinase
	Timp2	NM_021989.2	Tissue inhibitor of metalloproteinase
	Timp3	NM_012886.2	Tissue inhibitor of metalloproteinase
	Timp4	NM_001109393.1	Tissue inhibitor of metalloproteinase
	Ccn2	NM_022266.2	Growth factor
	Pdgfa	NM_012801.1	Growth factor
	Pdgfra	NM_012802.1	Growth factor/Receptor
	Dcn	NM_024129.1	Proteoglycan-ECM component
	Tgfb1	NM_021578.2	Growth factor
	Tgfbr1	NM_012775.2	Growth factor/Receptor
	Smad2	NM_001105817.1	Growth factor/Receptor
	Smad3	NM_013095.2	Signal transducer

Table 2.1 Customized Nanostring nCounter panel list, continued

Category	Gene	Accession	Classification
	Smad4	NM_019275.2	Signal transducer
	Col1a1	NM_053304.1	ECM component
	Col3a1	NM_032085.1	ECM component
	Itga1	NM_030994.2	ECM component
	Itgb1	NM_017022.2	Cell-matrix interaction
	Itga2	XM_345156.6	Cell-matrix interaction
	Itga2	XM_345156.6	Cell-matrix interaction
	Vwa1	NM_001013938.1	Cell-matrix interaction
Muscle anabolism/catabolism	Akt1	NM_033230.1	Anabolism/mTOR signaling
	Mtor	NM_019906.1	Anabolism/mTOR signaling
	Rheb	NM_013216.1	Anabolism/mTOR signaling
	Eif2b5	NM_138866.2	Anabolism/mTOR signaling
	Akt2	NM_017093.1	Anabolism/mTOR signaling
	Eif4b	NM_001008324.1	Anabolism/mTOR signaling
	Eif4e	NM_053974.2	Anabolism/mTOR signaling
	Eif4ebp1	NM_053857.1	Anabolism/mTOR signaling
	Eif4g1	XM_213569.6	Anabolism/mTOR signaling
	Grb10	NM_001109093.1	Anabolism
	Rps6ka1	NM_031107.1	Anabolism

Table 2.1 Customized Nanostring nCounter panel list, continued

Category	Gene	Accession	Classification
	Rps6kb1	NM_031985.1	mTOR signaling
	Gsk3b	NM_032080.1	Anabolism
	Junb	NM_021836.2	Anabolism
	Nol3	NM_053516.2	Apoptosis
	Ikbkb	NM_053355.1	Anabolism
	Nfkbia	XM_001075778.1	Anabolism
	Foxo1	NM_001191846.2	Catabolism
	Foxo3	NM_001106395.1	Catabolism
	Fbxo32	NM_133521.1	Catabolism
	Trim63	NM_080903.1	Catabolism
	Camkk1	NM_031662.1	Catabolism
	Mstn	NM_019151.1	Anabolism
	Ctsl	NM_013156.2	Catabolism
	Prkaa1	NM_019142.2	Catabolism
	Fst	NM_012561.1	Anabolism
	Ccn4	NM_031716.1	Cellular survival
	Has1	NM_172323.1	Cellular survival
	Has2	NM_013153.1	Cellular survival
Vascularization	Vegfa	NM_031836.2	Growth factor
	Vegfb	NM_053549.1	Growth factor
	Angpt1	NM_053546.1	Growth factor
	Angpt2	NM_134454.1	Growth factor
	Kdr	NM_013062.1	Growth factor/Receptor
	Flt1	NM_019306.1	Growth factor/Receptor
	Nrp1	NM_145098.2	Growth factor/Receptor

Table 2.1 Customized Nanostring nCounter panel list, continued

Category	Gene	Accession	Classification
	Tie1	NM_053545.1	Growth factor/Receptor
	Fgf2	NM_019305.2	Growth factor/Receptor
	Thsb1	NM_001013062.1	Cell-matrix interaction
	Mmp14	NM_031056.1	Metalloproteinase
Neuromuscular junctions	Erbb2	NM_017003.2	Growth factor/Receptor
	App	NM_019288.1	Receptor
	Dvl1	NM_031820.1	Cytoplasmic
	Ptn	NM_017066.2	Growth factor
	Tnc	NM_053861.1	ECM component
	Utrn	NM_013070.1	Cytoskeleton
	Musk	NM_031061.1	Receptor
	Agrn	NM_175754.1	Proteoglycan
Housekeeping	Gphn	NM_022865.3	Cytoskeleton
	Ap3d1	XM_001076208.1	
	Hprt1	NM_012583.2	
	Rpl13a	NM_173340.2	
	Rpl32	NM_013226.2	
	Rplp0	NM_022402.2	
	Tbp	NM_001004198.1	

Note: *Genes that were excluded since normalized mRNA counts were at the level of background for all conditions.

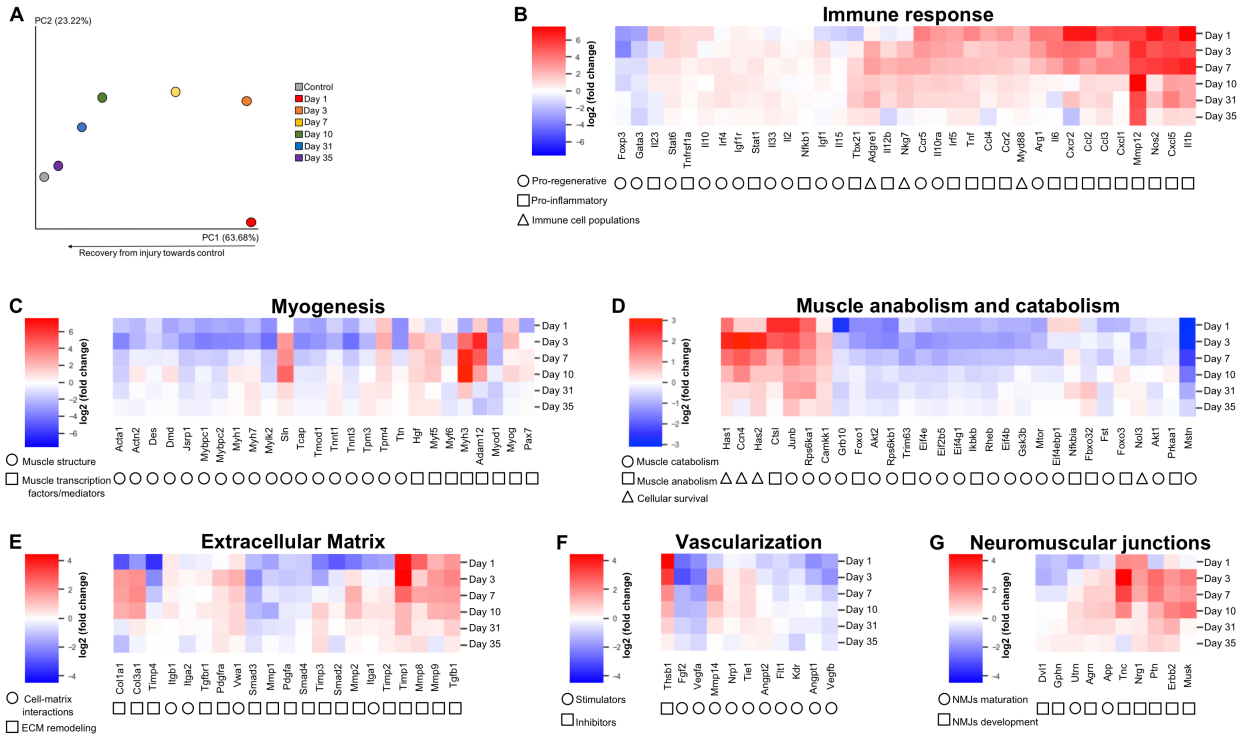

Figure 2.5. Simulated birth injury (SBI) leads to sustained inflammatory response, upregulation of ECM remodeling genes, and downregulation of genes involved in muscle anabolism.
(A) Transcriptional signatures of the pelvic floor muscles across different pathways were derived from the customized Nanostring nCounter panel with 150 genes. Principal component analysis includes gene expression in uninjured controls and at multiple time points during active muscle regeneration post-SBI. (B-G) Unsupervised clustered heat maps of fold changes at each time point with respect to control. Pathways examined include immune response (B), myogenesis (C), muscle anabolism and catabolism (D), extracellular matrix (E), vascularization (F), and neuromuscular junctions (G).

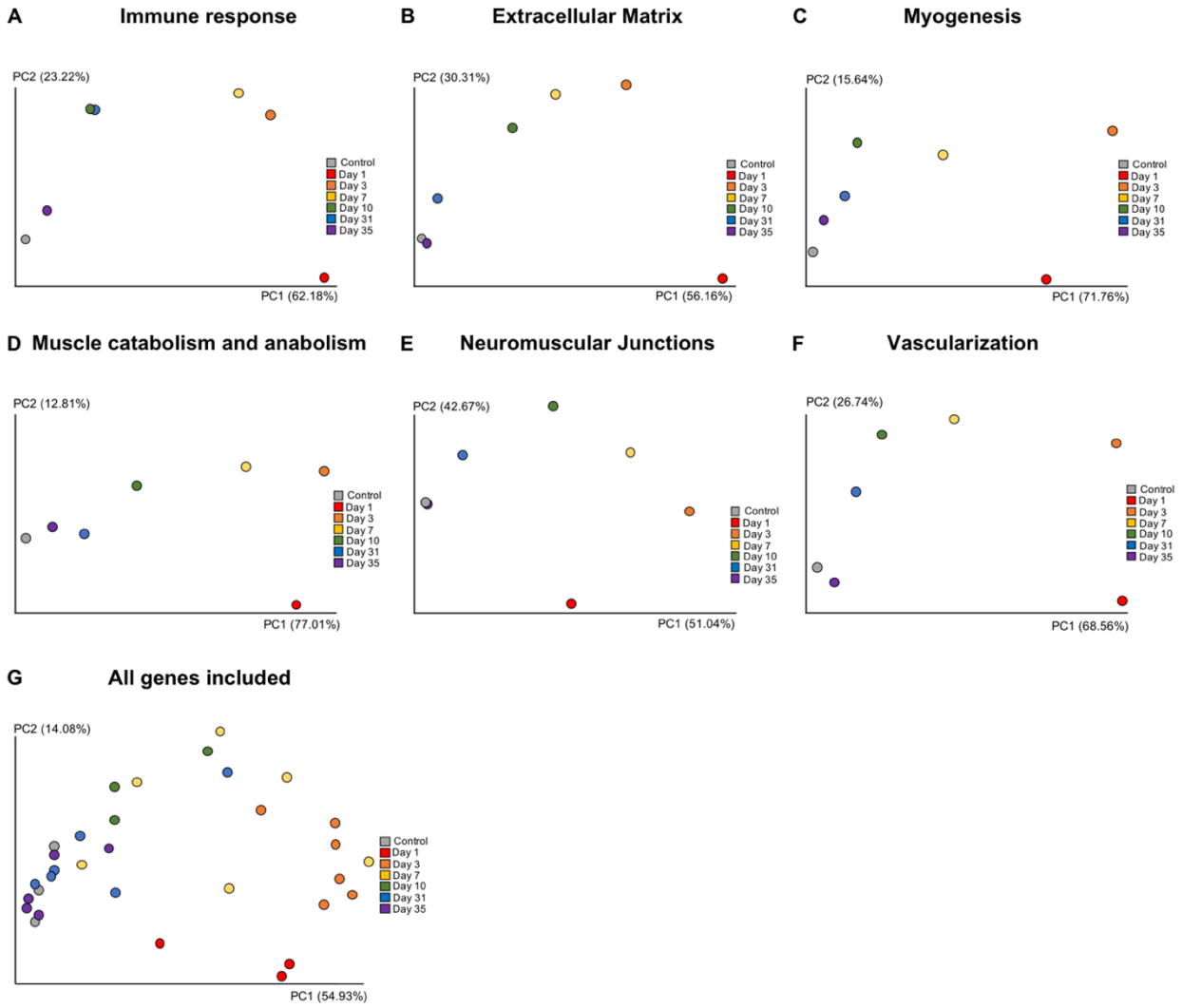

Figure 2.6. Principal component analysis of transcriptional signatures during active regeneration of the pelvic floor muscles following simulated birth injury.
Customized Nanostring nCounter panel included genes involved in the following pathways: immune response (A), extracellular matrix (B), myogenesis (C), muscle anabolism and catabolism (D), neuromuscular junctions (E), vascularization (F). Average of normalized expression at each time point was included for all the pathways. (G) Principal component analysis for all genes including all replicates for each time point. Gene expression values were normalized to the following housekeeping genes Ap3d1, Hprt1, Rpl13a, Rpl32, Rplp0, and Tbp.

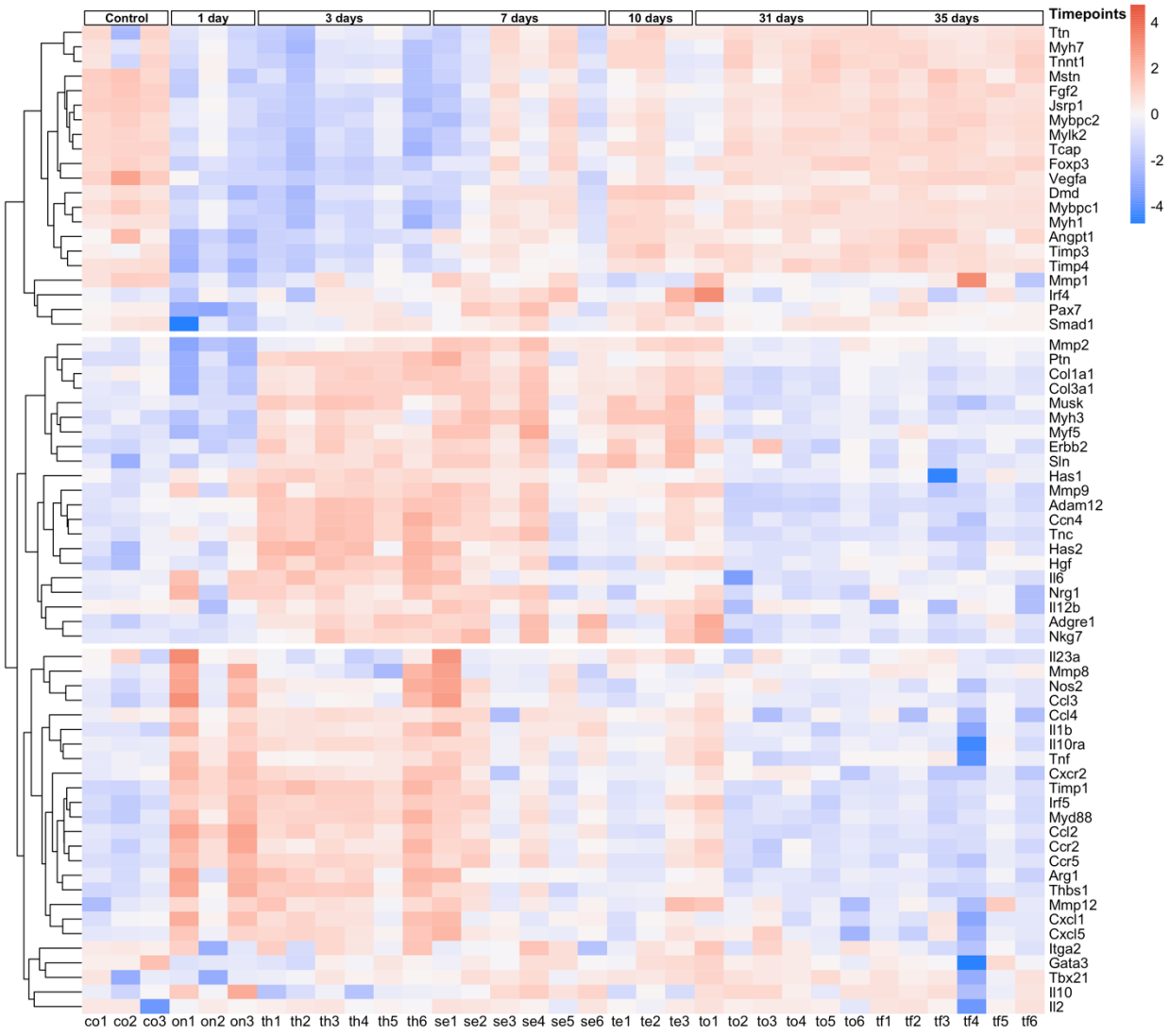

Figure 2.7. Gene expression profile across the samples per timepoint post-simulated birth injury. Heat map of genes with the highest variation in the dataset. N= 3/6 per group.

Table 2.2. Immune response related genes throughout the different time points after simulated birth injury.
P and q values are indicated for significantly differentially expressed genes compared to uninjured group. FC= Log2FC

	Days after Simulated Birth Injury																	
Gene	1			3			7			10			31			35		
	FC	p	q	FC	p	q	FC	p	q	FC	p	q	FC	p	q	FC	p	q
Adgre1	0.38			2.6	0.001	0.002	2.85	0.0005	0.001	1.68	0.04	0.12	2.27	0.004	0.07	0.93		
Arg1	4.04	2.60E-06	9.40E-06	2.98	0.0001	0.0002	2	0.006	0.1	0.4			0.26			-0.09		
Ccl2	6.98	1.60E-11	4.50E-10	4.14	2.40E-06	6.20E-06	2.83	0.0004	0.001	1.12			0.98			0.31		
Ccl3	5.29	1.10E-06	4.60E-06	2.6	0.004	0.006	3.61	0.0002	0.0009	0.89			1.24			0.81		
Ccl4	2.6	0.001	0.002	1.61	0.01	0.02	1.73	0.01	0.02	0.63			0.38			-0.88		
Ccr2	2.99	5.50E-08	3.10E-07	1.94	7.10E-05	0.0001	1.54	0.001	0.003	0.99			0.82			0.026		
Ccr5	3.84	1.10E-07	6.10E-07	3.05	4.20E-06	1.00E-05	2.49	0.0001	0.0005	1.38	0.03	0.1	1.16			0.15		
Cxcl1	5.68	0.0001	0.003	3.51	0.006	0.008	3.43	0.007	0.01	0.89			0.06			0.14		
Foxp3	-3.07	8.40E-01	9.70E-09	-3.66	0	0	-0.99	0.009	0.01	-1.27	0.006	0.04	-0.17			-0.18		
Gata3	-2.68	1.10E-05	3.80E-05	-1.58	0.0003	0.0006	-1.04	0.01	0.02	-0.67			-0.93	0.04	0.1	-1.32	0.01	0.25
Igf1	-1.06	0.01	0.02	1.04	0.007	0.01	0.64			0.31			-0.08			-0.19		
Igf1r	0.46			0.47	0.03	0.04	0.42			0.72	0.003	0.03	0.55	0.01	0.1	0.24		
Il10	1.1	0.0003	0.0006	-0.19			0.68	0.01	0.02	-0.05			0.63	0.02	0.1	0.39		
Il10ra	2.96	4.70E-05	0.0001	2.71	5.20E-05	0.0001	2.04	0.001	0.003	1.52	0.02	0.1	1.17			-0.07		
Il12b	-0.59			1.15			2.21	0.007	0.01	1.34			1.02			-1.29		
Il15	-1.4	9.20E-07	4.00E-06	-0.32			0.06			0.03			-0.12			0.23		
Il1b	7.52	2.10E-06	7.80E-06	5.22	0.0001	0.0002	6.6	9.00E-06	0.0001	2.64	0.03	0.11	2.72	0.02	0.1	1.06		
Il2	-0.06			0.23			0.42			-0.14			0.24			0.34		
Il33	-0.44			0.72	0.001	0.001	0.25			0.33			0.7	0.001	0.03	0.49	0.02	0.44
Il6	3.96	0.0001	0.0003	4.11	5.40E-05	0.001	2.72	0.003	0.007	0.24			-0.94			0.01		
Irf4	-0.16			0.24			0.74			0.82			0.84			0.12		
Irf5	2.67	5.70E-07	2.60E-06	2.45	7.30E-07	1.90E-06	1.92	6.20E-05	0.0003	1.34	0.008	0.055	1.1	0.01	0.1	0.59		
Myd88	2.13	2.60E-08	1.80E-07	1.94	2.80E-08	1.20E-07	1.23	0.0002	0.0009	0.77	0.03	0.1	0.58			0.26		
Nfkb1	0.11			0.29			0.14			0.09			0.17			-0.01		
Nkg7	-0.26			1.95	0.01	0.01	2.57	0.001	0.003	1.75	0.03	0.1	1.63	0.02	0.1	-0.35		
Nos2	6.99	5.90E-05	0.0001	5.06	2.20E-08	9.70E-08	5.81	1.40E-11	1.90E-09	0.75			1.8			0.44		
Stat1	0.25			0.44			0.78	0.001	0.003	0.6	0.02	0.1	0.44			0.28		
Stat6	1.33	4.40E-05	0.0001	1.27	1.70E-05	3.90E-05	0.85	0.003	0.006	0.55			0.59	0.03	0.1	0.26		
Tnfrsf1a	1.02	2.80E-05	8.20E-05	1.01	4.00E-06	9.80E-06	0.37			0.24			0.13			-0.04		

Table 2.3. Myogenesis related genes throughout the different time points after simulated birth injury.
P and q values are indicated for significantly differentially expressed genes compared to uninjured group. Log2FC

	Days after Simulated Birth Injury																	
Gene	1			3			7			10			31			35		
	FC	p	q	FC	p	q	FC	p	q	FC	p	q	FC	p	q	FC	p	q
Pax7	-2.19	2.10E-08	1.50E-07	-0.08			0.46			0.58			-0.16			0.12		
Acta1	-1.37	0.02	0.03	-2.94	6.50E-09	3.60E-08	-1.3	0.01	0.01	-1.14			-0.77			-0.21		
Actn2	-1.69	0.0002	0.0005	-1.74	3.30E-06	8.20E-06	-0.4			0.57			-0.07			-0.24		
Adam12	0.87			3.78	1.60E-07	5.50E-07	2.88	2.50E-05	0.0002	1.64	0.01	0.1	-0.46			-1.08		
Des	-0.76	0.006	0.01	-1.01	1.70E-05	3.90E-05	-0.46			-0.16			-0.27			-0.08		
Dmd	-2.15	1.80E-06	6.80E-06	-1.7	2.10E-06	5.50E-06	-0.4			0.72			-0.09			-0.07		
Hgf	0.43			1.73	9.30E-07	2.40E-06	0.94	0.006	0.01	0.96	0.01	0.07	0.65			0.53		
Mybpc1	-2.25	2.70E-05	8.20E-05	-3.06	1.10E-12	1.60E-11	-1.1	0.01	0.01	-0.24			-0.41			-0.35		
Mybpc2	-2	0.002	0.003	-2.87	8.70E-08	3.30E-07	-1.26	0.01	0.02	-0.81			-0.63			-0.14		
Myf5	-0.89	0.02	0.03	1.12	0.001	0.002	1.48	2.70E-05	0.0002	1.34	0.0005	0.01	0.05			0.49		
Myf6	0.25			-1.5	8.20E-09	4.30E-08	-0.64	0.01	0.02	0.08			-0.75	0.004	0.07	-0.58	0.02	0.4
Myh1	-2.24	0.0003	0.0006	-2.84	1.40E-08	7.00E-08	-0.6			0.48			0.11			0.1		
Myh3	-1.96	0.03	0.04	3.51	0.0001	0.0002	5.6	3.60E-08	6.20E-07	6.11	1.40E-08	1.00E-06	1.38			-0.27		
Myh7	-1.62	0.02	0.03	-2.4	6.10E-05	0.0001	-0.28			0.4			0.6			0.56		
Mylk2	-2.64	0.0003	0.0006	-3.42	5.10E-09	2.90E-08	-1.28	0.02	0.03	-1.15			-0.32			-0.01		
Myod1	-2.13	3.00E-08	2.00E-07	-1.62	1.40E-07	4.90E-07	-1.8	4.70E-09	9.60E-08	-0.39			-1.26	4.60E-05	0.003	-1.09	0.0004	0.01
Myog	1.09	0.001	0.003	1.65	3.20E-07	9.80E-07	0.32			1.01	0.003	0.03	-0.32			-0.14		
Sln	-0.04			2.46	3.00E-05	6.50E-05	2.76	4.40E-06	5.60E-05	3.65	4.40E-08	2.00E-06	0.88			0.43		
Tcap	-1.96	0.0005	0.0009	-2.83	7.00E-10	5.70E-09	-1.35	0.003	0.006	-0.52			-0.4			-0.19		
Tmod1	-2.27	6.10E-07	2.70E-06	-2.5	5.40E-12	6.80E-11	-1.09	0.002	0.005	-0.59			-0.41			-0.21		
Tnnt1	-1.11			-1.91	5.80E-05	0.0001	-0.31			0.24			0.47			0.5		
Tnnt3	-1.97	0.0001	0.0003	-3.43	5.50E-16	1.50E-14	-1.29	0.001	0.004	-0.62			-0.51			-0.2		
Tpm3	-0.75			-1.73	9.50E-05	0.0001	-0.5			0.03			0.53			0.53		
Tpm4	1.4	0.0002	0.0004	1.98	3.40E-08	1.40E-07	1.09	0.001	0.003	0.85	0.02	0.1	0.57			0.15		
Ttn	-2.69	0.006	0.009	-2.63	0.0006	0.001	-0.71			0.2			0.06					

Table 2.4. Muscle anabolism and catabolism related genes throughout the different time points after simulated birth injury.
P and q values are indicated for significantly differentially expressed genes compared to uninjured group. Log2FC

	Days after Simulated Birth Injury																	
Gene	1			3			7			10			31			35		
	FC	p	q	FC	p	q	FC	p	q	FC	p	q	FC	p	q	FC	p	q
Has1	1.73			2.76	1.90E-07	6.60E-07	1.72	0.001	0.002	0.89			0.41			0.33		
Akt1	-0.29			-0.39			-0.44	0.0002	0.0009	-0.02			-0.37			-0.2		
Akt2	-1.4	3.30E-08	2.00E-07	-1.38	2.70E-11	2.90E-10	-0.77	0.0002	0.0009	-0.45			-0.49	0.02	0.1	-0.26		
Camkk1	0.18			0.78	0.002	0.003	0.7	0.005	0.01	0.52			0.39			0.41		
Ctsl	2.58	4.50E-12	1.50E-10	2.02	2.00E-09	1.40E-08	0.84	0.007	0.01	0.65			0.18			-0.04		
Eif2b5	-0.93	0.0002	0.0005	-1.26	2.90E-09	1.90E-08	-1	2.10E-06	2.90E-05	-0.49	0.04	0.1	-0.35			-0.2		
Eif4b	-0.96	0.0001	0.0003	-1.21	1.10E-08	5.70E-08	-0.73	0.0006	0.001	-0.37			-0.05			0.07		
Eif4e	-0.63	0.0001	0.0002	-1.36	0	0	-0.8	4.90E-09	9.60E-08	-0.47	0.003	0.03	-0.4	0.003	0.07	-0.19		
Eif4ebp1	0.49	0.01	0.02	-0.25			-0.66	0.0001	0.0007	-0.28			-0.07			0.02		
Eif4g1	-0.95	0.0004	0.0007	-1.15	3.20E-07	9.80E-07	-0.83	0.0002	0.0009	-0.33			-0.21			-0.11		
Fbxo32	-0.37			-0.13			-0.37			-0.33			0.72			0.32		
Foxo1	-1.4	1.50E-06	5.90E-06	-1.22	3.70E-07	1.00E-06	-0.6	0.01	0.01	-0.15			-0.19			-0.18		
Foxo3	-0.85	0.0001	0.0003	-0.07			-0.15			0.3			0.15			0.01		
Fst	-0.91	0.005	0.008	-0.32			-0.65	0.01	0.02	-0.03			-0.4			-0.38		
Grb10	-2.69	1.10E-16	1.50E-14	-0.74	0.004	0.006	-0.35			-0.3			-0.56	0.03	0.1	-0.4		
Gsk3b	-0.96	8.30E-05	0.0002	-1.06	2.00E-07	6.60E-07	-0.64	0.001	0.003	-0.06			0.44			-0.19		
Ikbkb	-0.95	9.40E-05	0.0002	-1.14	1.50E-08	7.20E-08	-0.78	0.0001	0.0005	-0.53	0.02	0.1	0.41			0.33		
Junb	2.59	4.40E-08	2.60E-07	2.17	4.90E-07	1.40E-06	1.63	9.50E-05	0.0005	1.01	0.02	0.1	1.12	0.005	0.08	0.76		
Mstn	-3.08	0.0001	0.0003	-2.97	2.20E-06	5.60E-06	-2.32	0.0001	0.0008	-1.69	0.02	0.1	-1			-0.5		
Mtor	-1.1	4.30E-05	0.0001	-0.83	0.0002	0.0003	-0.63	0.004	0.008	-0.24			-0.07			0.02		
Nfkbia	0.47			-0.27			0.23			-0.02			0.57			0.53		
Nol3	-0.48			-0.86	0.002	0.004	-0.54			-0.02			0.18			-0.04		
Prkaa1	-0.29			-0.34			-0.27			0.18			1.12			0.76		
Rheb	-0.81	6.60E-05	0.0001	-1.12	3.40E-11	3.40E-10	-0.75	1.10E-05	0.0001	-0.44	0.02	0.1	-0.38			-0.21		
Rps6ka1	1.87	1.00E-05	3.60E-05	1.59	3.50E-05	7.40E-05	1.25	0.0009	0.002	0.91	0.02	0.1	1.23	0.001	0.03	0.31		
Rps6kb1	-1.59	5.50E-11	9.50E-10	-1.47	8.80E-14	1.30E-12	-0.7	0.0004	0.001	-0.3			-0.5	0.01	0.1	-0.33		
Ccn4	0.59			3.1	6.20E-08	2.40E-07	2.01			1.46	0.01	0.06	0.44			-0.19		
Trim63	-0.39			-1	0.01	0.01	-1.11	0.005	0.01	-0.5			-0.24			-0.05		

Table 2.5. Extracellular matrix remodeling related genes throughout the different time points after simulated birth injury.
P and q values are indicated for significantly differentially expressed genes compared to uninjured group. Log2FC

Gene	1			3			7			10			31			35		
	FC	p	q	FC	p	q	FC	p	q	FC	p	q	FC	p	q	FC	p	q
Mmp8	2.74	0.002	0.004	0.84			1.58	0.04	0.06	0.47			0.33			0.6		
Col1a1	-3.03	1.30E-05	4.30E-05	1.75	0.003	0.005	1.66	0.005	0.01	1.4	0.03	0.1	-0.35			-1.15	0.03	0.4
Col3a1	-1.82	0.0009	0.001	1.92	0.0001	0.0002	2.08	5.10E-05	0.0003	1.66	0.002	0.02	0.36			-0.19		
Itga1	-1.76	4.40E-11	9.50E-10	-0.16			0.24			0.52	0.04	0.1	0.21			0.02		
Itga2	-0.35			0.16			-0.1			-0.05			0.075			-0.517		
Itgb1	0.39	0.04	0.05	0.35	0.04	0.05	0.18			0.42	0.03	0.1	0.02			0.007		
Mmp1	-1.6	0.0009	0.001	-0.85			-0.39			-1.46	0.008	0.053	-0.52			-0.06		
Mmp2	-2.35	1.60E-09	1.70E-08	0.49			1.39	4.70E-05	0.0003	1.13	0.002	0.02	0.33			0.14		
Mmp9	1.32	0.02	0.03	1.79	0.001	0.001	1.66	0.002	0.005	1.38	0.01	0.1	0.28			-0.41		
Pdgfa	-0.8	1.30E-05	4.30E-05	-0.99	1.00E-10	9.40E-10	-0.56	0.0002	0.0009	-0.35			-0.42	0.007	0.08	-0.21		
Pdfgra	-0.06			1.06	4.00E-05	8.40E-05	0.5	0.04	0.06	0.45			0.41			0.44		
Smad3	-1.19	0.006	0.009	-2.02	1.50E-08	7.20E-08	-1.44	5.30E-05	0.0003	-1.18	0.006	0.04	-0.71	0.04	0.1	-0.49		
Smad4	-0.92	2.80E-07	1.50E-06	-0.89	3.70E-09	2.30E-08	-0.5	0.0008	0.002	-0.29			-0.06			0.01		
Tgfb1	1.84	3.50E-05	0.0001	2.15	2.60E-07	8.30E-07	1.74	1.80E-05	0.0001	1.44	0.001	0.01	0.85	0.02	0.1	0.36		
Tgfbr1	-0.27			0.28	0.0002	0.0003	-0.01			-0.35			-0.06			-0.07		
Timp1	4.28	7.20E-09	5.50E-08	4.46	4.70E-10	4.10E-09	2.66	3.60E-05	0.0002	1.28			1.25	0.03	0.1	0.44		
Timp2	-1.57	4.80E-11	9.50E-10	-0.22			0.43	0.03	0.05	0.49	0.03	0.1	0.34			0.28		
Timp3	-2.26	2.60E-09	2.20E-08	-1.55	2.60E-07	8.30E-07	-0.15			0.84	0.02	0.1	0.54			0.61		
Timp4	-3.56	3.10E-12	1.40E-10	-2.03	1.10E-07	4.20E-07	-1.02	0.008	0.01	-0.26			0.08			-0.004		
Vwa1	0.48			1.39	6.10E-06	1.40E-05	0.92	0.002	0.005	0.72	0.03	0.1	0.74	0.01	0.1	0.14		

Table 2.6. Vascularization related genes throughout the different time points after simulated birth injury.
P and q values are indicated for significantly differentially expressed genes compared to uninjured group. Log2FC

Days after Simulated Birth Injury																		
Gene	1			3			7			10			31			35		
	FC	p	q	FC	p	q	FC	p	q	FC	p	q	FC	p	q	FC	p	q
Thsb1	4.7	4.00E-10	5.00E-09	3.6	9.80E-08	3.60E-07	2	0.0007	0.002	1.46	0.02	0.1	0.87			0.25		
Angpt1	-2.12	1.00E-13	7.20E-12	-1.35	1.50E-09	1.10E-08	-0.45	0.04	0.06	-0.006			-0.29			0.001		
Angpt2	-0.95	0.0001	0.0004	-0.42	0.04	0.06	0.05			-0.04			0.33			0.28		
Fgf2	-2.68	5.30E-07		-3.2	4.40E-14	7.80E-13	-1.3	0.0009	0.002	-1.35	0.007	0.05	-0.83	0.04	0.18	-0.48		
Flt1	-0.69	0.009	0.01	-0.74	0.001	0.001	-0.57	0.01	0.01	-0.2			-0.05			-0.22		
Kdr	-1.05	0.0002	0.0004	-0.47	0.04	0.06	-0.14			-0.1			-0.31			-0.83	0.0006	0.02
Mmp14	-0.87			1.29	0.002	0.003	1.75	5.50E-05	0.0003	1.05	0.02	0.1	0.51			-0.01		
Nrp1	-0.14			0.3			0.26			0.41			0.1			-0.25		
Tie1	-0.3			0.76	0.0001	0.0002	0.64	0.001	0.003	0.68	0.002	0.02	0.42	0.03	0.14	0.2		
Vegfa	-2	2.00E-09	2.00E-08	-2.54	0	0	-1.78	1.10E-10	3.20E-09	-1.27	0.0001	0.002	-1.09	8.10E-05	0.003	-0.71	0.01	0.25
Vegfb	-1.62	1.10E-06	4.60E-06	-2	3.60E-14	7.80E-13	-0.98	0.0003	0.001	-0.39			-0.59	0.03	0.14	-0.46		

Table 2.7. Neuromuscular junctions related genes throughout the different time points after simulated birth injury.
P and q values are indicated for significantly differentially expressed genes compared to uninjured group. Log2FC

Days after Simulated Birth Injury																		
Gene	1			3			7			10			31			35		
	FC	p	q	FC	p	q	FC	p	q	FC	p	q	FC	p	q	FC	p	q
Dvl1	-1.58	2.10E-10	3.00E-09	-1.69	1.10E-16	3.80E-15	-0.77	0.0001	0.0007	-0.3			-0.43	0.03	0.14	-0.16		
Agrn	-1.16	0.0004	0.0007	0.04			0.43			0.47			0.25			-0.19		
App	-0.78	0.0002	0.0004	0.29			0.43	0.01	0.02	0.62	0.003	0.03	0.22			-0.1		
Erbb2	0.06			1.43	0.0001	0.0002	1.24	0.001	0.002	1.72	3.90E-05	0.0009	0.95	0.01	0.1	0.23		
Gphn	-1.34	1.70E-06	6.60E-06	-1.4	1.20E-09	9.80E-09	-0.79	0.0006	0.001	-0.38			-0.23	0.32	0.55	-0.05		
Musk	-0.52			1.84	4.60E-06	1.00E-05	1.48	0.0002	0.0008	2.05	3.20E-06	8.80E-05	-0.21			-0.24		
Nrg1	1.58	0.008	0.01	1.33	0.01	0.01	1.12	0.03	0.05	-0.002			0.03			0.12		
Ptn	-1.18	0.01	0.02	2.08	5.80E-06	1.30E-05	1.91	2.50E-05	0.0002	0.96	0.04	0.12	0.58			0.38		
Tnc	1.61	0.03	0.04	3.93	6.90E-07	1.90E-06	2.82	0.0001	0.0007	1.69	0.02	0.1	-0.1			-0.85		
Utrn	-1.79	3.50E-09	2.90E-08	-0.63	0.01	0.01	-0.12			0.21			0.15			-0.04		

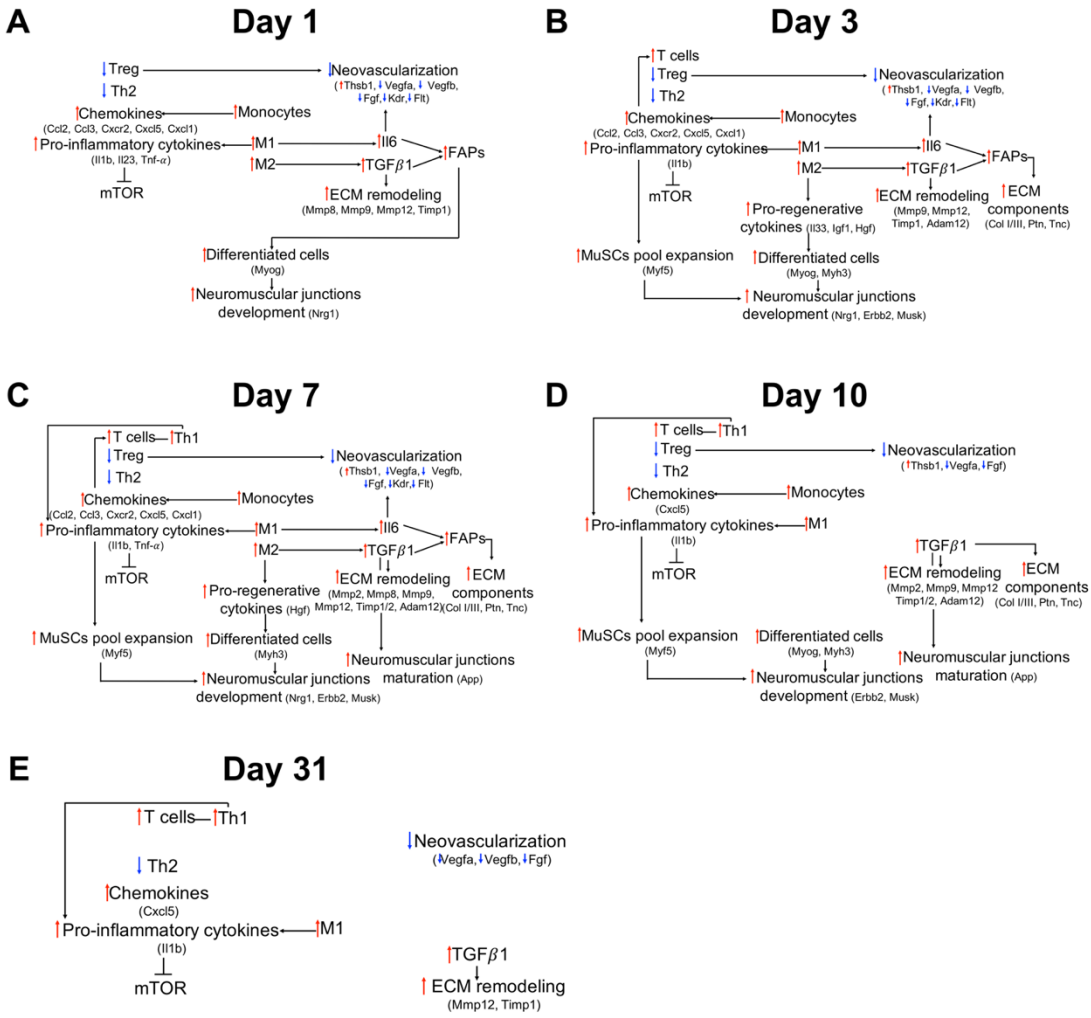

Figure 2.8. Schematic interpretation of the interplay between different pathways analyzed at multiple time points following simulated birth injury.
1 day (A), 3 days (B), 7 days (C), 10 days (D), 31 days (E).

2.3 Discussion

We demonstrate, for the first time, that pubovisceralis, which sustains the highest strains during vaginal delivery, exhibits substantial myofiber atrophy and severe fibrosis in parous women with symptomatic pelvic organ prolapse. The widespread degeneration observed in this group was not evident in PFMs procured from age-comparable nulliparous cadaveric donors without

history of PFDs. Furthermore, we recapitulated these pathological alterations in the rat model of SBI. Analyses of the PFM transcriptional signatures across multiple time points post SBI demonstrate a sustained inflammatory response, impairment in muscle anabolism, and persistent expression of ECM remodeling genes. These transcriptional alterations point towards putative mechanisms that account for PFM atrophy and fibrosis.

Maternal PFM birth injury and subsequent muscle dysfunction are major inciting events that lead to the development of pelvic floor disorders, especially pelvic organ prolapse, later in life. Radiologically detected PFM avulsions have been the widely acknowledged phenotype associated with PFDs and the primary focus of the literature to date. However, the radiological evidence of such mechanical uncoupling is not present in all women with decreased PFM strength, suggesting the existence of other causes of PFM dysfunction. Furthermore, published clinical studies indicate that a sizable proportion of PFM avulsions observed on imaging shortly after childbirth are no longer evident 1 year postpartum,[5] while large-scale cadaveric investigations demonstrate absence of radiologically-detected “avulsions” on direct anatomic dissections. [4] Together with our findings in the rat model [7], the above supports our notion that PFM birth injury can result in pathological transformations, other than avulsions, not detectable by routine imaging modalities. Expanding our understanding of PFM injuries beyond mechanical uncoupling is of utmost importance to foster identification of novel therapeutic targets and approaches. Previous studies have demonstrated that the morphological PFM changes associated with pelvic organ prolapse are muscle thinning and decreased volume identified with magnetic resonance imaging, indicative of muscle atrophy. [16, 17] In addition to myofiber atrophy, we identified dramatic fibrotic degeneration of PFMs in parous women with pelvic organ prolapse. To understand the mechanism of injury leading to such phenotype, we relied on an animal model to investigate PFM response to strains associated with birth injury.

The constructive regeneration of acutely injured limb muscles that returns them to the pre-injury state is mainly completed within a 4-week recovery period [9, 18]. In contrast, we demonstrate that the endogenous regenerative potential of PFMs is insufficient to restore the muscle to its baseline following SBI, resulting in PFM atrophy and fibrosis. Multiple studies conducted in the appendicular and trunk muscles conclude that acute skeletal muscle injury is followed by a temporally regulated immune response. The pro-inflammatory phase lasts up to 3-4 days post-injury, followed by the pro-regenerative phase that promotes tissue remodeling and repair. The transition towards the latter phase is influenced by a subpopulation of T-helper cells (Tregs) [19]. In our study, the pro-inflammatory and pro-regenerative phases overlapped during the acute period post-SBI (Fig. 2.8) with a sustained inflammatory response until day 31 post-injury. This could be attributed to the downregulation of Foxp3 gene, which is a transcription factor that is uniquely expressed in Tregs.[20] Our data suggest that the chronic inflammatory response of PFMs following SBI negatively impacts pathways related to muscle growth, acute ECM remodeling, and vascularization.

Skeletal muscle growth and repair occur via myogenesis (i.e., cellular turnover) or through increase in protein synthesis (i.e, anabolism). In limb muscles, the source of de novo myofibers observed acutely after muscle injury is committed MuSCs poised for immediate differentiation without proliferation. Following this swift differentiation, between 5 to 7 days post injury, the majority of remaining MuSCs self-renew to replenish the stem cell pool [13]. In our study, the early brief upregulation of pro-regenerative mediators correlated with the increased expression of genes associated with the MuSC differentiation and myofiber regeneration from 1 to 10 days (Fig. 2.8) and the increased density of differentiated $Myog^{+}$ MuSCs at 3 days post SBI (Fig. 2.4C). Consistently, the upregulation of pro-inflammatory cytokines coincided with the upregulation of genes involved in MuSC expansion from 3 to 10 days (Fig. 2.8); this was further correlated with the increased density of $Pax7^{+}$ MuSCs at 7 days (Fig. 2.4C). Given that myogenesis of PCa

followed the expected time course after SBI, we focused on the protein turnover pathways to determine potential mechanism responsible for PFM atrophy. The AkT/mTOR pathway plays a key role in protein synthesis and its activation is negatively influenced by prolonged inflammation[21]. Our data suggest that persistent inflammation after birth injury could be a culprit in the downregulation of the AkT/mTOR pathway, as indicated by the persistent downregulation of one of its main downstream targets (Rpskb1) until 31 days post injury. Furthermore, Il1, known to promote decrease in mTOR signaling, leading to muscle atrophy [21], was upregulated until day 31. The principal mechanism for activation of the AkT/mTOR pathway involves phosphorylation of its components, which we did not assess in the current study; however, published studies demonstrate correlation of this signaling pathway at the transcriptional, translational and post-translational levels during muscle anabolism. [22, 23]

Following acute muscle injury, a temporal increase in ECM deposition is crucial to provide a scaffold that regulates MuSC function and muscle repair. However, excessive ECM production and dysregulation of ECM metabolism leads to a pathological increase in intramuscular ECM components, mainly collagen I.[10] ECM remodeling mediators are secreted by damaged myofibers, immune cells, and fibroadipogenic progenitors (FAPs), which also support MuSC differentiation. [24] In our study, upregulation of Pdgfra, a gene that encodes the marker of FAPs in skeletal muscles [24], was followed by the increase in genes related to MuSC differentiation and ECM production from 3 to 10 days (Fig. 2.8). Although we observed an expected upregulation of genes associated with the temporal ECM deposition, we suggest that the sustained expression of Tgfb1, a master regulator of fibrosis, and Timp1, involved in inhibition of ECM degradation [10], lead to the long-term pathological increase in PFM collagen content.

After muscle injury, inflammation has been shown to alter vascularization with unknown overall impact on the intramuscular blood flow. [9, 12] In our study, the sustained inflammatory response was associated with the increased vessel number, specifically smaller arterioles. At the

gene expression level, we observed upregulation of the indirect stimulators of arteriogenesis (Ccl2, Tnfa, Tgfb1); however, direct stimulators (Fgf2, Vegfa, Vegfb, Flt1, Kdr, Angpt2) [25] were downregulated. Due to our targeted biased approach, we did not investigate other direct stimulators (Fgf1, Fgf4 or Pdgfb) that could also contribute to arteriogenesis.

One of the limitations of our study relies on a biased approach in designing the custom gene panel. We selected key genes based on the published literature to cover different pathways relevant to skeletal muscle regeneration, however, we are aware that this limits an unbiased and in-depth analysis of pathways' regulation following PFM injury. Secondly, we performed our studies in non-pregnant model to obviate the potential confounding effects of the complex hormonal milieu associated with pregnancy, size and number of pups, and the effects of spontaneous parturition.

In conclusion, our study demonstrates that PFMs in parous women with symptomatic pelvic floor disorders exhibit severe atrophy and fibrotic degeneration. In addition, we show that the rat birth injury model recapitulates this phenotype, with long-term muscle atrophy and fibrosis associated with sustained inflammatory response. This study provides the basis for scientifically rationale therapeutics for PFM dysfunction due to parturition.

2.4 Materials and methods

2.4.1 Study design

The objectives of this study were to: 1) determine and compare morphological properties of PFMs in parous women with symptomatic pelvic organ prolapse and age-comparable nulliparous cadaveric donors without history of pelvic floor disorders; and 2) investigate the endogenous response of PFMs to birth injury along the biologically-relevant continuum using validated pre-clinical model of SBI. The sample size, indicated in the figure legends, was

calculated *a priori* (see Statistical Analysis). No outliers were excluded from the study. For the quantitative analyses, the investigators were blinded to the group identity.

2.4.2 Pelvic floor muscle collection from women with pelvic organ prolapse

The pubovisceralis biopsies were obtained during surgical pelvic organ prolapse correction (n=20). Study participants were enrolled in the Institutional Review Board approved study at two sites— Kaiser Permanente San Diego and the University of California San Diego. Relevant obstetrical, surgical, and medical history were collected for each subject. Immediately after procurement, muscle biopsies were pinned to a cork at slack length, snap-frozen in isopentane chilled with liquid nitrogen, transported on dry ice, and stored in -80°C. At the time of tissue processing, tissue was embedded in optimal cutting temperature material for cryosectioning and snap-frozen again. Ten micron-thick cross-sections were stained with Hematoxylin and Eosin for myofibrillar shape and packing, Oil-red-O for intramuscular fat content, and Gomori's trichrome for collagen content, fiber area, and centralized nuclei, using well-established methods.

2.4.3 Cadaveric pelvic floor muscle collection

Nulliparous cadaveric donors without history of pelvic floor disorders were used as controls (n=4). Samples were obtained through the Bequest Body Donation Program at the University of Minnesota, which provides relevant obstetrical, surgical, and medical history for each donor. Donors with history of gynecologic or colorectal malignancy, pelvic metastasis, pelvic radiation, connective tissue disorder, myopathy, rectal prolapse, colectomy, or proctectomy were excluded. Biopsies of pubovisceralis were obtained from the muscle mid-belly within 7 days post-mortem and immediately processed as described above.

2.4.4 Simulated birth injury rat model

All procedures were approved by the Institutional Animal Care and Use Committee at the University of California, San Diego. Three-month-old non-pregnant Sprague-Dawley female rats (Envigo, Indianapolis, IN) were anesthetized using 2.5% isoflurane with oxygen for the duration of the procedure. Vaginal distention was performed using an established protocol. [7].Briefly, a 12-French transurethral catheter (Bard Medical, Covington, GA) with the tip cut off was inserted into the vagina with 130 grams weight attached to the end of the catheter. The balloon was inflated to 5 ml and left in place for 2 hours, after which it was pulled through the introitus to replicate circumferential and downward strains associated with parturition.

2.4.5 Rat pelvic floor muscle collection to assess endogenous response to simulated birth injury

For subacute and long-term outcomes, animals were sacrificed and PCa was harvested 4 or 8 weeks post-SBI. To assess early response to SBI, PCa was harvested at 1, 3, 7, or 10 days post-injury to assess the overall tissue morphology by H&E and to quantify phases of myogenesis by immunohistochemistry. Harvested muscles were embedded in optimal cutting temperature material and snap-frozen in isopentane chilled with liquid nitrogen. Expression of genes relevant to muscle regeneration was performed using Nanostring to investigate putative mechanisms accountable for the long-term muscle phenotype. PCa was harvested at 1, 3, 7, 10, 31 and 35 days post-SBI—time points of ongoing muscle regeneration. Muscles were submerged in RNAlater™, stored at 4°C overnight, and transferred to -80°C before RNA isolation.

2.4.6 Histological analysis

Hematoxylin and Eosin (H&E), Oil-red-O, Masson's Trichrome (Polysciences kit) stainings were done as described previously [26]. Immunohistochemistry was done to stain laminin, vessels,

quiescent and activated muscle stem cells, and differentiated muscle stem cells. Histological analyses were done with a Leica Aperio ScanScope® CS^2 (H&E), Leica Ariol® (Laminin, vessels), and Leica DM600B (muscle stem cells). A pathologist—blinded to the time points after SBI—performed a qualitative assessment of the H&E images. For fiber area and centralized nuclei, anti-laminin antibody (Abcam, Cambridge, MA; 1:200) was used and an Alexa Fluor 488 conjugated secondary antibody (Invitrogen, Carlsbad, California; 1:500), and nuclei were counterstained with Hoechst 33342. Fiber area was measured using a custom ImageJ (NIH, Bethesda, MD) Macro for a total of approximately 10,000 fibers per sample, covering 8 tissue sections. Fibers with centralized nuclei were manually counted from the same tissue sections and divided by the total number of fibers per section. For vessels staining, arterioles were stained with an alpha-smooth muscle actin (αSMA) antibody (Dako, Carpinteria, California; 1:75) and an Alexa Fluor 488 conjugated secondary antibody (Invitrogen, Carlsbad, California; 1:500), and nuclei were counterstained with Hoechst 33342. Five regions of interest per tissue section at 10X were obtained throughout 5 sections per sample. The midline of arterioles was traced and the average feret (maximum and minimum) diameter was recorded using ImageJ. Muscle stem cells density was assessed by an anti-Pax-7 antibody (DSHB, Iowa city, Iowa; 1:100), co-stained with anti-laminin antibody (Abcam, Cambridge, MA; 1:200) and an Alexa Fluor 488 and 594 conjugated antibodies (Invitrogen, Carlsbad, California; 1:250), respectively, and nuclei were counterstained with Hoechst 33342. $Pax\text{-}7^+$ cells located below laminin were quantified in 4 regions of interest per section at 20X, for a total of 8 sections per sample. Number of cells was normalized to area per image, to obtain cell density. Differentiated muscle stem cells was performed with anti-myogenin antibody (Abcam, Cambridge, MA; 1:200), co-stained with anti-laminin antibody (Abcam, Cambridge, MA; 1:200) and an Alexa Fluor 488 and 594 conjugated antibodies (Invitrogen, Carlsbad, California; 1:250), respectively, and nuclei were counterstained with Hoechst 33342. Imaging analysis was performed as described for Pax7.

2.4.7 RNA isolation and Nanostring

Samples were thawed, homogenized with a sonicator (TissueRuptorII, Qiagen, Germantown, Maryland) and RNA was isolated with RNAeasy Fibrous Tissue Mini Kit following manufacturer instructions (Qiagen, Germantown, Maryland). We used NanoString nCounter ® MAX Analysis System with an nCounter® custom codeset designed for rat with different categories take into consideration (Table S1 for a complete gene list). Briefly, RNA concentration was measured using a Qubit 3.0 Fluorometer with a Qubit™ RNA HS Assay kit. The hybridization buffer (70 µl) was then mixed with the Custom Reporter CodeSet solution, and 8 µl of this master mix was then added separately to 50-100 ng of RNA per tissue sample, and RNA-free water up to 13 µl total. Then, 2 µl of Capture ProbeSet was added to the mixture, thoroughly mixed and placed on a thermocycler at 65°C for 16-48 hours and then maintained at 4°C for less than 24 hours. Using a two-step magnetic beads purification, probe excess was removed in PrepStation and target/probe complexes were bound on the cartridge. The data was collected by the digital analyzer (NanoString nCounter® Digital Analyzer) with images of immobilized fluorescent reporters in the sample cartridge. Results of barcode reads were analyzed by nSolver™ Analysis Software 4.0 and differential expression analysis was done with a custom R script. The nanostring data were visualized using QIIME 2 (https://view.qiime2.org/) and ggplot and pheatmap packages in R.

2.4.8 Statistical Analysis

Sample size for histological analysis was determined based on a previous study. [27] Using G*power software, 6 animals/group/timepoint were needed to achieve 90% power at a significance level of 0.05. For gene expression studies, preliminary data with qRT-PCR were used to obtain sample size. Ten animals/group/timepoint were needed to achieve 80% power at a significance level set to 0.05. Data that followed a parametric distribution were compared using a

Student's t-test, or a one-way analysis of variance followed by Tukey's post hoc pairwise comparisons. Non-parametrically distributed variables, such as fiber area, were analyzed by Mann-Whitney or Kruskal-Wallis test followed by Dunn's pairwise comparisons. [28, 29] Data were analyzed using GraphPad Prism v8.0, San Diego, CA. Gene expression normalization and differential expression was analyzed using the NanoStringDiff package in R, with a significance at a p value<0.05 and a fold change cutoff of 1 ± 0.25. [30]

2.5 Acknowledgements

Chapter 2, in part, is currently being prepared for re-submission for publication of the material, Pamela Duran, Francesca Boscolo Sesillo, Lindsey Burnett, Shawn A. Menefee, Mark Cook, Gisselle Zazueta-Damian, Monika Dzieciatkowska, Emmy Do, Saya French, Manali M. Shah, Clyde Sanvictores, Kirk C. Hansen, Matthew Shtrahman, Karen L. Christman, Marianna Alperin. "Pro-regenerative Extracellular Matrix Hydrogel Prevents and Mitigates Pathological Alterations of Pelvic Muscles Following Birth Injury". The dissertation author was the first author of this paper.

2.6 References

1. Brooks, S., Zerba, E., Faulkner, J., Injury to muscle fibres after single stretches of passive and maximally stimulated muscles in mice*. Journal of Physiology*. 1995; 488(2): p. 459-469.

2. Hoyte, L., M.S. Damaser, S.K. Warfield, G. Chukkapalli, A. Majumdar, D.J. Choi, A. Trivedi, and P. Krysl, Quantity and distribution of levator ani stretch during simulated vaginal childbirth*. Am J Obstet Gynecol*. 2008; 199(2): p. 198 e1-5.

3. Jing, D., J.A. Ashton-Miller, and J.O. DeLancey, A subject-specific anisotropic visco-hyperelastic finite element model of female pelvic floor stress and strain during the second stage of labor*. J Biomech*. 2012; 45(3): p. 455-60.

4. Da Silva, A.S., G.A. Digesu, C. Dell'Utri, H. Fritsch, P. Piffarotti, and V. Khullar, Do ultrasound findings of levator ani "avulsion" correlate with anatomical findings: A multicenter cadaveric study. *Neurourol Urodyn*. 2016; 35(6): p. 683-8.

5. van Delft, K.W., R. Thakar, A.H. Sultan, J. IntHout, and K.B. Kluivers, The natural history of levator avulsion one year following childbirth: a prospective study. *BJOG*. 2015; 122(9): p. 1266-73.

6. Alperin, M., L.J. Tuttle, B.R. Conner, D.M. Dixon, M.A. Mathewson, S.R. Ward, and R.L. Lieber, Comparison of pelvic muscle architecture between humans and commonly used laboratory species. *Int Urogynecol J*. 2014; 25(11): p. 1507-15.

7. Catanzarite, T., S. Bremner, C.L. Barlow, L. Bou-Malham, S. O'Connor, and M. Alperin, Pelvic muscles' mechanical response to strains in the absence and presence of pregnancy-induced adaptations in a rat model. *Am J Obstet Gynecol*. 2018; 218(5): p. 512 e1-512 e9.

8. Lieber RL, F.J., Mechanisms of muscle injury gleaned from animal models. . *Am J Phys Med Rehabil*. 2002; 81: p. 81-S79.

9. Hardy, D., A. Besnard, M. Latil, G. Jouvion, D. Briand, C. Thepenier, Q. Pascal, A. Guguin, B. Gayraud-Morel, J.M. Cavaillon, S. Tajbakhsh, P. Rocheteau, and F. Chretien, Comparative Study of Injury Models for Studying Muscle Regeneration in Mice. *PLoS One*. 2016; 11(1): p. e0147198.

10. Gillies, A.R. and R.L. Lieber, Structure and function of the skeletal muscle extracellular matrix. *Muscle Nerve*. 2011; 44(3): p. 318-31.

11. Ranjbar, K., F. Rahmani-Nia, and E. Shahabpour, Aerobic training and l-arginine supplementation promotes rat heart and hindleg muscles arteriogenesis after myocardial infarction. *J Physiol Biochem*. 2016; 72(3): p. 393-404.

12. Gibbons, M.C., A. Singh, O. Anakwenze, T. Cheng, M. Pomerantz, S. Schenk, A.J. Engler, and S.R. Ward, Histological Evidence of Muscle Degeneration in Advanced Human Rotator Cuff Disease. *J Bone Joint Surg Am*. 2017; 99(3): p. 190-199.

13. Rantanen, J., Hurme, T., Lukka, R., Heino, J., Kalimo., Satellite cell proliferation and the expression of myogenin and desmin in regenerating skeletal muscle: evidence for two different populations of satellite cells. *Lab Invest*. 1995; 72(3): p. 341-7.

14. Riuzzi, F., G. Sorci, R. Sagheddu, and R. Donato, HMGB1-RAGE regulates muscle satellite cell homeostasis through p38-MAPK- and myogenin-dependent repression of Pax7 transcription. *J Cell Sci*. 2012; 125(Pt 6): p. 1440-54.

15. Berberoglu, M.A., T.L. Gallagher, Z.T. Morrow, J.C. Talbot, K.J. Hromowyk, I.M. Tenente, D.M. Langenau, and S.L. Amacher, Satellite-like cells contribute to pax7-dependent skeletal muscle repair in adult zebrafish. *Dev Biol*. 2017; 424(2): p. 162-180.

16. Hoyte, L., M. Jakab, S.K. Warfield, S. Shott, G. Flesh, and J.R. Fielding, Levator ani thickness variations in symptomatic and asymptomatic women using magnetic

resonance-based 3-dimensional color mapping. *Am J Obstet Gynecol*. 2004; 191(3): p. 856-61.

17. Hoyte, L., L. Schierlitz, K. Zou, G. Flesh, and J.R. Fielding, Two- and 3-dimensional MRI comparison of levator ani structure, volume, and integrity in women with stress incontinence and prolapse. *Am J Obstet Gynecol*. 2001; 185(1): p. 11-9.

18. McCully, K., Faulkner, J., Injury to skeletal muscle fibers of mice following lengthening contractions. *Am J Physiol* 1985: p. 119-126.

19. Tidball, J.G., Regulation of muscle growth and regeneration by the immune system. *Nat Rev Immunol*. 2017; 17(3): p. 165-178.

20. Castiglioni, A., G. Corna, E. Rigamonti, V. Basso, M. Vezzoli, A. Monno, A.E. Almada, A. Mondino, A.J. Wagers, A.A. Manfredi, and P. Rovere-Querini, FOXP3+ T Cells Recruited to Sites of Sterile Skeletal Muscle Injury Regulate the Fate of Satellite Cells and Guide Effective Tissue Regeneration. *PLoS One*. 2015; 10(6): p. e0128094.

21. Costamagna, D., P. Costelli, M. Sampaolesi, and F. Penna, Role of Inflammation in Muscle Homeostasis and Myogenesis. *Mediators Inflamm*. 2015; 2015: p. 805172.

22. Morissette, M.R., S.A. Cook, C. Buranasombati, M.A. Rosenberg, and A. Rosenzweig, Myostatin inhibits IGF-I-induced myotube hypertrophy through Akt. *Am J Physiol Cell Physiol*. 2009; 297(5): p. C1124-32.

23. Boudra, R., R. Lagrafeuille, C. Lours-Calet, C. de Joussineau, G. Loubeau-Legros, C. Chaveroux, J.P. Saru, S. Baron, L. Morel, and C. Beaudoin, mTOR transcriptionally and post-transcriptionally regulates Npm1 gene expression to contribute to enhanced proliferation in cells with Pten inactivation. *Cell Cycle*. 2016; 15(10): p. 1352-62.

24. Biferali, B., D. Proietti, C. Mozzetta, and L. Madaro, Fibro-Adipogenic Progenitors Cross-Talk in Skeletal Muscle: The Social Network. *Front Physiol*. 2019; 10: p. 1074.

25. Carmeliet, P., Mechanisms of angiogenesis and arteriogenesis. *Nature Review*. 2000; 6(3): p. 389-395.

26. Phillips, D.I.W., Caddy, S., Ilic, V., Fielding, B.A., Frayn, K.N., Borthwick, A.C., Taylor, R., Intramuscular triglyceride and muscle insulin sensitivity: Evidence for a relationship in nondiabetic subjects. *Metabolism*. 1996; 45(8): p. 947-950.

27. Ungerleider, J.L., T.D. Johnson, M.J. Hernandez, D.I. Elhag, R.L. Braden, M. Dzieciatkowska, K.G. Osborn, K.C. Hansen, E. Mahmud, and K.L. Christman, Extracellular Matrix Hydrogel Promotes Tissue Remodeling, Arteriogenesis, and Perfusion in a Rat Hindlimb Ischemia Model. *JACC Basic Transl Sci*. 2016; 1(1-2): p. 32-44.

28. Baghdadi, M.B., D. Castel, L. Machado, S.I. Fukada, D.E. Birk, F. Relaix, S. Tajbakhsh, and P. Mourikis, Reciprocal signalling by Notch-Collagen V-CALCR retains muscle stem cells in their niche. *Nature*. 2018; 557(7707): p. 714-718.

29. Sun, X., Wu, J., Qiang, B., Romagnuolo, R., Gagliardi, M., Keller, G., Laflamme, M., Li, R., Nunes, S., Transplanted microvessels improve pluripotent stem cell–derived cardiomyocyte engraftment and cardiac function after infarction in rats*. Sci. Transl. Medi*. 2020; 12.

30. Raman, A.T., A.E. Pohodich, Y.W. Wan, H.K. Yalamanchili, W.E. Lowry, H.Y. Zoghbi, and Z. Liu, Apparent bias toward long gene misregulation in MeCP2 syndromes disappears after controlling for baseline variations*. Nat Commun*. 2018; 9(1): p. 3225.

Chapter 3: Pro-regenerative extracellular matrix hydrogel prevents and mitigates pathological alterations of pelvic floor muscles following birth injury

3.1 Introduction

Beyond the lack of fundamental knowledge regarding tissue- and cell-level alterations that govern pelvic floor muscle (PFM) dysfunction, there are currently minimal strategies to preempt the maladaptive recovery of PFMs following birth injury. As mentioned in chapter 1, PFM exercises have been recommended to compensate for PFM weakness in pregnant and postpartum women. However, this therapy is associated with poor adherence [1]. Furthermore, the existing treatments for PFM dysfunction and the associated pelvic floor disorders are plagued with high failure rates [2, 3], while the only preventative strategy for birth injury - Cesarean section – increases the risk of maternal morbidity and mortality compared to vaginal delivery [4]. Given the dramatic prevalence of pelvic floor disorders, novel preventative and therapeutic approaches are urgently needed to address this public health problem. One potential tactic is to potentiate constructive remodeling of PFMs following birth injury with the ultimate goal of preventing PFM dysfunction and the resultant pelvic floor disorders. We have previously demonstrated that a decellularized porcine skeletal muscle extracellular matrix (ECM) hydrogel (SKM) promoted constructive muscle remodeling and prevented atrophy in ischemic skeletal muscle through upregulation of pathways related to myogenesis and blood vessel development [5]. Therefore, our objective was to investigate the efficacy of SKM, administered at two clinically relevant time points, for the prevention and treatment of the pathological PFM alterations consequent to simulated birth injury, previously identified in chapter 2.

In the current study, we observed that a acellular pro-regenerative biomaterial prevented and mitigated the pathological alterations of PFMs by modulating the immune response and

enhancing myogenesis, signifying its potential as a new preventative therapy for PFM pathologies following birth injury.

3.2 Results

3.2.1 Skeletal muscle ECM hydrogel prevents pelvic floor muscle atrophy and mitigates fibrosis when administered at the time of simulated birth injury

As indicated on chapter 2, PFM undergo incomplete recovery after SBI. Thus, we then went on to investigate whether SKM, an ECM hydrogel derived from decellularized porcine skeletal muscle, could potentiate muscle recovery when injected directly into pubocaudalis (PCa) at the time of SBI. We hypothesized that the immunomodulatory properties of the SKM would counteract the sustained PFM inflammatory response to SBI by inducing an early transition to the pro-regenerative environment [5]. Injection of saline served as an experimental control (Fig. 3.1A). Data from animals at 4 weeks following SBI without any injection were used for comparison, given the reproducibility of our model (Fig. 3.2). Fiber area and collagen content were quantified 4 weeks post-SBI+injection. While saline injection increased fiber area compared to untreated SBI ($P<0.0001$), SKM injection resulted in a substantially greater increase in fiber area compared to saline ($P<0.0001$), with return of fiber size to the uninjured levels (SBI+SKM vs controls: $P>0.99$, Fig. 3.1B). SKM also lowered collagen deposition relative to untreated SBI ($P=0.02$), bringing intramuscular collagen content down to the level not significantly different from uninjured pubocaudalis ($P=0.6$). However, this response was similar to that observed in the SBI+saline group ($P=0.5$, Fig. 3.1C). These results indicate that SKM prevents PFM atrophy, restoring fiber size to the uninjured state, and mitigates fibrotic degeneration of the PFMs consequent to birth injury. With respect to vascularization, the arteriole density in the SKM group did not differ significantly compared to saline ($P=0.5$), untreated SBI ($P=0.4$), or uninjured controls ($P=0.1$); whereas it was significantly higher in the saline group compared to uninjured controls ($P=0.01$,

Fig. 3.1D). Analysis of the arteriole density by size revealed that the smaller arterioles (11-25 μm) decreased in SKM group relative to untreated SBI (P=0.002); however, this decrease did not reach statistically significant difference compared to saline (P=0.09, Fig. 3.1E). The above suggests that SKM mitigates the arteriole-level vascular alterations of PFMs observed after birth injury.

We went on to assess transcriptional regulation of the changes in the PFM phenotype induced by SKM injection at the time of birth injury. PCa was harvested 3 or 7 days post-SBI+injection (Fig. 3.1A) and analyzed with the same Nanostring panel (Table 2.1) for comparisons with the untreated SBI group. These timepoints correspond to the early inflammatory response and peak cell infiltration into the material, respectively. Based on the principal component analysis, SKM, saline and untreated SBI groups did not cluster separately at either time point (Fig. 3.1F-G); however, several genes were differentially expressed. Gene expression profiles across the samples per each timepoint are demonstrated in Figures 3.3-4. Clustered heat maps for each pathway, indicating fold change of SKM and saline in relation to untreated SBI and with differentially expressed genes between SKM and saline, are shown in Figures 3.1H-I, with pairwise comparisons illustrated in Figure 3.5.

At the earlier timepoint (3 days post SBI), SKM decreased the inflammatory response, as indicated by downregulation of Nos2, Il1b, Cxcl1, Ccl2, Ccl3, all of which are associated with a pro-inflammatory environment. In addition, we observed upregulation of genes associated with MuSC pool expansion (Pax7, Myf5) and a trend towards upregulation of a muscle transcription factor that encodes for de novo or fused myofibers (Myh3, P=0.06) at this timepoint. We also observed decreased expression of ECM remodeling genes at both timepoints (3 days: Mmp8, Mmp9; 7 days: Ccn2, Itga1) together with a trending downregulation of collagen I (Col1a1, P=0.07) at 7 days. Decreased expression of Vegfa and Kdr, both associated with vascularization, was observed at both timepoints. Downregulation of Tnc, involved in the development of

neuromuscular junctions, was identified at 7 days. Altogether, our results indicate that compared to saline, SKM treatment at the time of birth injury decreases inflammatory response and ECM remodeling related PFM genes and upregulates genes in the myogenesis pathway early on.

Figure 3.1. Injection of skeletal muscle extracellular matrix hydrogel (SKM) at the time of simulated birth injury (SBI) prevents pelvic floor muscle atrophy and mitigates fibrosis.
(A) Study timeline. Pubocaudalis muscle of uninjured controls; and animals subjected to SBI, SBI + saline injection, or SBI + SKM injection were compared with respect to fiber cross-sectional area (B); collagen content (C); overall vessel (arteriole) density (D); and vessel (arteriole) density separated by size (E). Principal components analysis of transcriptional signatures at 3 (F) and 7 (G) days post-SBI with and without injection. Supervised heat map of fold changes for SKM and saline with respect to untreated SBI at 3 (H) and 7 (I) days. Heat map includes significantly differentially expressed genes based on the pairwise comparison between SKM and saline groups. N=6/group for histological assessments, and 8-9/group for gene expression analyses. *P*-values derived from one-way ANOVA followed by pairwise comparisons with Tukey's range test for parametric data and Kruskal-Wallis followed by pairwise comparisons with Dun's test for non-parametrically distributed data. Gene expression analysis was analyzed based on NanoStringDiff package in R. *$p<0.05$, **$p<0.01$, ****$p<0.0001$, mean±SEM.

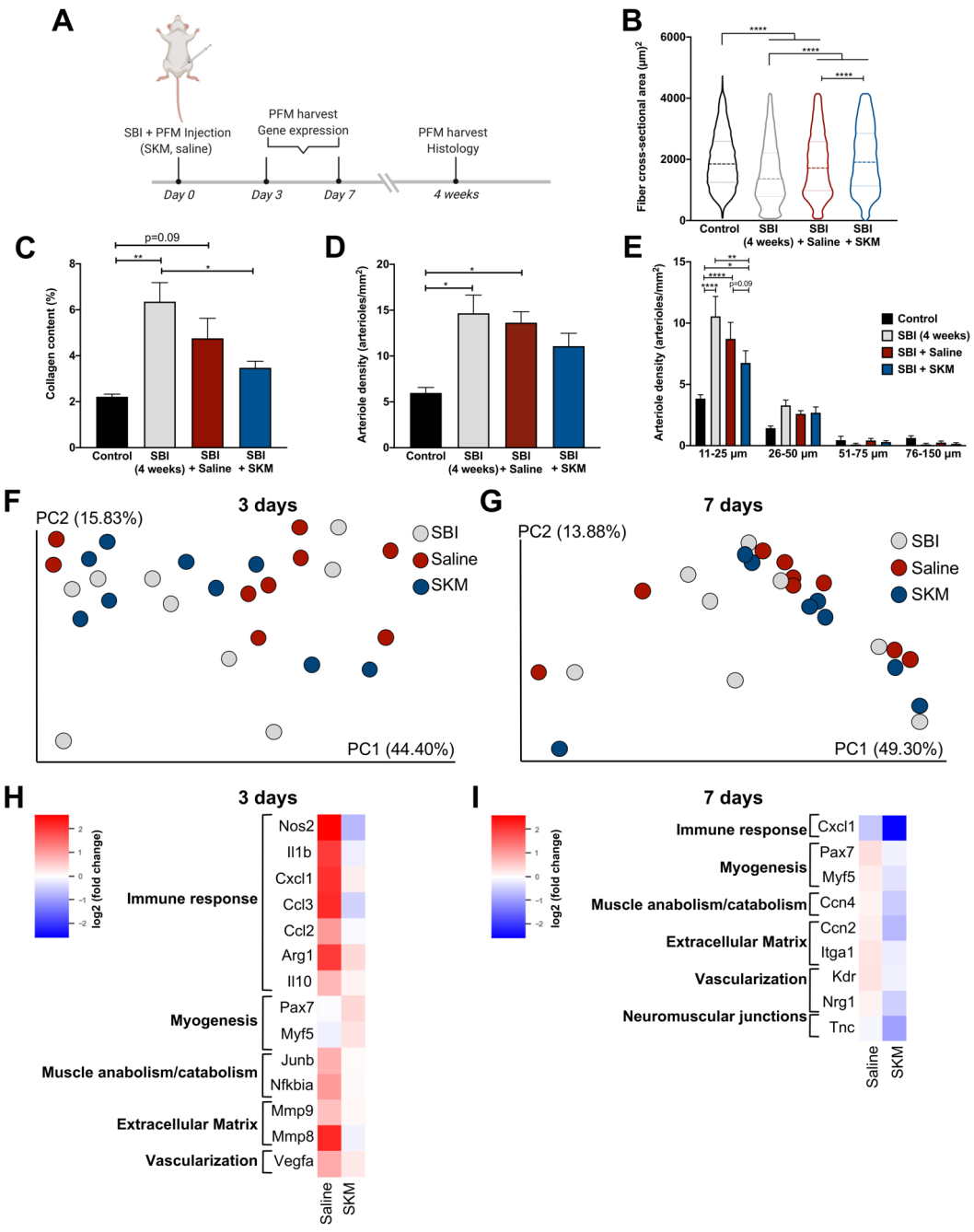
A
SBI + PFM Injection
(SKM, saline)
PFM harvest
Gene expression
PFM harvest
Histology
Day 0
Day 3
Day 7
4 weeks
B
Fiber cross-sectional area (µm)²
Control
SBI (4 weeks)
SBI + Saline
SBI + SKM
C
Collagen content (%)
p=0.09
D
Arteriole density (arterioles/mm²)
E
Arteriole density (arterioles/mm²)
11-25 µm
26-50 µm
51-75 µm
76-150 µm
F
3 days
PC2 (15.83%)
PC1 (44.40%)
SBI
Saline
SKM
G
7 days
PC2 (13.88%)
PC1 (49.30%)
H
3 days
log2 (fold change)
Immune response
Nos2
Il1b
Cxcl1
Ccl3
Ccl2
Arg1
Il10
Myogenesis
Pax7
Myf5
Muscle anabolism/catabolism
Junb
Nfkbia
Extracellular Matrix
Mmp9
Mmp8
Vascularization
Vegfa
Saline
SKM
I
7 days
Immune response
Cxcl1
Myogenesis
Pax7
Myf5
Muscle anabolism/catabolism
Ccn4
Extracellular Matrix
Ccn2
Itga1
Vascularization
Kdr
Neuromuscular junctions
Nrg1
Tnc
Saline
SKM

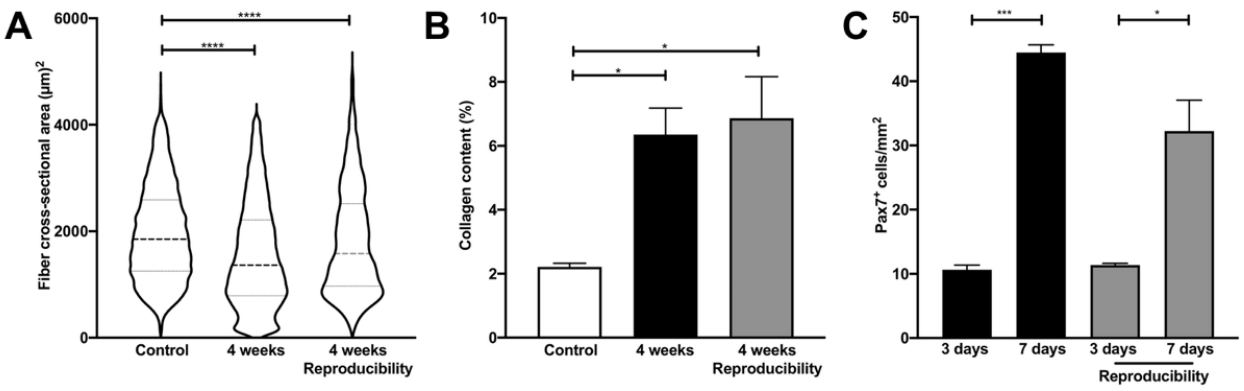

Figure 3.2. Reproducibility of simulated birth injury (SBI).
A separate set of animals underwent SBI to assure the reproducibility of the main study outcomes. (A) Violin plot of fiber cross-sectional area. (B) Collagen content quantification. (C) Cell density of muscle stem cells. SBIs and quantification analyses for this set of animals were performed by the researchers not involved in the SBI experiments or analyses described in the main results. N=3-7/group. P-values derived from Student's t-tests or one-way ANOVA followed by pairwise comparisons with Tukey's range test for parametric and Mann-Whitney tests for non-parametric data.*p<0.05, ****p<0.0001, mean±SEM.

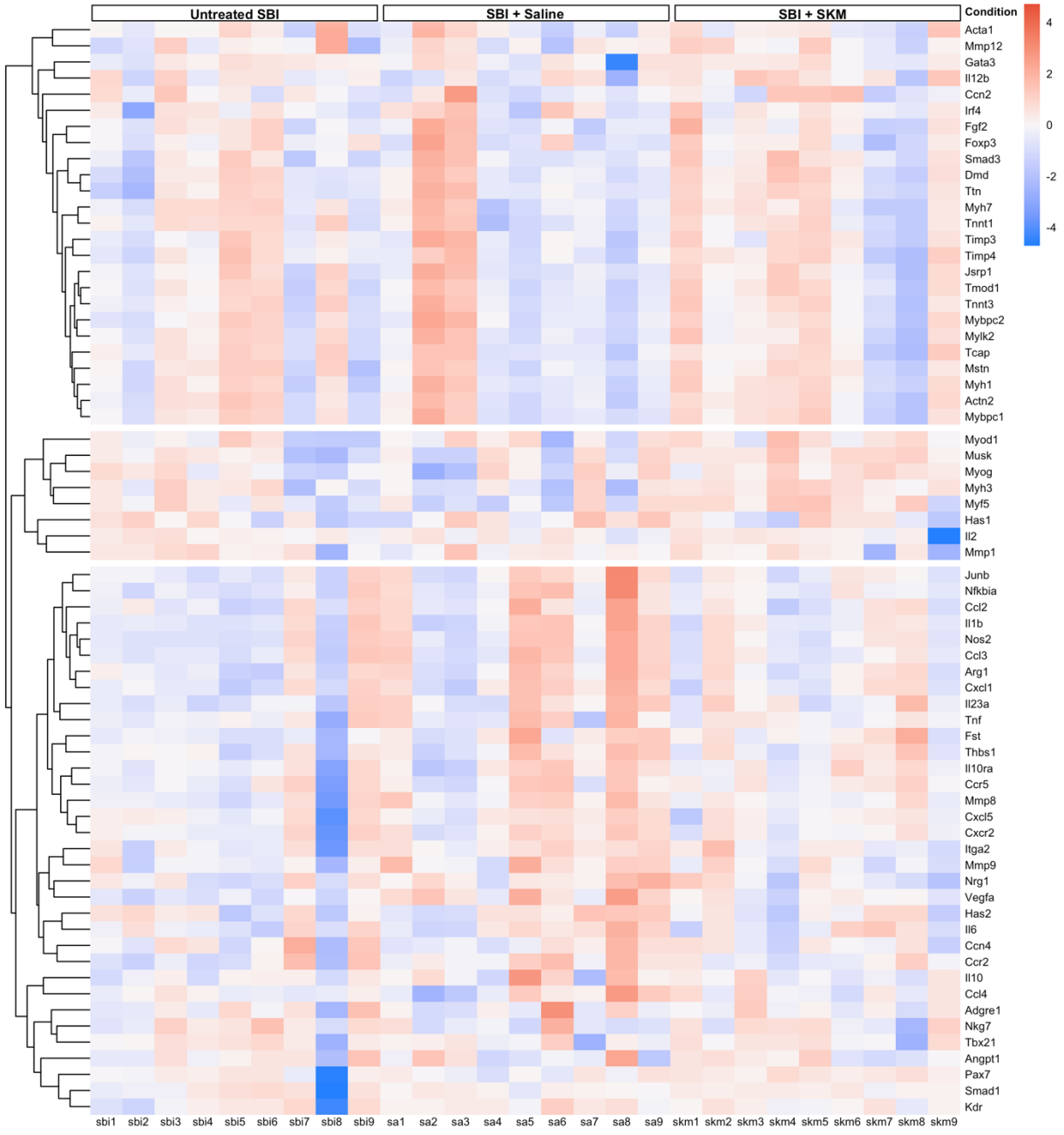

Figure 3.3. Gene expression profile across the samples 3 days after immediate injection of skeletal muscle extracellular matrix (SKM) hydrogel.
Heat map of genes with the highest variation in the dataset. N=8/9 per group.

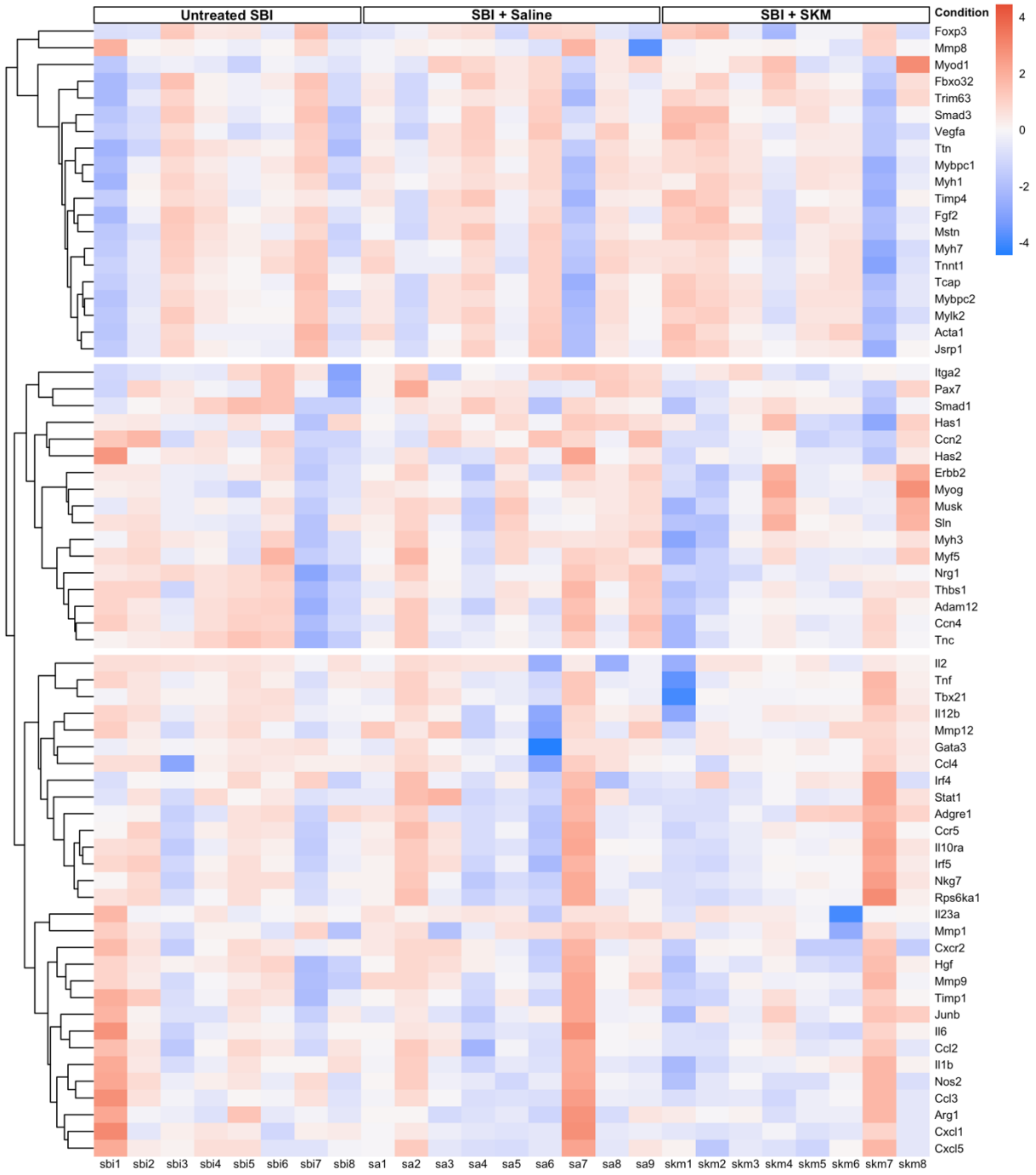

Figure 3.4. Gene expression profile across the samples 7 days after immediate injection of skeletal muscle extracellular matrix (SKM) hydrogel.
Heat map of genes with the highest variation in the dataset. N=8/9 per group.

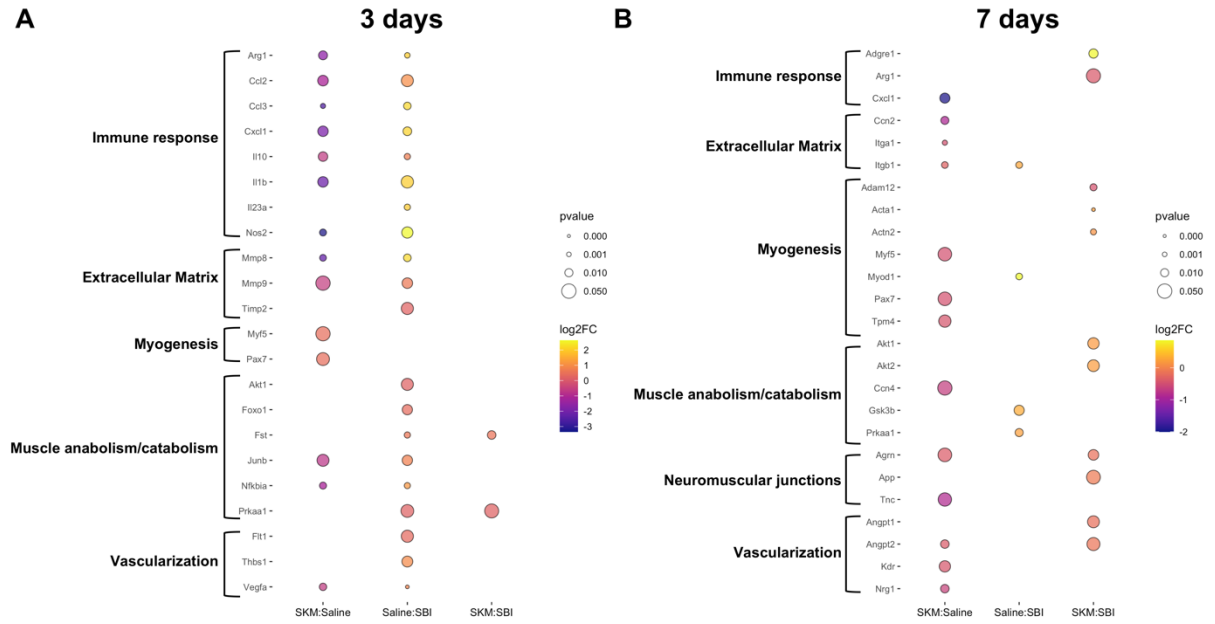

Figure 3.5. Pairwise comparisons after immediate injection of skeletal muscle extracellular matrix (SKM) hydrogel.
Significantly differentially expressed genes at 3 (A) and 7 (B) days.

3.2.2 Delayed injection of skeletal muscle ECM hydrogel prevents pelvic floor muscle atrophy and mitigates fibrosis

Given that delayed injection corresponding to the timing of a routine post-partum visit may be even more clinically relevant, we next evaluated whether treatment with SKM 4 weeks post-SBI can prevent PFM atrophy and fibrosis consequent to birth injury. SKM injection 4 weeks post-SBI (Fig. 3.6A) potentiated muscle recovery long-term, as evident from the increased fiber area compared to saline at 8 weeks post-SBI ($P<0.0001$). Interestingly, SKM administration at this time point resulted in the fiber area greater than that in uninjured controls ($P<0.0001$) (Fig. 3.6B). Saline injection also increased fiber area compared to untreated SBI ($P<0.0001$) but failed to return fiber size to the uninjured level ($P<0.0001$). We then analyzed fiber area 12 weeks post-SBI to visualize the effect of the biomaterial at an even longer time point (Fig. 3.6C). SKM injection

continued to demonstrate improvement in relation to saline ($P<0.001$) and untreated SBI ($P<0.05$) as observed by the increased fiber area. Surprisingly, SKM administration led to a smaller fiber area compared to uninjured controls ($P<0.001$). In addition, saline injection resulted in decreased fiber area in relation to untreated SBI ($P<0.001$). SKM decreased the fibrotic response compared to untreated SBI at both 8 weeks and 12 weeks post-SBI ($P=0.01$) restoring ECM collagen content to the uninjured levels (8 weeks; $P=0.8$, 12 weeks; $P=0.99$). Surprisingly, saline also significantly decreased collagen accumulation post injury relative to the untreated SBI group ($P=0.006$) at 8 weeks with a similar response 12 weeks post-injury ($P=0.1$) resulting in levels analogous to the uninjured controls (8 weeks; $P=0.8$, 12 weeks; $P=0.54$), similar to the effect of SKM (8 weeks; $P=0.9$, 12 weeks; $P=0.9$) (Fig. 3.6D-E). For arteriole density, both SKM and saline led to a decrease in the overall arteriole density (Fig. 3.6F), and specifically of smaller arterioles (Fig. 3.6G) compared to untreated SBI, restoring arteriole density to the uninjured levels ($P=0.9$). These results indicate that SKM administered 4 weeks after birth injury prevents PFM atrophy, mitigates fibrosis and restores vascularization. In addition, saline injection was sufficient to also mitigate fibrosis and restore vascularization to baseline levels.

We next analyzed the acute and subacute transcriptional changes in the PFM response to the delayed SKM injection, using the same Nanostring panel as described in chapter 2 (Table 2.1). PCa was harvested at 3- or 7-days post-injection, i.e. 31 and 35 days post-SBI (Fig. 3.6A). The PFM was also harvested at 8 weeks post-injection (Fig. 3.6A) to visualize the gene expression profile at the longer-term time point. Despite similar response to SKM and saline with respect to intramuscular collagen content and vascularization, the principal component analysis revealed that at the earliest time points, SKM mostly clustered separately from saline and untreated SBI, especially at 3-day time point, while saline clustered together with untreated SBI (Fig. 3.6H-I). At 8 weeks, the groups did not cluster separately, potentially due to the stabilization of the tissue after the injection (Fig. 3.6J). Gene expression profiles for each timepoint are

summarized in Figures 3.7-9. Clustered heat maps for each pathway indicating fold change in SKM and saline groups relative to untreated SBI and with differentially expressed genes between SKM and saline are shown in Figures 3.6K-M. Pairwise comparisons are shown in Figure 3.10. At both time points, SKM led to upregulation of genes related to the immune response, specifically monocytes (Myd88), macrophages (Adgre1), macrophages type 1 (Nos2, Irf5, Stat1), macrophages type 2 (Arg1, Irf4, Stat6), T cells (Nkg7), and T helper cells type 1 (Tbx21). We identified increased expression of genes associated with pro-inflammatory (Il12b, Il1b, Tnf, Ccl2, Ccl3, Ccl4, Ccr2, Ccr5, Cxcl1, Cxcl5, Cxcr2), as well as pro-regenerative (Il10ra, Il33, Igf1) mediators. In addition, genes that code for mediators of myogenesis (3 days: Hgf; 7 days: Hgf, Adam12) and cellular survival (7 days: Has1, Ccn4) were upregulated. Genes associated with muscle structure were downregulated (3 days: Tnnt1, Tpm3, Tcap, Mylk2, Mybpc1, Mybpc2, Myh1, Acta1, Actn2, Myh7, Tnnt3, Tpm4, Ttn). While upstream genes of muscle anabolism pathway (Junb, Rps6ka1, Fst) were upregulated at 3 and 7 days, the downstream targets remained unchanged. Upregulation of ECM remodeling genes was identified at both time points (Mmp2, Mmp9, Timp1, Tgfb1, Ccn2), with increased expression of collagens I and III (Col1a1, Col3a1) at 7 days. Although receptor genes related to vascularization pathway were upregulated (Kdr, Nrp1, Tie1), the ligands were not differentially expressed. Lastly, we observed upregulation of genes involved in the development (Agrn, Erbb2, Ptn, Tnc) and maturation (App, Utrn) of neuromuscular junctions at 3 and 7 days. At the long-term time point of 8 weeks post-injection, SKM resulted in significant differential expression of only 4 genes, which could be associated with the stabilization of the tissue after the injection and the degradation of the hydrogel.[6] Upregulation of genes associated with the immune response were identified. This included macrophages (Adgre1), specifically type 2 phenotype (Irf4), and T cells (Nkg7). In addition, we observed downregulation of an ECM remodeling gene (Mmp8). Taken together, while at the acute and subacute timepoints studied, SKM increases the expression of genes associated with both pro-

inflammatory and pro-regenerative immune responses, at the long-term time point SKM upregulates few genes with one related to type 2 pro-regenerative response. In addition, ECM remodeling genes were upregulated at the earliest time points, with downregulation at 8 weeks. At last, SKM results in increased expression of genes related to myogenesis, and neuromuscular junction development and maturation within one week post-injection.

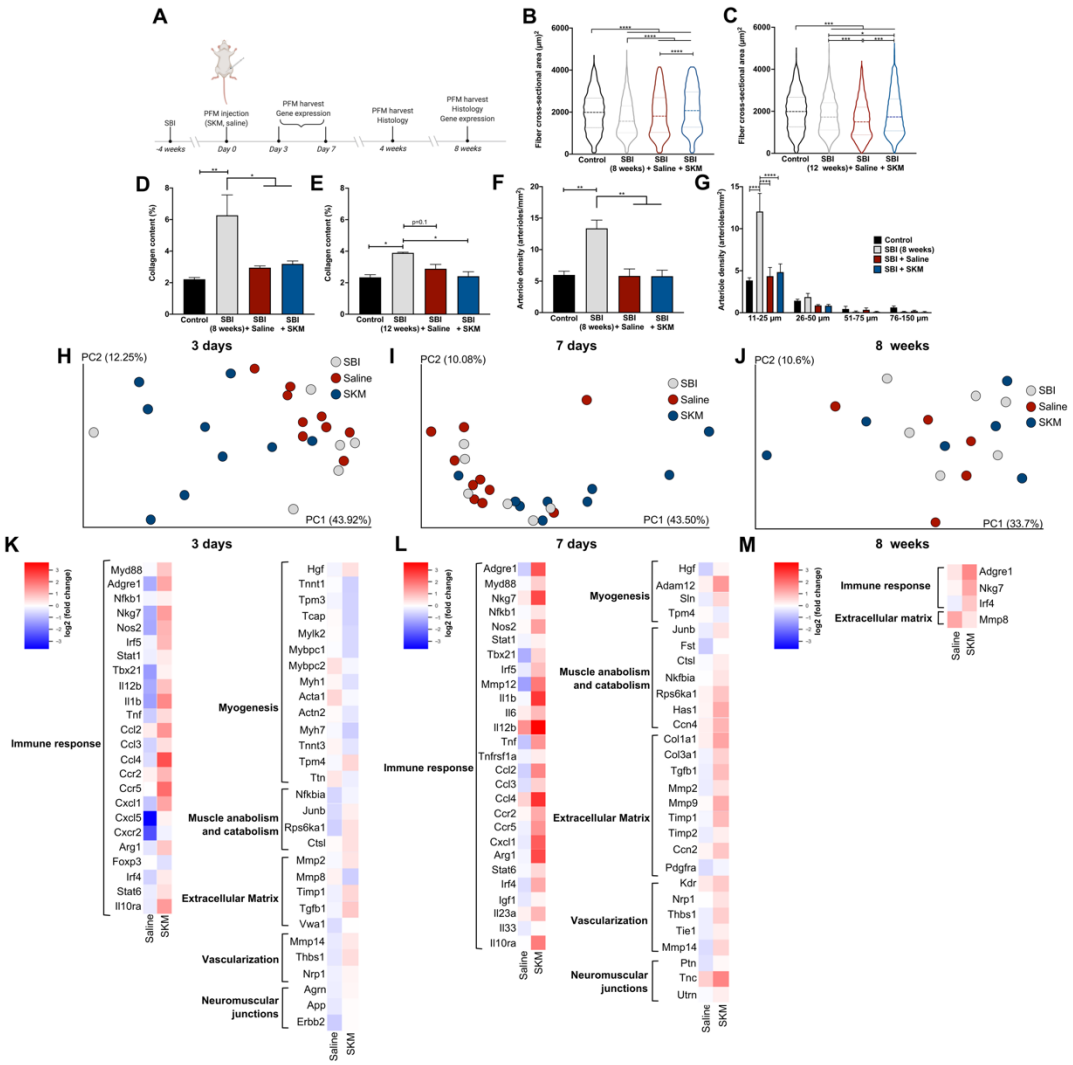

Figure 3.6. Delayed injection of skeletal muscle extracellular matrix hydrogel (SKM) prevents pelvic floor muscle atrophy and mitigates fibrosis.
(A) Study timeline. Pubocaudalis muscle of uninjured controls; and animals subjected to SBI, SBI + saline injection, or SBI + SKM injection were compared with respect to fiber cross-sectional area (B,C); collagen content (C,E); overall vessel density (F); and vessel density separated by size (G). Principal components analysis of transcriptional signatures at 3 (H), 7 (I) days, and 8 weeks (J) post-injection. Supervised heat map of fold changes for SKM and saline with respect to untreated SBI at 3 (K), 7 (L) days, and 8 weeks (M). Heat map includes significantly differentially expressed genes based on the pairwise comparison between SKM and saline groups. N=6/group for histological assessments, and 6-10/group for gene expression analyses. *P*-values derived from one-way ANOVA followed by pairwise comparisons with Tukey's range test for parametric data and Kruskal-Wallis followed by pairwise comparisons with Dun's test for non-parametrically distributed data. Gene expression analysis was analyzed based on NanoStringDiff package in R. *p<0.05, **p<0.01, ****p<0.0001, mean±SEM.

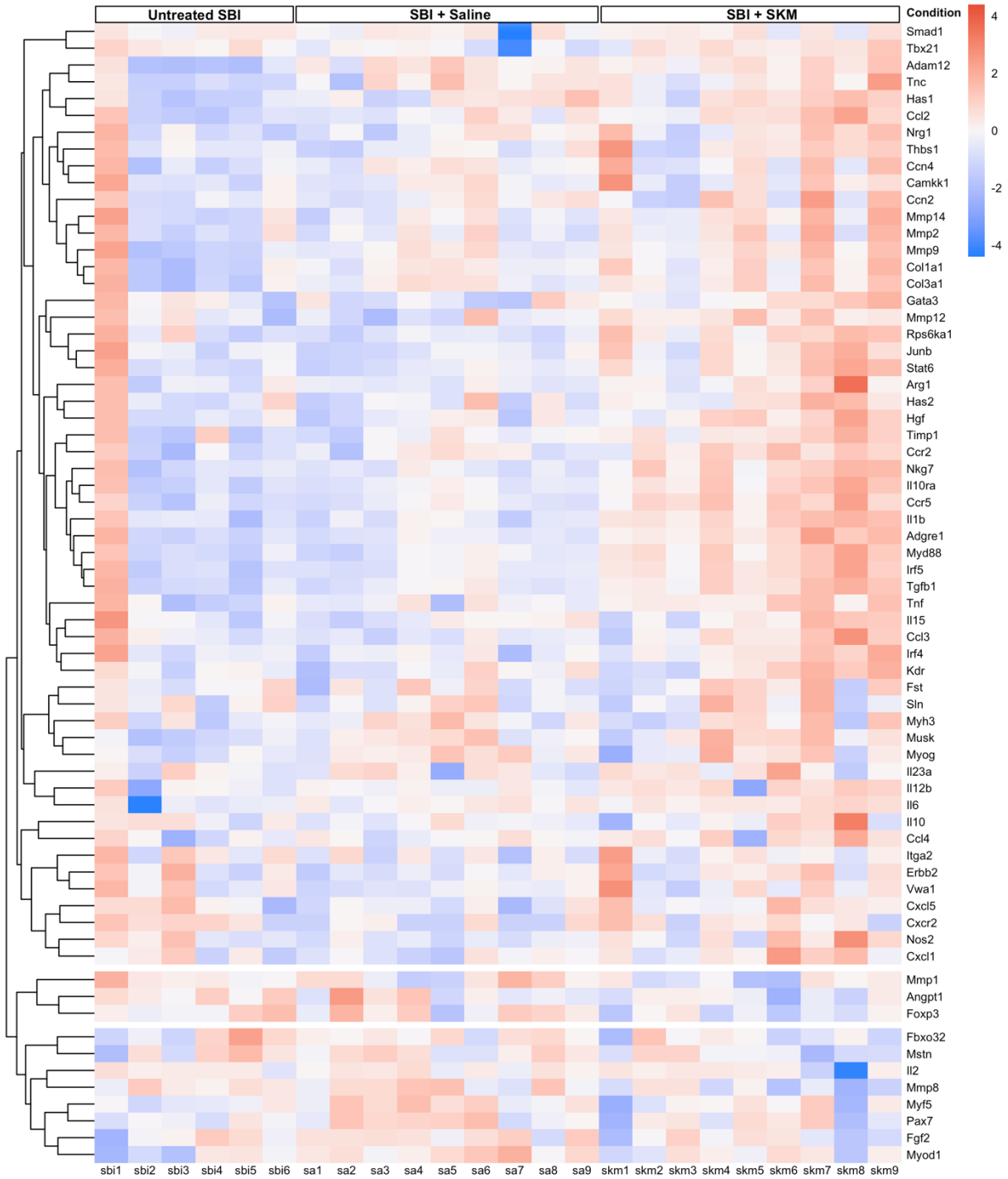

Figure 3.7. Gene expression profile across the samples 3 days after delayed injection of skeletal muscle extracellular matrix (SKM) hydrogel.
Heat map of genes with the highest variation in the dataset. N=6/9 per group.

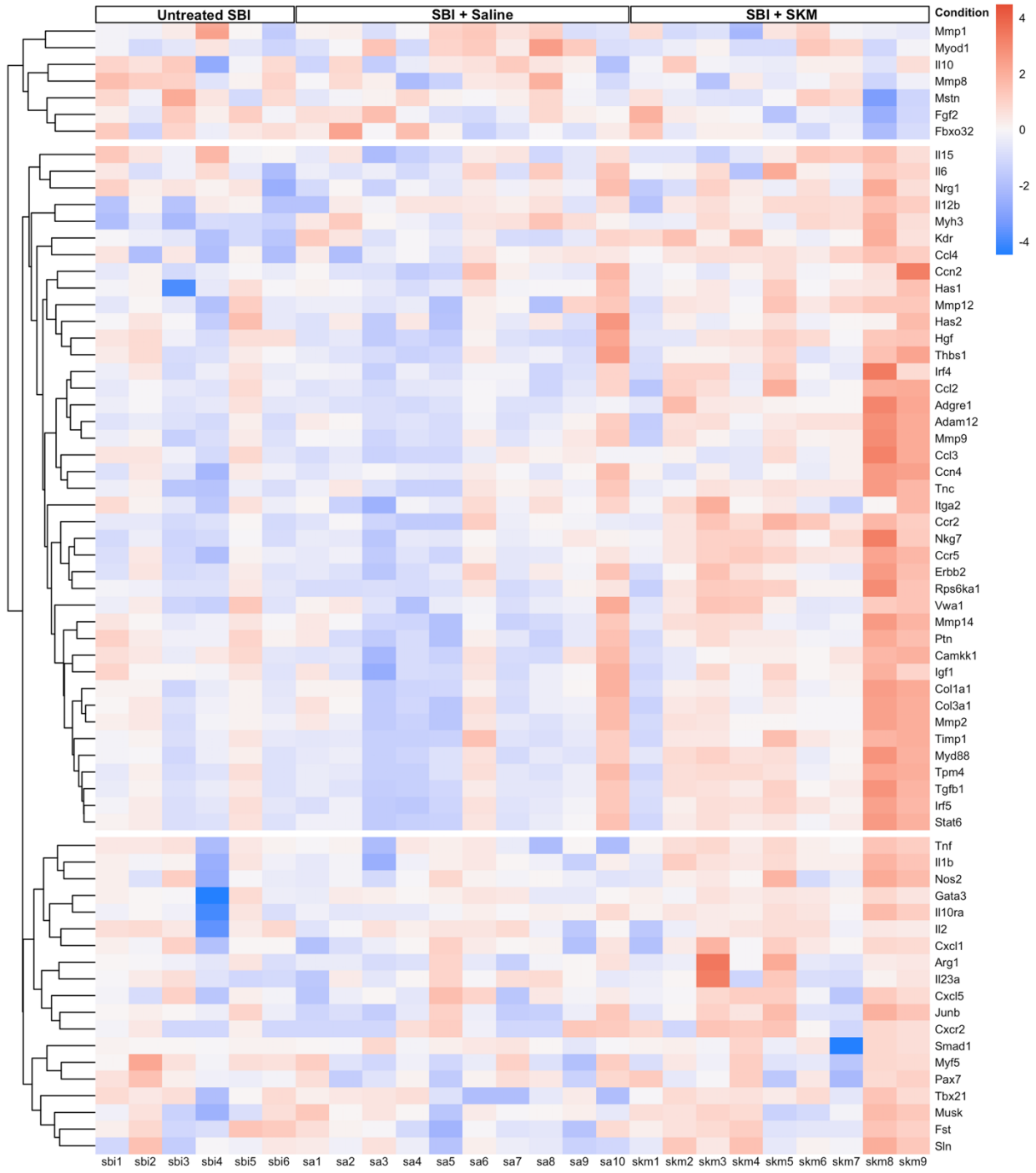

Figure 3.8. Gene expression profile across the samples 7 days after delayed injection of skeletal muscle extracellular matrix (SKM) hydrogel.
Heat map of genes with the highest variation in the dataset. N=6/10 per group.

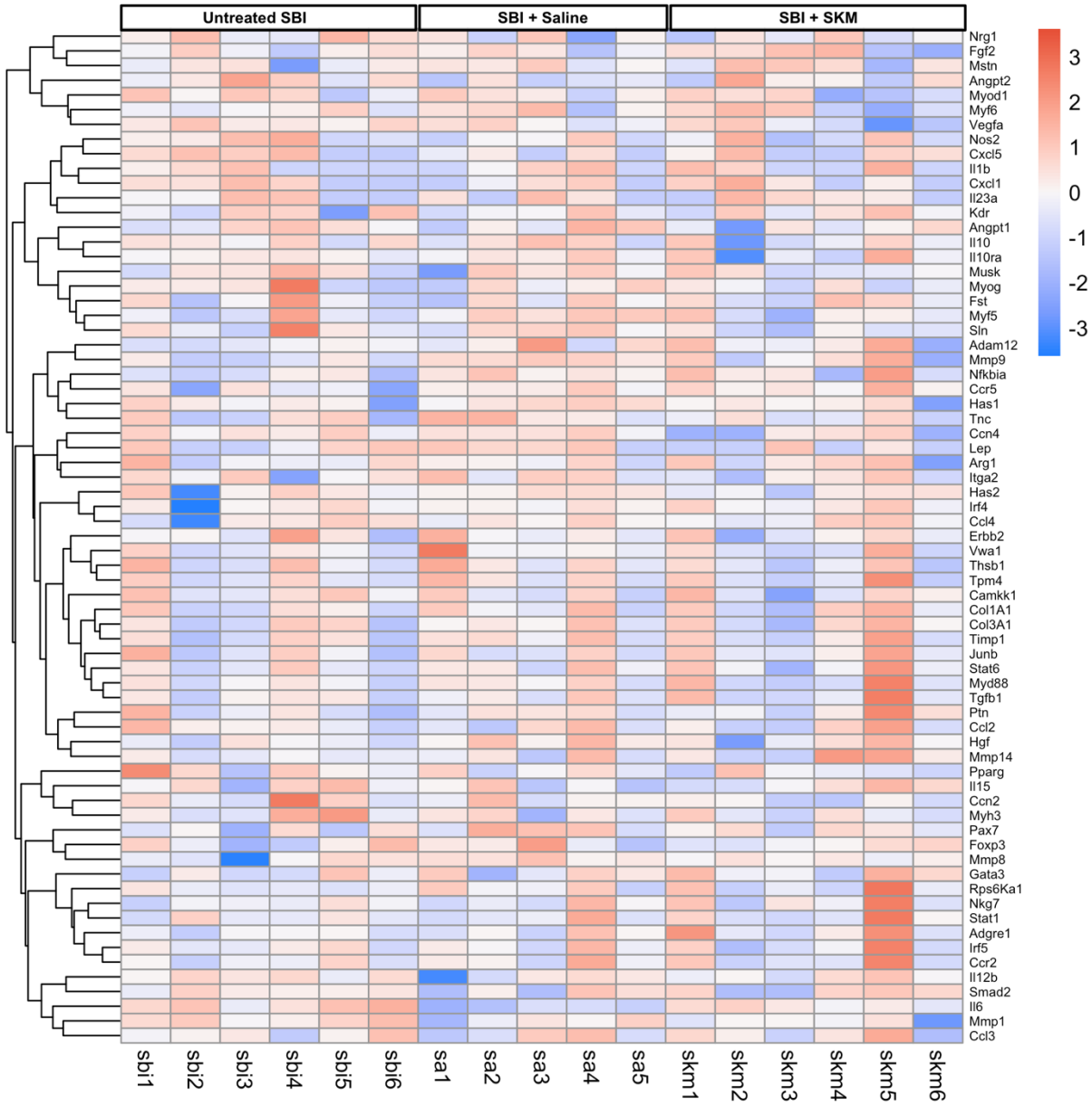

Figure 3.9. Gene expression profile across the samples 8 weeks after delayed injection of skeletal muscle extracellular matrix (SKM) hydrogel.
Heat map of genes with the highest variation in the dataset. N=5/6 per group.

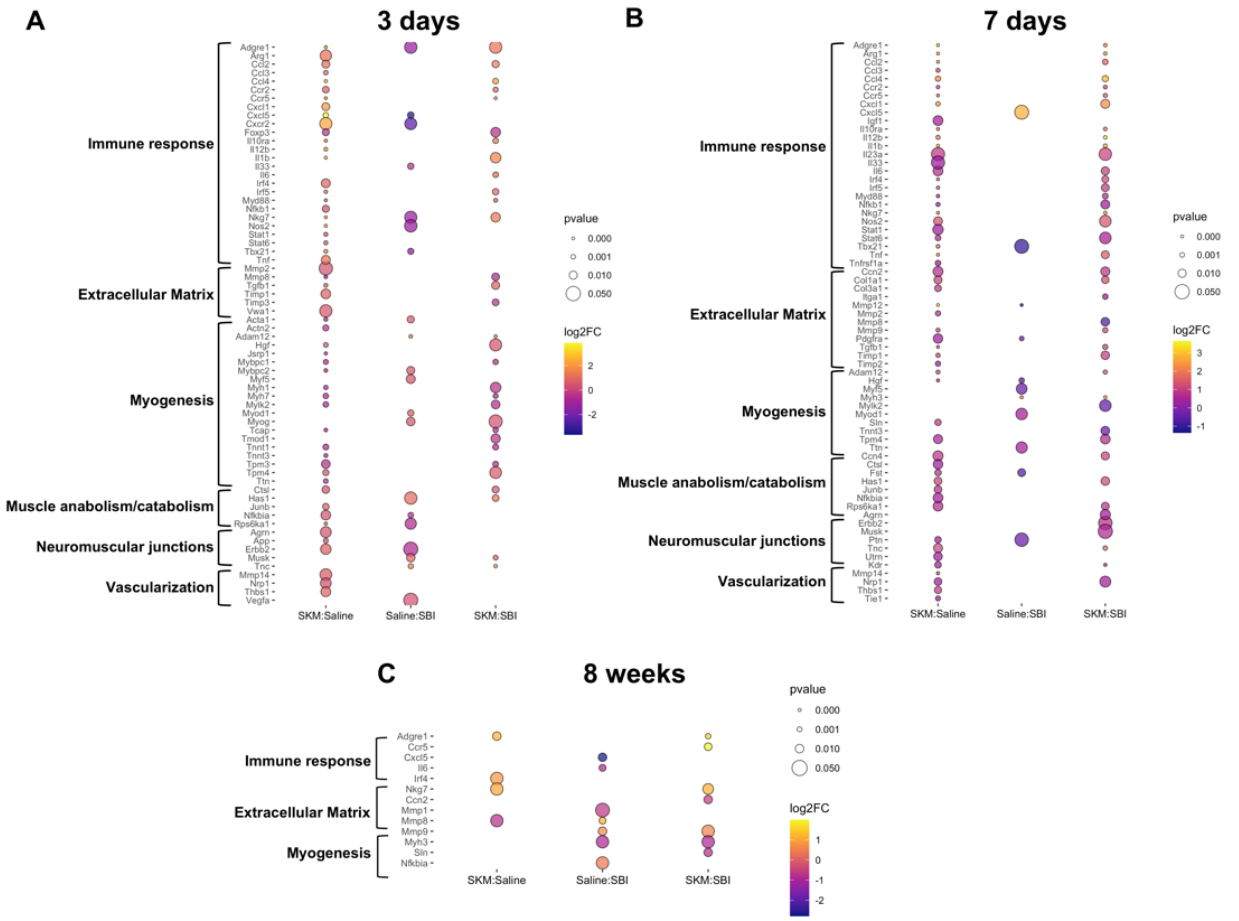

Figure 3.10. Pairwise comparisons after delayed injection of skeletal muscle extracellular matrix (SKM) hydrogel.
Significantly differentially expressed genes at 3 (A) 7 (B) days, and 8 weeks (C).

3.3 Discussion

Current preventative and therapeutic approaches for PFM dysfunction are limited to PFM rehabilitation, plagued by low overall success rates and poor long-term adherence. [1] Among regenerative strategies, cell-based therapies introduce challenges related to survival and engraftment, potential tumorigenicity, high costs and short shelf life. [7, 8] Several clinical trials have investigated the safety and efficacy of stem cell-based therapies for the treatment of urinary or fecal incontinence by targeting other skeletal muscle components of the pelvic floor that mainly

influence these disorders (i.e., urinary and anal sphincters).[9] These studies showed a lack of efficacy after the stem cell treatment. For example, a clinical trial of adipose stem cells injections showed a minimal improvement of the continence mechanism due to a bulking effect rather than muscle regeneration.[10] On the other hand, acellular immunomodulatory biomaterials can be used to potentiate endogenous regeneration [11], as we have previously shown in ischemic limb muscles.[5]

Here, we investigated whether SKM could be used to treat injured PFMs at the time of SBI or 4 weeks post injury. Our overarching goal is to develop therapeutic approaches for vaginally parous women - the most vulnerable population with respect to PFM injury and pelvic floor disorders. Thus, these time points were chosen to reflect two translationally relevant opportunities to use SKM. As a preventative measure, SKM could be used on Labor and Delivery for women at high risk for PFM injury (i.e. operative vaginal delivery, prolonged second stage of labor, macrosomia, obstetrical laceration).[12] As a therapeutic intervention, SKM could be used for women with clinically detected PFM weakness, identified by digital palpation or with the use of perineometer [13] at the post-partum visit, routinely scheduled within 2 months after childbirth. Moreover, SKM could be injected with minimal invasiveness directly into PFMs, identified by palpation, a technique familiar to most obstetricians and gynecologists, or with an ultrasound available on Labor and Delivery units and in outpatient office settings. A similar injectable ECM hydrogel derived from porcine myocardium was developed and tested in a Phase I clinical trial in myocardial infarction patients [14, 15], which demonstrates the translational potential of an ECM hydrogel therapy.

Immediate delivery of SKM following SBI led to decreased expression of several key pro-inflammatory genes, although pro-regenerative genes were not impacted at the time points studied. With respect to the observed improvement in PFM phenotype, we suggest that the increase in PFM fiber area in response to SKM is due to the material's enhancement of the

expanding MuSC population rather than upregulation of the muscle anabolism, as the downstream targets of the mTOR pathway were unchanged. Indeed, upregulation of genes associated with MuSCs together with a trending increase of genes related to de novo or fused myofibers were observed early on (3 days). Previous studies, indicating that SKM increases the MuSC recruitment [5, 6], are consistent with our current findings that SKM supports PFMs' stem cell function. With respect to the intramuscular collagen content, we suggest that SKM mitigates fibrosis by downregulating ECM remodeling genes, such as Ccn2 (connective tissue growth factor), involved in ECM deposition.[16] Lastly, immediate injection of SKM mitigates the altered vascularization, observed at the levels of arterioles, after birth injury. The above could be an indirect consequence of the downregulation of pro-inflammatory related genes or a direct result of decreased Vegfa expression.[17]

Interestingly, although the long-term improvements in PFM phenotype were similar after SKM administration at either time point, the differential gene expression in response to SKM vs saline was more prominent for the delayed injection (Fig. 3.6H, I). One month after birth injury, the tissue environment is not as dynamic as immediately after SBI. ECM hydrogels are known immunomodulators[18], and indeed we found shifts in both the pro-inflammatory and pro-regenerative responses, with increased expression of a pro-regenerative gene even at 8 weeks post-injection. While delayed SKM injection did not upregulate genes directly associated with MuSC function, it upregulated genes that aid in myogenesis, specifically Hgf and Adam12. The former is involved in the migration and activation of MuSCs [19], while the latter one is expressed transiently during muscle regeneration at the time of MuSC differentiation and fusion [20]. Thus, similar to the effects of SKM at the time of birth injury, biomaterial administration 4 weeks post SBI appears to increase the PFM fiber size at both time points analyzed via SKM impact on the myogenesis, rather than muscle anabolism. In addition, both SKM and saline mitigated fibrosis and restored arteriole density to the uninjured levels, which is, at least partially, a likely

consequence of the acute inflammatory response to the micro-injury associated with the process of injection,[21] although the gene expression profile following SKM or saline injection did differ. Moreover, delayed injection of SKM potentiated expression of genes associated with neuromuscular junction development and maturation, which contribute to overall muscle repair. We analyzed the morphological properties and gene expression at a later time point for this particular study since delayed administration of the biomaterial seems a more promising therapeutic window to separate women who did and did not get injured after childbirth. Even weeks after the hydrogel has been degraded,[6] we observed efficacy of the acellular biomaterial.

As with the previous chapter, we performed a biased analysis with Nanostring to identify potential mechanisms for the observed PFM phenotype after SKM injection. This approach can limit our investigation to uncover the influence of the biomaterial on other pathways. In addition, the studies were also performed on non-pregnant animals first as a proof-of-concept and to segregate the influence of other variables associated with pregnancy.

In conclusion, this study provides evidence to support the novel use of a minimally-invasive acellular regenerative biomaterial therapy at two clinically relevant interventional time points to prevent and mitigate pathological alterations of PFMs consequent to birth injury.

3.4 Materials and methods

3.4.1 Study design

This study investigated the efficacy of SKM at two translationally relevant time points following birth injury. Non-pregnant animals were randomized for the biomaterial-related studies. The sample size, indicated in the figure legends, was calculated *a priori* (see Statistical Analysis). No outliers were excluded from the study. For the quantitative analyses, the investigators were

blinded to the group identity. Simulated birth injury was performed as previously described for chapter 2 (2.4.4).

3.4.2 Pelvic Floor Muscle Collection after Biomaterial Injection

SKM was fabricated and characterized as described in Figure 3.11, and Table 3.1. For the immediate injection, animals were subjected to SBI, followed by 10 µl saline (experimental control) or SKM injection directly into the rostral portion of PCa. For the delayed injection, either saline or SKM (10 µl) was injected 4 weeks post-SBI. The minimally invasive injection via transobturator approach (Fig. 3.12) was performed using Hamilton syringe with a 30G needle. To assure reliable SKM injection, we first performed multiple injections with biomaterial prelabeled with India ink or Alexa fluor 568 (Fig. 3.12B-C). The material was consistently observed in the rostral/enthesial portion of PCa. This region of pubovisceralis and PCa is known to experience the highest strains during the human parturition and SBI in the rat model, respectively [22, 23]. We performed a long-term efficacy study, where saline and SKM groups were compared to each other and to the untreated SBI group. We then performed another study to assess gene expression changes at 3 and 7 days post-injection, as well as 8 weeks. Methods for histological analysis, RNA isolation, and Nanostring gene expression analysis are described in chapter 2 (2.4.6-7).

3.4.3 Statistical Analysis

Sample size for histological analysis was determined based on the previous study assessing efficacy of SKM. [5] Using G*power software, 6 animals/group/timepoint were needed to achieve 90% power at a significance level of 0.05. For gene expression studies, preliminary data with qRT-PCR were used to obtain sample size. Ten animals/group/timepoint were needed to achieve 80% power at a significance level set to 0.05. Data that followed a parametric distribution were compared using a Student's t-test, or a one-way analysis of variance followed by Tukey's post hoc pairwise comparisons. Non-parametrically distributed variables, such as fiber area, were

analyzed by Mann-Whitney or Kruskal-Wallis test followed by Dunn's pairwise comparisons. [24, 25] Data were analyzed using GraphPad Prism v8.0, San Diego, CA. Gene expression normalization and differential expression was analyzed using the NanoStringDiff package in R, with a significance at a p value<0.05 and a fold change cutoff of 1 ± 0.25. [26]

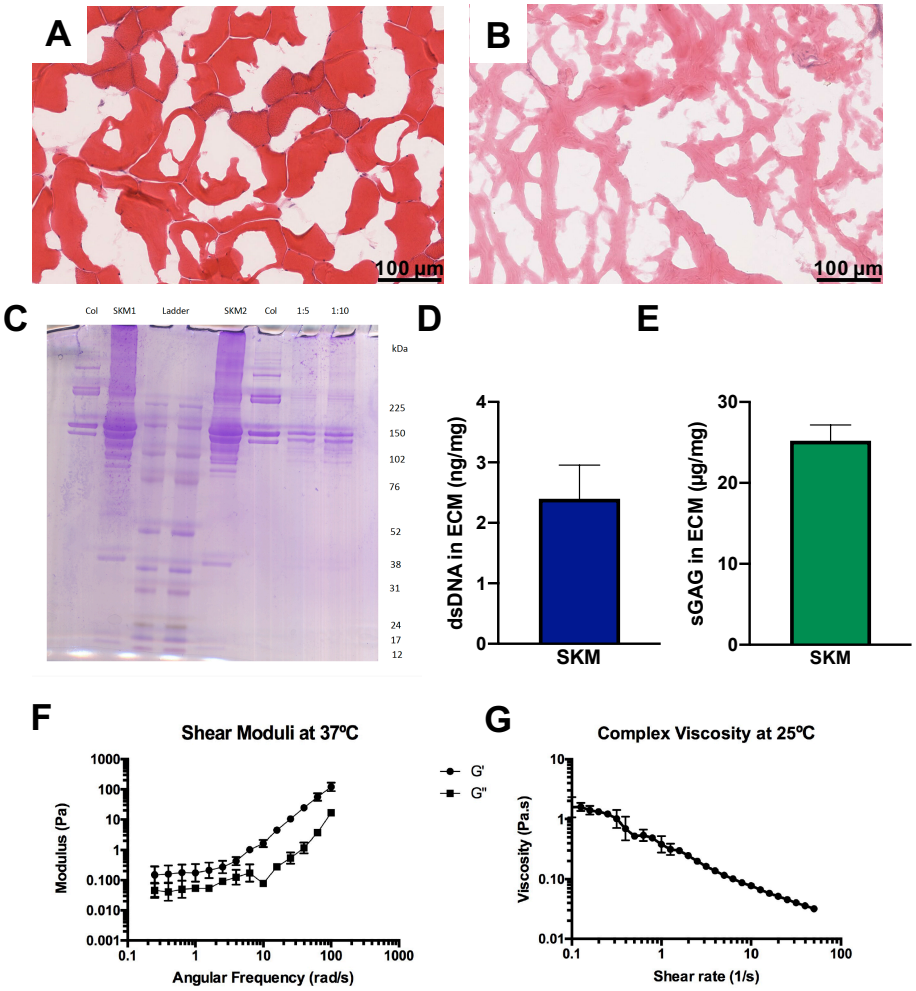

Figure 3.11. Characterization of skeletal muscle extracellular matrix (SKM).
H&E of fresh porcine longissimus dorsi skeletal muscle (A), and decellularized SKM (B). C) SDS-PAGE of SKM replicates (SKM1, SKM2) and dilutions (1:5, 1:10) compared to a single ECM component, collagen (Col). The dsDNA (D) and the sGAG (E) composition in SKM (n=3). F, G) Mechanical properties of SKM, indicating storage (G') and loss (G") moduli for SKM (F) and complex viscosity traces of liquid SKM (G), indicating a shear thinning material.

Table 3.1. Composition of decellularized porcine skeletal muscle ECM.

Protein Abundance in Porcine Skeletal Muscle Matrix (nmol/g)			
Protein	**Gene**	**Functional Classification**	**Average**
Collagen alpha-1(IV) chain(Arresten/Core Protein)	COL4A1	Basement Membrane	25.55
Collagen alpha-1/5(IV) chain(Arresten/Core Protein)	COL4A1/5	Basement Membrane	92.89
Collagen alpha-2(IV) chain(Canstatin/Core Protein)	COL4A2	Basement Membrane	19.35
Laminin Beta-1	LAMB1	Basement Membrane	0.15
Laminin Beta-2	LAMB2	Basement Membrane	0.17
Laminin Gamma-1	LAMC1	Basement Membrane	0.21
Perlecan	HSPG2	Basement Membrane	2.99
Collagen alpha-1(XIV) chain	COL14A1	FACIT Collagen	0.40
Collagen alpha-1(I) chain	COL1A1	Fibrillar Collagen	1393.12
Collagen alpha-1(V) chain	COL5A1	Fibrillar Collagen	35.55
Collagen alpha-2(I) chain	COL1A2	Fibrillar Collagen	1272.17
Collagen alpha-2(V) chain	COL5A2	Fibrillar Collagen	39.68
Collagen alpha-1(VI) chain	COL6A1	Matricellular	28.34
Collagen alpha-2(VI) chain	COL6A2	Matricellular	3.36
Collagen alpha-3(VI) chain	COL6A3	Matricellular	23.05
Dermatopontin	DPT	Matricellular	1.30
Emilin 1	EMILIN1	Matricellular	0.22
Fibronectin 1(type-III 4 domain)	FN1	Matricellular	4.53
Lumican	LUM	Matricellular	13.65
Fibrillin 1	FBN1	Structural ECM	3.12
Actin (All Isoforms)	ACT	Cytoskeletal	9.00
Myosin(Myosin-3,4,6,7)	MYH	Cytoskeletal	3.12

Note, low cytoskeletal components indicate sufficient decellularization.

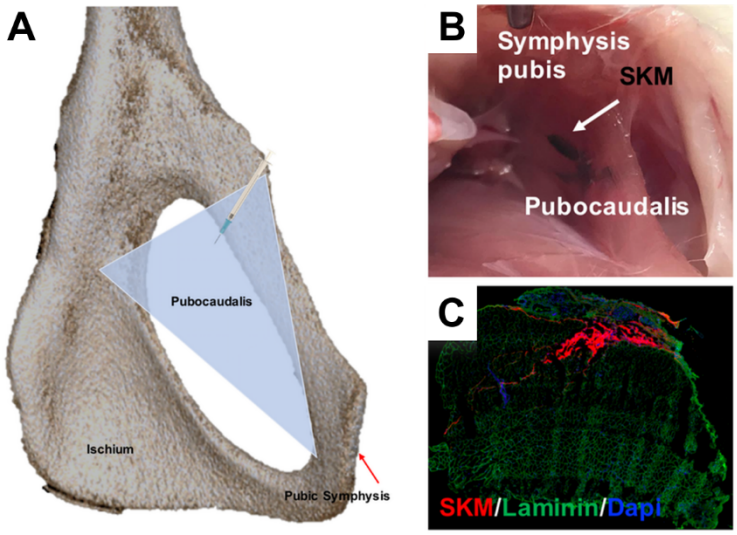

Figure 3.12. Intramuscular injection of decellularized skeletal muscle extracellular matrix (SKM) hydrogel.
(A) Computer tomography image of the female rat pelvis demonstrating that SKM was delivered using the obturator foramen as a therapeutic window were the syringe passed through and injected the proximal (i.e., enthesial) region of pubocaudalis. We performed practice injections to assure a reliable delivery of SKM by prelabeling either with india ink (B) or Alexa Fluor 568 (C).

3.5 Acknowledgements

Chapter 3, in part, is currently being prepared for re-submission for publication of the material, Pamela Duran, Francesca Boscolo Sesillo, Lindsey Burnett, Shawn A. Menefee, Mark Cook, Gisselle Zazueta-Damian, Monika Dzieciatkowska, Emmy Do, Saya French, Manali M. Shah, Clyde Sanvictores, Kirk C. Hansen, Matthew Shtrahman, Karen L. Christman, Marianna Alperin. “Pro-regenerative Extracellular Matrix Hydrogel Prevents and Mitigates Pathological Alterations of Pelvic Muscles Following Birth Injury”. The dissertation author was the first author of this paper.

3.6 References

1. Wallace, S.L., L.D. Miller, and K. Mishra, Pelvic floor physical therapy in the treatment of pelvic floor dysfunction in women. *Curr Opin Obstet Gynecol*. 2019; 31(6): p. 485-493.

2. Gormley, E.A., Evaluation and management of the patient with a failed midurethral synthetic sling. *Can Urol Assoc J*. 2012; 6(5 Suppl 2): p. S123-4.

3. Anil, G., Kalmar, K., Panarese, A., Dudding, T., Nicholls, R., Vaizey, C., Long-term outcomes of sacral nerve stimulation for fecal incontinence. *Dis Colon Rectum*. 2012; 55(3): p. 302-6.

4. Sandall, J., R.M. Tribe, L. Avery, G. Mola, G.H.A. Visser, C.S.E. Homer, D. Gibbons, N.M. Kelly, H.P. Kennedy, H. Kidanto, P. Taylor, and M. Temmerman, Short-term and long-term effects of caesarean section on the health of women and children. *The Lancet*. 2018; 392(10155): p. 1349-1357.

5. Ungerleider, J.L., T.D. Johnson, M.J. Hernandez, D.I. Elhag, R.L. Braden, M. Dzieciatkowska, K.G. Osborn, K.C. Hansen, E. Mahmud, and K.L. Christman, Extracellular Matrix Hydrogel Promotes Tissue Remodeling, Arteriogenesis, and Perfusion in a Rat Hindlimb Ischemia Model. *JACC Basic Transl Sci*. 2016; 1(1-2): p. 32-44.

6. DeQuach, J., Lin, J., Cam, C., Hu, D., Salvatore, M., Sheikh, F., Christman, K., Injectable skeletal muscle hydrogel promotes neovascularization and muscle cell infiltration in a hindlimb ischemia model. *Eur Cell Mater*. 2012; 23: p. 400-412.

7. Dodson, B.P. and A.D. Levine, Challenges in the translation and commercialization of cell therapies. *BMC Biotechnol*. 2015; 15: p. 70.

8. Lee, A.S., C. Tang, M.S. Rao, I.L. Weissman, and J.C. Wu, Tumorigenicity as a clinical hurdle for pluripotent stem cell therapies. *Nat Med*. 2013; 19(8): p. 998-1004.

9. Manodoro, S., M. Frigerio, M. Barba, S. Bosio, L.A. de Vitis, and A.M. Marconi, Stem Cells in Clinical Trials for Pelvic Floor Disorders: a Systematic Literature Review. *Reprod Sci*. 2021.

10. Aragon, I.M., B.H. Imbroda, and M.F. Lara, Cell Therapy Clinical Trials for Stress Urinary Incontinence: Current Status and Perspectives. *Int J Med Sci*. 2018; 15(3): p. 195-204.

11. Christman, K.L., Biomaterials for tissue repair. *Science*. 2019; 363(6425): p. 340-341.

12. Friedman, S., Blomquist, J., Nuget, J., McDermott, K., Muñoz, A., Handa, V., Pelvic Muscle Strength After Childbirth. *Obstet Gynecol*. 2012; 120(5): p. 1021-1028.

13. Frawley, H.C., M.P. Galea, B.A. Phillips, M. Sherburn, and K. Bo, Reliability of pelvic floor muscle strength assessment using different test positions and tools. *Neurourol Urodyn*. 2006; 25(3): p. 236-242.

14. Self-Naraghi, S.S., J.; Salvatore, M.; Osborn, K.; Wang, J.; Sampat, U.; Kwan, O.; Strachan, M.; Wong, J.; Schup-Magoffin, P.; Braden, R.; Bartels, K.; DeQuach, J.; Preul, M.; Kinsey, A.; DeMaria, A.; Dib, N.; Christman, K., Safety and Efficacy of an Injectable Extracellular Matrix Hydrogel for Treating Myocardial Infarction. *Sci. Transl. Medi*. 2013; 5(173): p. 173ra25.

15. Traverse, J.H., T.D. Henry, N. Dib, A.N. Patel, C. Pepine, G.L. Schaer, J.A. DeQuach, A.M. Kinsey, P. Chamberlin, and K.L. Christman, First-in-Man Study of a Cardiac Extracellular Matrix Hydrogel in Early and Late Myocardial Infarction Patients*. JACC Basic Transl Sci*. 2019; 4(6): p. 659-669.

16. Gillies, A.R. and R.L. Lieber, Structure and function of the skeletal muscle extracellular matrix*. Muscle Nerve*. 2011; 44(3): p. 318-31.

17. Carmeliet, P., Mechanisms of angiogenesis and arteriogenesis*. Nature Review*. 2000; 6(3): p. 389-395.

18. Dziki, J.L., L. Huleihel, M.E. Scarritt, and S.F. Badylak, Extracellular Matrix Bioscaffolds as Immunomodulatory Biomaterials*. Tissue Eng Part A*. 2017; 23(19-20): p. 1152-1159.

19. Dhawan, J. and T.A. Rando, Stem cells in postnatal myogenesis: molecular mechanisms of satellite cell quiescence, activation and replenishment*. Trends Cell Biol*. 2005; 15(12): p. 666-73.

20. Galliano, M., Huet, C., Frygelius, J., Polgren, A., Wewer, U., Engvall, E., Binding of ADAM12, a Marker of Skeletal Muscle Regeneration, to the Muscle-specific Actin-binding Protein, α-Actinin-2, Is Required for Myoblast Fusion*. Journal of Biological Chemistry*. 2000; 275: p. 13933-13939.

21. Thuilliez, C., L. Dorso, P. Howroyd, S. Gould, F. Chanut, and R. Burnett, Histopathological lesions following intramuscular administration of saline in laboratory rodents and rabbits*. Exp Toxicol Pathol*. 2009; 61(1): p. 13-21.

22. Catanzarite, T., S. Bremner, C.L. Barlow, L. Bou-Malham, S. O'Connor, and M. Alperin, Pelvic muscles' mechanical response to strains in the absence and presence of pregnancy-induced adaptations in a rat model*. Am J Obstet Gynecol*. 2018; 218(5): p. 512 e1-512 e9.

23. Jing, D., J.A. Ashton-Miller, and J.O. DeLancey, A subject-specific anisotropic visco-hyperelastic finite element model of female pelvic floor stress and strain during the second stage of labor*. J Biomech*. 2012; 45(3): p. 455-60.

24. Baghdadi, M.B., D. Castel, L. Machado, S.I. Fukada, D.E. Birk, F. Relaix, S. Tajbakhsh, and P. Mourikis, Reciprocal signalling by Notch-Collagen V-CALCR retains muscle stem cells in their niche*. Nature*. 2018; 557(7707): p. 714-718.

25. Sun, X., Wu, J., Qiang, B., Romagnuolo, R., Gagliardi, M., Keller, G., Laflamme, M., Li, R., Nunes, S., Transplanted microvessels improve pluripotent stem cell–derived cardiomyocyte engraftment and cardiac function after infarction in rats*. Sci. Transl. Medi*. 2020; 12.

26. Raman, A.T., A.E. Pohodich, Y.W. Wan, H.K. Yalamanchili, W.E. Lowry, H.Y. Zoghbi, and Z. Liu, Apparent bias toward long gene misregulation in MeCP2 syndromes disappears after controlling for baseline variations. *Nat Commun*. 2018; 9(1): p. 3225.

Chapter 4: Repeated birth injuries lead to pelvic floor muscle dysfunction and impairment in regeneration

4.1 Introduction

As described in chapter 1, vaginal delivery has been consistently identified as a key risk factor for pelvic floor muscle (PFM) injury and the associated pelvic floor disorders (PFDs).[1] In addition, multiparity further increases this risk, especially for the development of pelvic organ prolapse (POP).[2-5] Despite the established epidemiological risk factors, the mechanisms leading to PFM dysfunction in primiparous and multiparous women remain elusive.

In chapter 2, we discovered that despite an 8-week recovery period following vaginal distention, pubocaudalis (PCa)—analogous to human pubovisceralis[6]—exhibits atrophic and fibrotic pathological alterations in the rat pre-clinical model. The above morphological aberrations are associated with sustained inflammatory response, impairment in muscle anabolism, and persistent extracellular matrix remodeling. To investigate whether these long-term pathological alterations impact PFM function, the first objective of the current study was to assess how simulated birth injury (SBI) affects mechanical muscle properties.

Studies investigating the effect of repeat injuries on the limb muscle recovery demonstrate profound muscle atrophy associated with loss of regenerative capacity.[7, 8] To our knowledge, there are no published studies examining the impact of repeat large mechanical strains on the female PFMs. In a previous study, focused on the effect of multiple vaginal distentions on external urethral sphincter recovery, the investigators observed a profound decrease in leak point pressure after repeated SBIs in the rat model.[9] However, it is not clear whether active regeneration of the striated urethral sphincter was completed at the time of the repeated injury in the above study. Several investigations have indicated that muscle response is dramatically affected when a second injury is performed during active muscle regeneration.[7, 10] Thus, the second objective of

the current study was to test the following hypotheses: 1) repeated SBI, imposed on the PFMs after completion of an active recovery period following the first SBI, further overwhelms PFM regenerative capacity, leading to more substantial pathological alterations than a single birth injury and 2) pathological alterations in the intrinsic PFM components incited by repeated SBIs result in PFM dysfunction, a known risk factor for clinically relevant PFDs observed in multiparous women.

In chapter 3, we investigated the efficacy of a skeletal muscle-derived extracellular matrix (SKM) hydrogel at two clinically relevant therapeutic time points. In both cases, the pro-regenerative biomaterial prevented and mitigated the pathological alterations of the PFMs after a single birth injury. To further analyze the efficacy of the acellular hydrogel in multiparous women, the third objective of the study was to test the hypothesis that SKM enhances muscle regeneration after repeated SBIs.

In this study, we found that repeated SBIs lead to increased pathological alterations and decreased active force production in relation to a single injury. In addition, a prolonged inflammatory response, impairment in muscle anabolism, upregulation of genes associated with muscle catabolism, and sustained ECM remodeling were observed with respect to a first SBI. Furthermore, administration of SKM resulted in improved PFM phenotype, and modulation of the immune response.

4.2 Results

4.2.1 The impact of single and repeat simulated birth injuries on the pelvic floor muscle function

To determine whether myofiber atrophy and fibrotic degeneration of the PFMs consequent to a single SBI are functionally relevant, we performed *ex vivo* active mechanical testing (Fig. 4.1A-B). Immediately following the 1st SBI, PCa demonstrated a decrease in the force-frequency curve (Fig. 4.1C), with significant reduction in the specific peak force compared to uninjured

controls (P<0.01, Fig. 4.1E). At 4 weeks post-1st SBI, the pattern of the force-frequency curve (Fig. 4.1C) and the specific peak force (Fig. 4.1E) were similar to controls despite ongoing muscle regeneration (P=0.99) (Fig. 4.1C, E). These mechanical parameters remained unchanged at 8 weeks post SBI, when muscle regeneration was completed, compared to the 4-week time point (P>0.99, Fig. 4.1C, E). Taken together, these data indicate that despite atrophy and fibrosis—which are known to affect active muscle mechanical properties[11, 12]—of the PCa in response to a single SBI, muscle force production was not affected long-term.

Given the above and motivated by the epidemiological studies that identify increased incidence of pelvic floor dysfunction and the associated PFDs in multiparous women compared to women with history of only one vaginal delivery[2], we went on to assess PFM function after repeat birth injuries. Immediately after repeat SBI, the force-frequency curve demonstrated decreased force production compared to uninjured controls, with a reduction in peak force (P<0.01, Fig. 4.1D, E). In contrast to the functional muscle recovery observed 4 weeks after a single SBI, PCa force was significantly decreased at 4 weeks post-2nd SBI relative to uninjured controls (Fig. 4.1D, E). A reduction in muscle force was identified even at 12 weeks after 2nd SBI (P<0.01, Fig. 4.1D, E). These results indicate that repeated birth injuries deleteriously affect PFM contractile function.

Besides assessing active mechanical properties, investigation of passive parameters is essential as a pathological increase in collagen (i.e., fibrosis) can affect muscle stiffness—which is known to affect muscle force transmission.[11] To assess this, we performed passive mechanical testing at the fascicle level (Fig. 4.2A, B). Interestingly, although active muscle function was not affected after a single SBI, at 8 weeks post-1st SBI we observed an upward shift of the stress-strain curve compared to uninjured controls (Fig. 4.2C) together with an increase in stiffness at low strains (Fig. 4.2D). This pattern was also observed at 12 weeks post-2nd SBI (Fig. 4.2C, D), indicating that a single or repeated birth injury affect muscle passive mechanical properties.

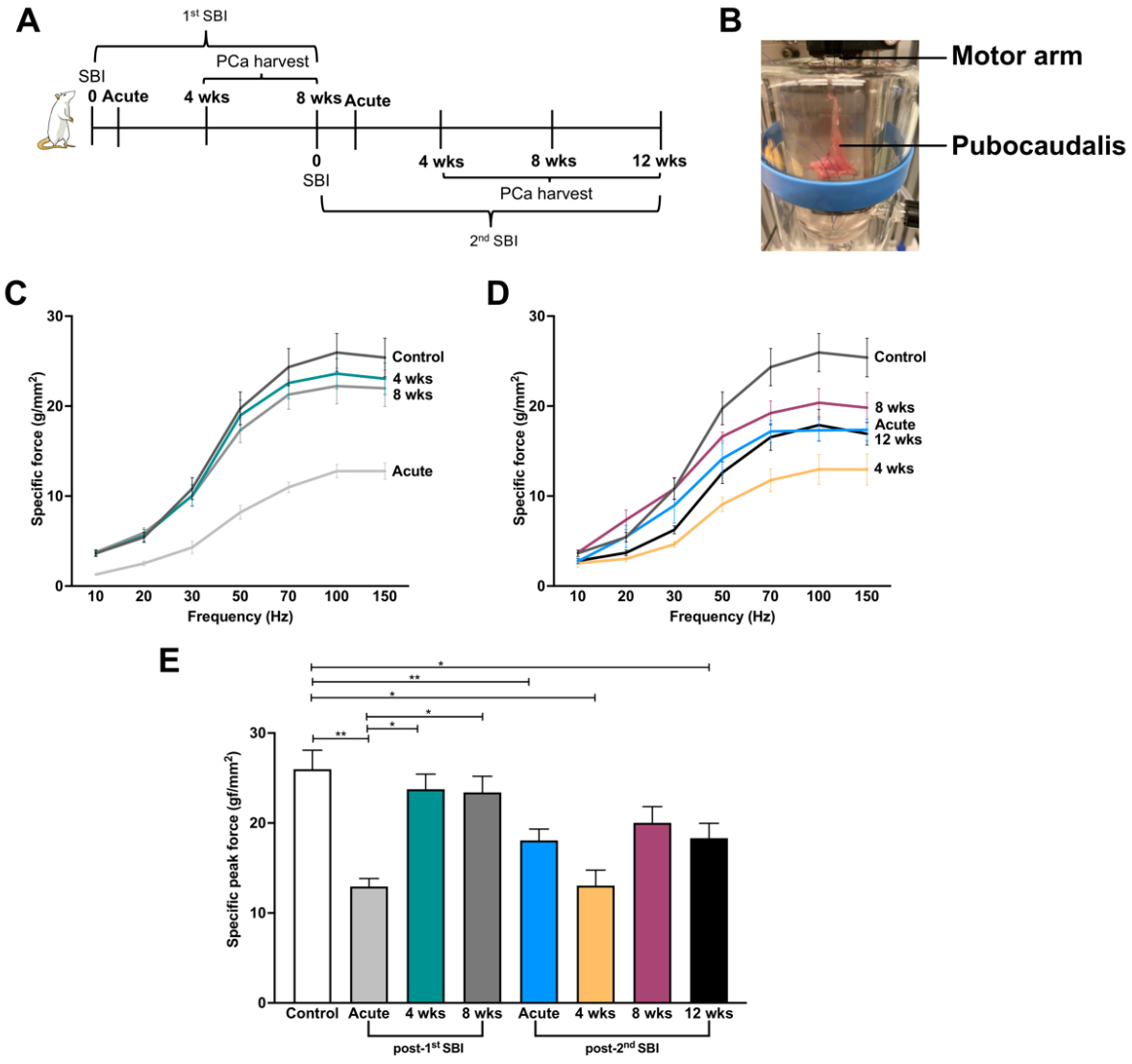

Figure 4.1 Pelvic floor muscle active function after single and repeated simulated birth injuries. (A) Timeline of experimental design. (B) Example of pubocaudalis (PCa) in organ bath attached to the force transducer by the tendon at the insertion and fixed to the arm with the pubic bone. Force-frequency curves at various timepoints after a single (C) or repeated (D) simulated birth injury and specific peak force (E). N=3-7/group. *P*-values derived from two-way ANOVA followed by pairwise comparisons with Sidak's range test. *p<0.05, **p<0.01, ***p<0.001, mean±SEM.

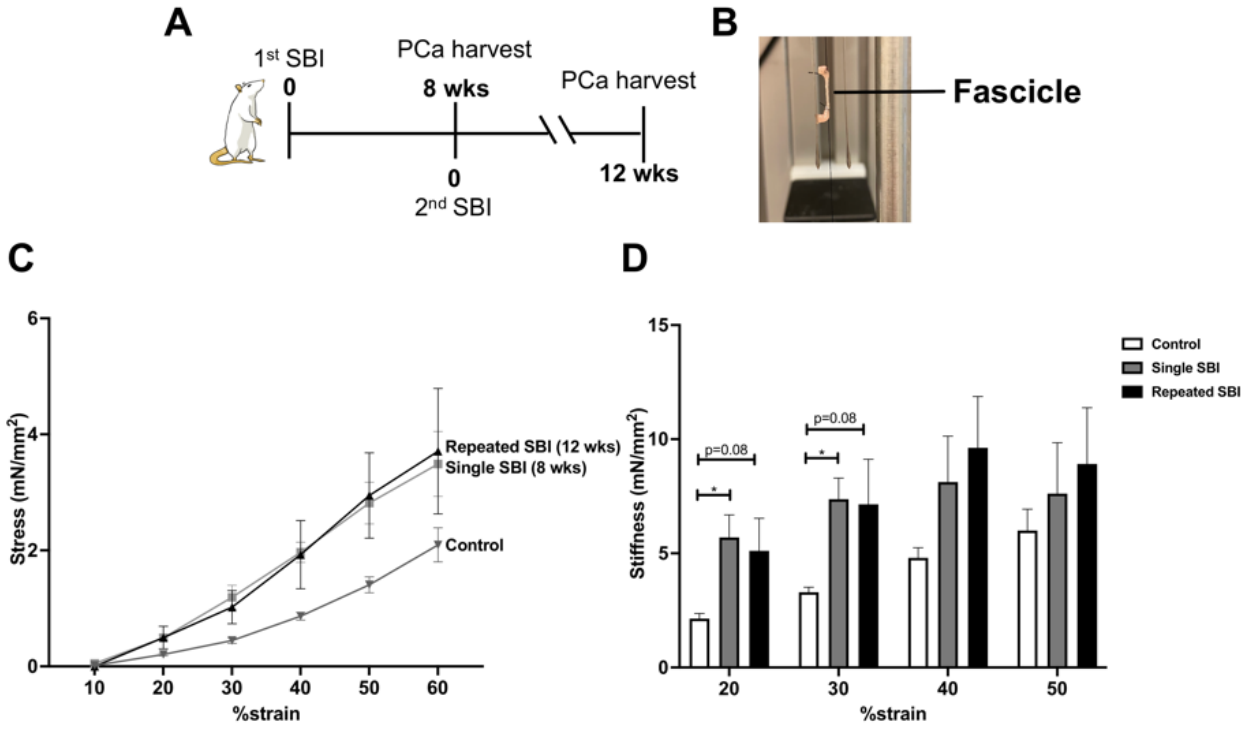

Figure 4.2 Passive mechanical properties of the pelvic floor muscle after a single or repeated simulated birth injuries.
(A) Timeline of experimental design. (B) Example of fascicle attached to motor arm for mechanical testing. Stress-strain curves (C) and stiffness (D) were obtained after a single or repeated birth injury. N=3/group. P-values derived from one-way ANOVA followed by pairwise comparisons with Dunnett's range test. mean±SEM.

4.2.2 Repeated birth injuries negatively impact pelvic floor muscle regeneration

As the first step in determining potential causes of the observed PFM dysfunction after repeated SBIs, we went on to assess the impact of repeated birth injuries on PFM histomorphometric properties (Fig. 4.3A) and to compare to the findings in animals subjected to a single SBI.

PCa fiber size decreased at 4 weeks post-2nd SBI compared to controls and to animals allowed to recover for 4- or 8-weeks post single SBI ($P<0.0001$, Fig. 4.3B). Fiber area distribution

did not change between 4 and 8 weeks following the 2nd injury (P>0.9, Fig. 4.3B). This was in contrast to the findings following a single SBI, after which PCa fiber size increased between 4 and 8 weeks following the injury. We further analyzed fiber area at 12 weeks after repeated injury as we also observed a reduction in force production at this time point. While fiber size was increased at 12 weeks in relation to 8 weeks post-2nd SBI (P<0.0001), fiber area was still decreased compared to uninjured controls (P<0.0001, Fig. 4.3B).

To assess muscle regeneration, we quantified the proportion of fibers with centralized nuclei—an index of regeneration.[13] The number of fibers with centralized nuclei post-2nd SBI was not different at 4 weeks following the injury compared to controls (P=0.5, Fig. 4.3C). At 8 weeks after the 2nd injury, the number of regenerating myofibers was substantially increased compared to uninjured controls (P<0.01, Fig. 4.3C). As opposed to the impact of a single SBI, after which the percent of regenerating myofibers returned to baseline by 8 weeks post injury, the proportion of centralized nuclei remained high at this time point after the 2nd SBI (P<0.01, Fig. 4.3C). Since these results indicated ongoing muscle regeneration at this time point, we analyzed the proportion of regenerated myofibers at 12 weeks post-repeated injury. Surprisingly, even at this long-term time point, the percent of centralized nuclei was still increased in relation to controls (P<0.0001), without differences compared to the 8-weeks period (P=0.8, Fig. 4.3C). All together, these findings suggest an impairment in muscle regeneration after repeated birth injuries.

We also assessed changes in the intramuscular collagen content in response to multiple SBIs, as pathological increase in collagen I, the main constituent of the intramuscular extracellular matrix, can negatively affect muscle active and passive mechanical properties.[14] At 4 weeks post-2nd SBI, PCa collagen content was unchanged relative to controls (P=0.0.5) and lower than that observed at 4 weeks post-1st SBI (P<0.05, Fig. 4.3D). Eight weeks after repeated SBI, intramuscular collagen content was significantly increased relative to controls (P<0.01) and compared to the 4-week time point (P<0.05), without differences in relation to the 12-week time

point (P>0.99, Fig. 4.3D). These results demonstrate that fibrotic degeneration of the PFMs subjected to repeated large strains occurs later than following a single vaginal distention.

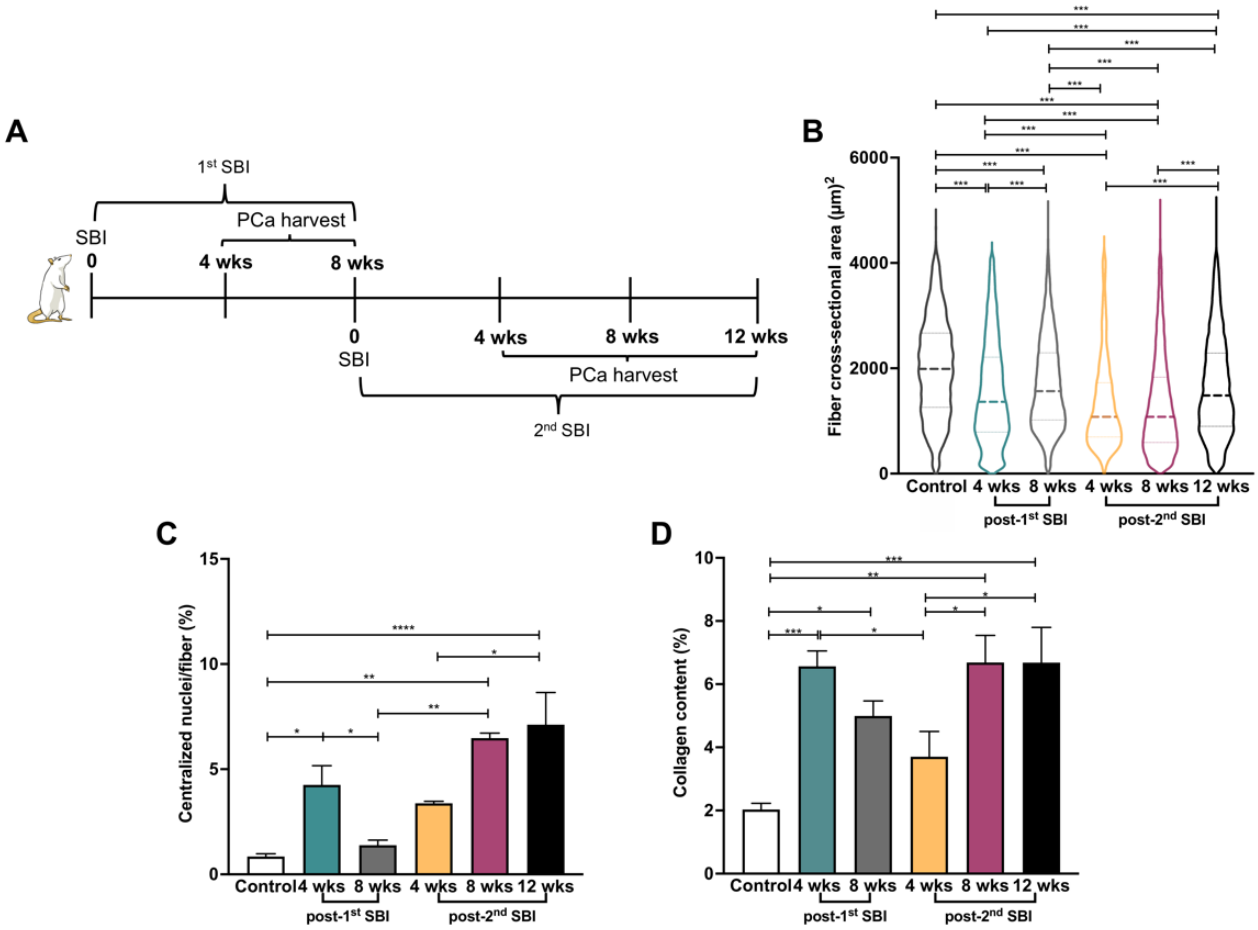

Figure 4.3 Repeated simulated birth injuries (SBI) lead to an impairment in pelvic floor muscle regeneration.
(A) Timeline of experimental design. Quantification of fiber cross-sectional area (B), centralized nuclei (E) and collagen content (F) after a single or repeated birth injury. N=3-6/group. *P*-values derived from two-way ANOVA followed by pairwise comparisons with Sidak's range test. *p<0.05, **p<0.01, ***p<0.001, ****p<0.0001, mean±SEM.

4.2.3 Prolonged inflammatory response of the pelvic floor muscles after repeated birth injuries

To investigate potential mechanisms behind the profound reduction in fiber size, impairment in regeneration and muscle fibrosis after repeated injuries, we then performed a gene expression study capitalizing on the customized Nanostring panel (Table 2.1) used in previous

chapters. PCa was harvested at acute, subacute and long-term time points as with a single SBI to analyze pathways essential for muscle regeneration after an injury.[15-17] We first assessed patterns across the injury time points through a Principal component (PC) analysis (Fig. 4.4A). PC1 that corresponded to the highest variability, indicated the time course of return to the uninjured state for both 1st and 2nd SBI. In addition, the same time points after single and repeated injury mostly clustered together.

We then investigated the longitudinal patterns in gene expression with respect to the uninjured state by evaluating the differentially expressed genes (Tables 2.2-7, 4.1-6). Figure 4.5 indicates the gene expression profile across the replicates per timepoint post-1st and 2nd SBI. Unsupervised clustered heat maps of the fold change in relation to the uninjured controls are visualized in Figure 4.4B-G. For the immune response category (Fig. 4.4B), the majority of inflammatory related genes clustered together. As with a single injury, at the acute time points after 2nd SBI, increased expression of pro-inflammatory genes was identified together with upregulation of few pro-regenerative genes. Prolonged expression of inflammatory genes (Il1b, Irf5, Stat1) was observed at the longer-term time point (63 days) which were not identified around this time point after a single injury. For myogenesis pathway (Fig. 4.4C), the gene expression pattern was similar after a repeated injury in relation to a single one—genes related to muscle structure were downregulated at the acute time points, with upregulation of muscle transcription factors and mediators. Notably, Myf5 and Myh3, which are involved in the regeneration of myofibers, were upregulated until day 21 post-2nd SBI. For muscle anabolism and catabolism category (Fig. 4.4D), following the pattern observed after a first injury, repeated injuries led to decreased expression of genes associated with muscle anabolism even at the long-term time points (Eif2b5, Rps6kb1). Uniquely, upregulation of genes associated with muscle catabolism (Foxo1, Foxo3) were identified at the longer time point. As with a single SBI, genes associated with extracellular matrix (ECM) remodeling (Mmp2, Mmp9, Tgfb1, Timp1) were observed at the

acute time points post-2nd SBI (Fig. 4.4E). From these genes, the ones that promote collagen synthesis (Tgfb1, Timp1) were still upregulated at the longer time point, which were not identified around this time point after a single injury. At last, similar patterns of differentially expressed genes were observed after a single and repeated injury for vascularization (Fig. 4.4F) and neuromuscular junctions (Fig. 4.4G) categories. All together the results suggest that repeated birth injuries lead to a prolonged inflammatory response, impairment in muscle anabolism, upregulation of genes associated with catabolism, and sustained expression of ECM remodeling genes in relation to a single SBI.

Figure 4.4 Repeated simulated birth injuries (SBI) lead to prolonged inflammatory response, sustained expression of ECM remodeling genes, impairment in muscle anabolism, and upregulation of muscle catabolism related genes.
(A) Principal component analysis that includes gene expression in uninjured controls and at several time points after a single and repeated SBI. (B-G) Unsupervised clustered heat maps of fold changes at each time point in relation to uninjured controls. Pathways include immune response (B), myogenesis (C), muscle anabolism and catabolism (D), extracellular matrix (E), vascularization (F), and neuromuscular junctions (G).

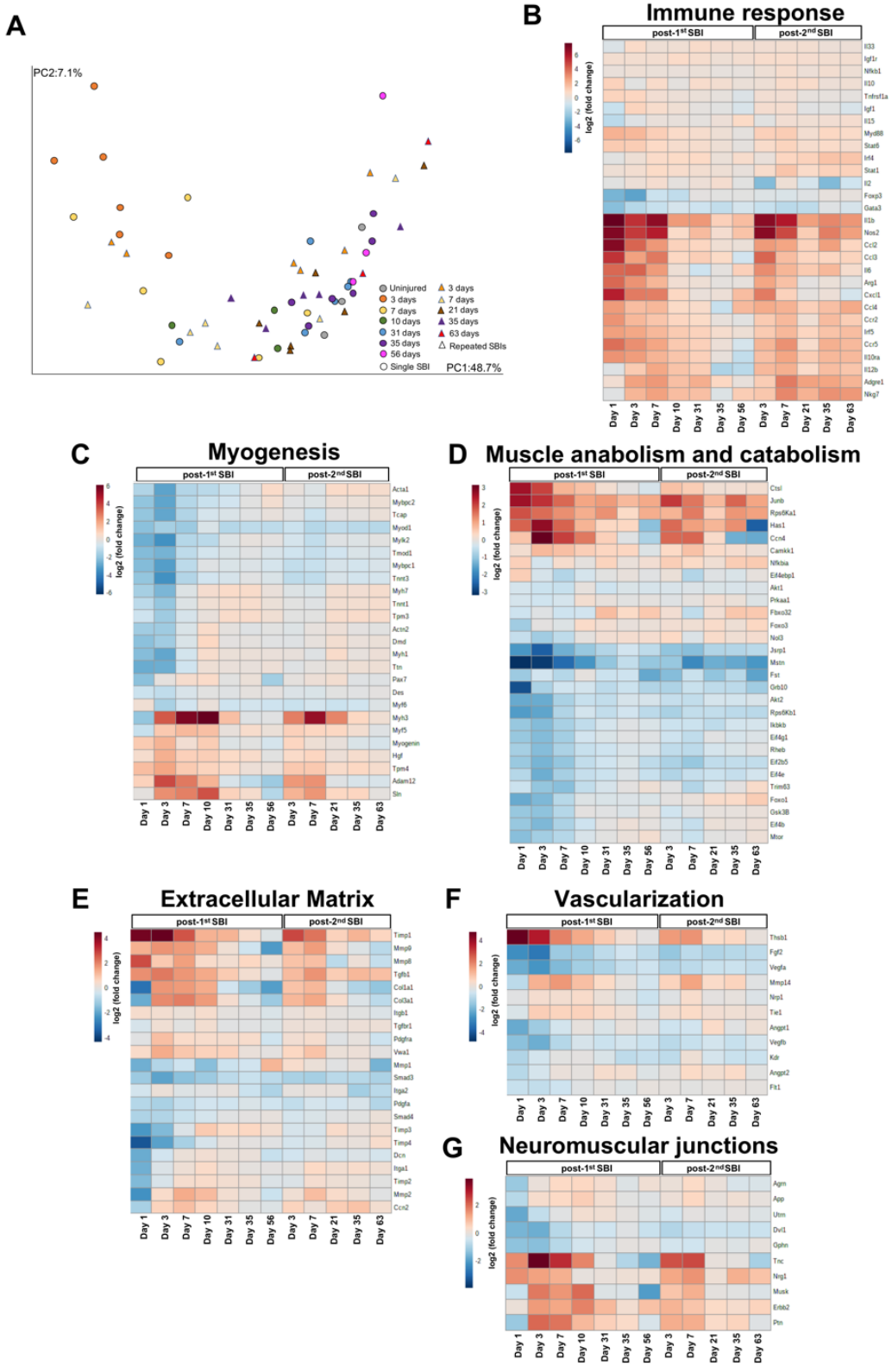
A
PC2:7.1%
PC1:48.7%
Uninjured
3 days
7 days
10 days
31 days
35 days
56 days
Single SBI
3 days
7 days
21 days
35 days
63 days
Repeated SBIs
B
Immune response
post-1st SBI
post-2nd SBI
log2 (fold change)
Il33
Igf1r
Nfkb1
Il10
Tnfrsf1a
Igf1
Il15
Myd88
Stat6
Irf4
Stat1
Il2
Foxp3
Gata3
Il1b
Nos2
Ccl2
Ccl3
Il6
Arg1
Cxcl1
Ccl4
Ccr2
Irf5
Ccr5
Il10ra
Il12b
Adgre1
Nkg7
Day 1
Day 3
Day 7
Day 10
Day 31
Day 35
Day 56
Day 3
Day 7
Day 21
Day 35
Day 63
C
Myogenesis
post-1st SBI
post-2nd SBI
log2 (fold change)
Acta1
Mybpc2
Tcap
Myod1
Mylk2
Tmod1
Mybpc1
Tnnt3
Myh7
Tnnt1
Tpm3
Actn2
Dmd
Myh1
Ttn
Pax7
Des
Myf6
Myh3
Myf5
Myogenin
Hgf
Tpm4
Adam12
Sln
Day 1
Day 3
Day 7
Day 10
Day 31
Day 35
Day 56
Day 3
Day 7
Day 21
Day 35
Day 63
D
Muscle anabolism and catabolism
post-1st SBI
post-2nd SBI
log2 (fold change)
Ctsl
Junb
Rps6Ka1
Has1
Ccn4
Camkk1
Nfkbia
Eif4ebp1
Akt1
Prkaa1
Fbxo32
Foxo3
Nol3
Jsrp1
Mstn
Fst
Grb10
Akt2
Rps6Kb1
Ikbkb
Eif4g1
Rheb
Eif2b5
Eif4e
Trim63
Foxo1
Gsk3B
Eif4b
Mtor
Day 1
Day 3
Day 7
Day 10
Day 31
Day 35
Day 56
Day 3
Day 7
Day 21
Day 35
Day 63
E
Extracellular Matrix
post-1st SBI
post-2nd SBI
log2 (fold change)
Timp1
Mmp9
Mmp8
Tgfb1
Col1a1
Col3a1
Itgb1
Tgfbr1
Pdgfra
Vwa1
Mmp1
Smad3
Itga2
Pdgfa
Smad4
Timp3
Timp4
Dcn
Itga1
Timp2
Mmp2
Ccn2
Day 1
Day 3
Day 7
Day 10
Day 31
Day 35
Day 56
Day 3
Day 7
Day 21
Day 35
Day 63
F
Vascularization
post-1st SBI
post-2nd SBI
log2 (fold change)
Thsb1
Fgf2
Vegfa
Mmp14
Nrp1
Tie1
Angpt1
Vegfb
Kdr
Angpt2
Flt1
Day 1
Day 3
Day 7
Day 10
Day 31
Day 35
Day 56
Day 3
Day 7
Day 21
Day 35
Day 63
G
Neuromuscular junctions
post-1st SBI
post-2nd SBI
log2 (fold change)
Agrn
App
Utrn
Dvl1
Gphn
Tnc
Nrg1
Musk
Erbb2
Ptn
Day 1
Day 3
Day 7
Day 10
Day 31
Day 35
Day 56
Day 3
Day 7
Day 21
Day 35
Day 63

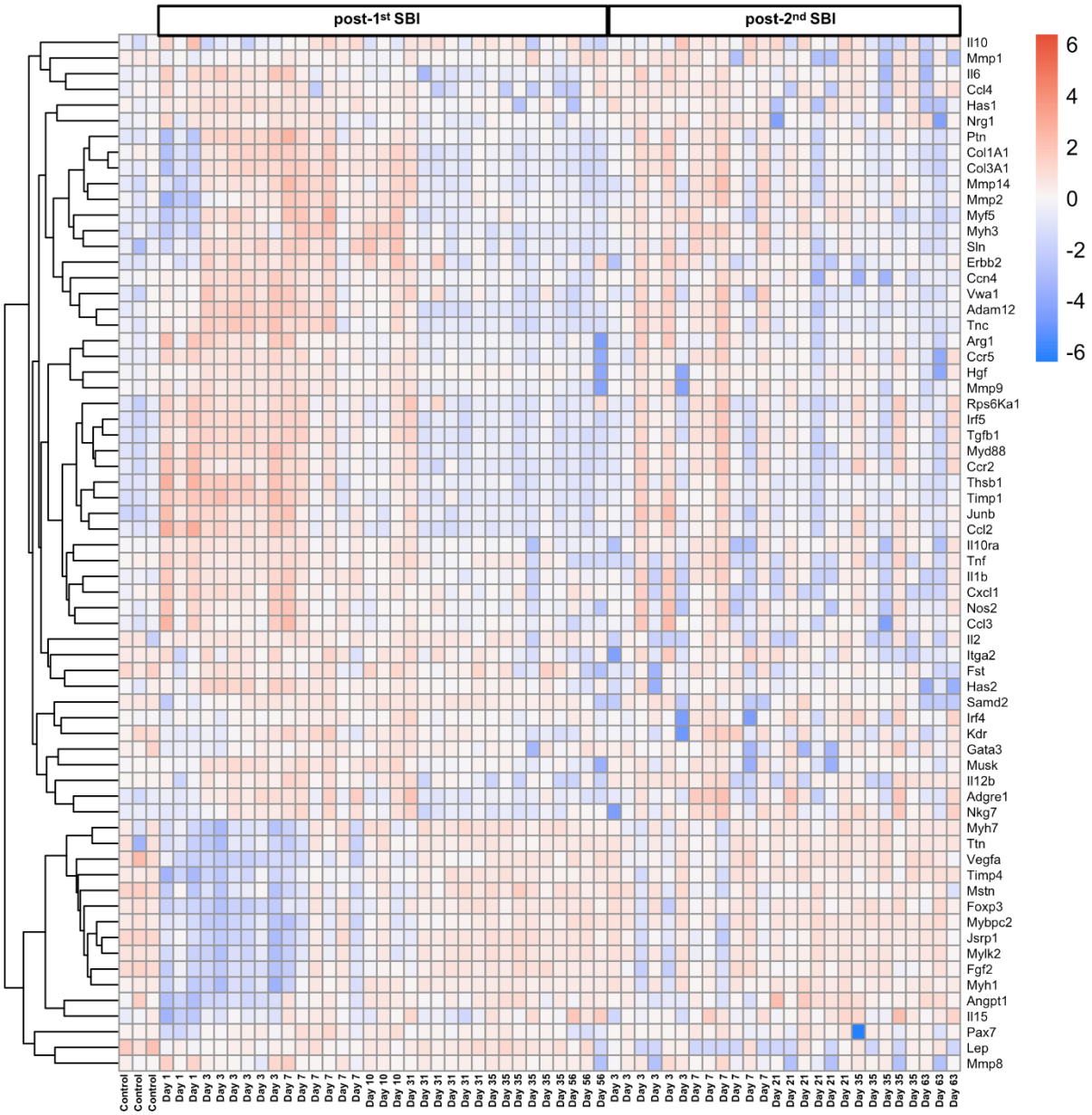

Figure 4.5 Gene expression profile across the replicates per time point after single and repeated simulated birth injury.
Heat map of genes with the highest variation in the dataset. N=3/7 per group.

Table 4.1. Immune response related genes throughout the different time points after repeated simulated birth injuries.
P and q values are indicated for significantly differentially expressed genes compared to uninjured group. FC= Log2FC

	Days after 2nd Simulated Birth Injury														
Gene	3			7			21			35			63		
	FC	p	q	FC	p	q	FC	p	q	FC	p	q	FC	p	q
Adgre1	1.31553789			3.55627507	0	0	2.61525684	0.01	0.08	2.529661	0.01	0.08	2.07202034		
Arg1	2.47717966	0	0.02	1.64061668			-0.1775432			0.13685368			-0.2287393		
Ccl2	2.80655752	0	0.01	2.46072917	0.006	0.01	1.11463903			2.68913478	0.003	0.03	1.00945403		
Ccl3	4.11776569	0	0	1.76777647			1.01452302			1.01265361			1.03009956		
Ccl4	2.3352731	0	0	2.13016896	0	0	1.15190687			1.68022553			2.34035449	0.005	0.05
Ccr2	1.34081704	0.02	0.06	1.90713463	0	0.01	0.31443285			1.80931201	0.004	0.04	1.27484094		
Ccr5	1.98280117	0.04	0.1	3.02550858	0.004	0.01	0.62804597			2.16814896	0.03	0.1	1.85722485		
Cxcl1	3.57829369	0.01	0.03	1.10774696			-0.0616809			0.22605741			-0.6684862		
Foxp3	-0.3917188			-0.5248428			-0.3137782			-0.041802			-0.0352335		
Gata3	-1.1133997			-1.4412141	0.03	0.05	-1.3379966			-0.3238518			-0.6341679		
Igf1	0.48787423			0.50704644			-0.2652431			-0.2237509			-0.5481125		
Igf1r	0.65565008	0	0	0.61258357	0.002	0.01	0.50389617	0.01	0.09	0.43836134	0.04	0.1	0.45572202		
Il10	0.24608613			0.68189705	0.01	0.02	0.70288497	0.01	0.09	0.18316467			0.33546007		
Il10ra	1.69596356			2.4842666	0.01	0.03	1.31647514			1.96860543			1.90944274		
Il12b	1.89969165	0.01	0.04	2.2159074	0	0	0.74877339			1.75069959	0.04	0.1	1.523696		
Il15	-0.198507			0.4068818			0.30165052			0.39873005			0.5367961		
Il1b	6.88124101	6.88E-14	2.39E-12	5.95816588	1.77E-15	8.23E-14	2.68458831	2.26E-14	1.04E-12	3.27976173	1.56E-14	1.08E-12	2.87962109	2.28E-14	1.59E-12
Il2	-2.8195227			0.25147327			-0.7021953			-2.9179119			-0.8913273		
Il33	0.36490963			0.44270045			0.44091491			0.22056838			0.23811717		
Il6	3.11479884	4.20E-05	0	2.00489386	0.006	0.01	1.32688326			1.91843524	0.01	0.07	0.55574405		
Irf4	0.09390505			0.96870481			1.08682157			1.56894436	0.01	0.08	1.51991042	0.03	0.19
Irf5	1.34407122	0.01	0.04	1.97142312	0	0	0.96774616			1.61031704	0.005	0.05	1.7505996	0.005	0.05
Myd88	1.14664026	0.01	0.04	1.30307144	0.005	0.01	0.43713789			0.91432487			0.72353769		
Nfkb1	0.27768821			0.5680915	0.03	0.07	0.23257477			0.42910188			0.25915407		
Nkg7	1.46460434			3.28311875	0	0	2.11834116	0.01	0.09	3.01591203	0.001	0.01	2.86095584	0.003	0.03
Nos2	6.87477916	3.12E-13	8.68E-12	4.73589435	0.02	0.04	1.27919391			3.51951931	3.39E-09	1.18E-07	2.6596629		
Stat1	0.60692927			1.5003169	0	0	0.72283543			1.09022946	0.01	0.08	1.12299278	0.02	0.16
Stat6	0.68416169			1.04042504	0.007	0.01	0.56874348			0.74609423			0.50843211		
Tnfrsf1a	0.38892727			0.38531613			-0.0588726			-0.0593433			-0.105608		

Table 4.2. Myogenesis related genes throughout the different time points after repeated simulated birth injuries.
P and q values are indicated for significantly differentially expressed genes compared to uninjured group. FC= Log2FC

	Days after 2nd Simulated Birth Injury														
Gene	3			7			21			35			63		
	FC	p	q	FC	p	q	FC	p	q	FC	p	q	FC	p	q
Pax7	-0.09			0.16			0.37			-0.25			-0.26		
Acta1	0.02316936			-0.3000812			0.58008995			0.56558299			0.46083841		
Actn2	-0.3249137			-0.0452203			0.17152183			-0.1001479			-0.1789316		
Adam12	2.25623937	0	0	2.41424305	0	0	-0.2462			-0.4756179			-0.4449533		
Des	-0.3392639			-0.3868541			-0.1548618			-0.2043479			-0.1316071		
Dmd	-0.2629371			-0.0392671			0.34949445			0.06310284			0.12853762		
Hgf	0.58899434			0.76688986			0.14596382			0.46351249			0.19603451		
Mybpc1	-0.9647268	0	0.02	-0.9015688	0.01	0.02	-0.4799291			-0.593721			-0.4656967		
Mybpc2	-0.2110009			-0.3021629			0.16940731			0.12526474			0.21432811		
Myf5	0.92194386	0	0	0.79706794	0	0	0.73801075	0.007	0.06	0.33679825			-0.2852865		
Myf6	-0.821629	0	0	-0.5857951	0.009	0.02	-0.8068009	0	0.005	-0.6843907	0.003	0.03	-0.3194646		
Myh1	0.01195634			-0.2487938			0.52803377			-0.0115645			0.18481157		
Myh3	2.81544654	0	0	5.25742584	2.71E-07	4.71E-06	2.65528892	0	0.03	0.75108399			0.27900562		
Myh7	-0.317075			-0.4144545			0.37514331			0.3214762			0.43807999		
Mylk2	-0.5360198			-0.9701489	0.04	0.08	-0.2859813			-0.2997333			-0.1645212		
Myod1	-0.7678297	0.01	0.04	-1.2865482	4.87E-05	0	-1.0082759	0	0.02	-1.1671528	0	0.007	-1.2080089	0.001	0.02
Myog	0.81063011	0	0.02	0.22940258			0.00566239			-0.412943			-0.506345		
Sln	1.62742805	0.01	0.04	2.3211714	0	0	0.76373956			0.78811659			-0.0686495		
Tcap	-0.2345825			-0.806663	0.04	0.08	-0.1391563			-0.0671382			0.13954969		
Tmod1	-0.7000945	0.03	0.07	-0.9272155	0.004	0.01	-0.6639865	0.04	0.19	-0.4042975			-0.4825921		
Tnnt1	-0.1440658			-0.2422662			0.35086716			0.35739569			0.4321472		
Tnnt3	-1.0871174	0	0.02	-1.0422206	0.009	0.02	-0.4381052			-0.6057715			-0.5354041		
Tpm3	-0.1672384			-0.1447604			0.52567842			0.53401076			0.52503759		
Tpm4	1.11113252	0	0.02	1.1130846	0.005	0.01	0.56239046			0.72901099			0.44673377		
Ttn	-0.2838444			-0.0821689			0.10928269			0.2159503			0.22653365		

Table 4.3. Muscle anabolism and catabolism related genes throughout the different time points after repeated simulated birth injuries.
P and q values are indicated for significantly differentially expressed genes compared to uninjured group. FC= Log2FC

	Days after 2nd Simulated Birth Injury														
Gene	3			7			21			35			63		
	FC	p	q	FC	p	q	FC	p	q	FC	p	q	FC	p	q
Has1	1.63	0.02	0.05	1.08			0.81			1.24			-2.49		
Akt1	-0.231723			-0.1722273			-0.2015771			-0.229714			-0.1886912		
Akt2	-0.4652612	0.03	0.07	-0.4924408	0.02	0.04	-0.2897174			-0.3163823			-0.2346297		
Camkk1	0.34601646			0.67307267	0.01	0.03	0.31531649			0.20860987			0.0898435		
Ctsl	0.66778891	0.03	0.08	0.53543334			0.13569182			0.14969831			0.17911889		
Eif2b5	-0.7510263	5.16E-05	0	-0.9539257	2.32E-07	4.61E-06	-0.5199577	0.005	0.05	-0.5124645	0.008	0.05	-0.5036815	0.02	0.1
Eif4b	-0.239648			-0.464939	0.006	0.01	0.0688716			0.00730212			0.08677879		
Eif4e	-0.6869186	0	0	-0.4830864	0.009	0.02	-0.4015353	0.03	0.15	-0.4843876	0.01	0.07	-0.3122299		
Eif4ebp1	0.06499577			-0.6718313	1.37E-08	3.19E-07	-0.1354139			-0.2080245			-0.0157674		
Eif4g1	-0.3752678			-0.5232425	0.005	0.01	-0.1131203			-0.2607579			-0.1760917		
Fbxo32	0.15592488			-0.5352283			0.16298208			0.5890172			0.58180934		
Foxo1	-0.0684141			0.02047918			0.27164583			0.30360012			0.52989642	0.002	0.031
Foxo3	0.16472942			0.14308394			0.28564863			0.10835136			0.36890497	0.02	0.18
Fst	-1.1383531	4.18E-05	0	-0.4274297			-1.0452085	0	0.004	-0.6323033	0.03	0.1	-1.5115167	8.31E-05	0.001
Grb10	-0.7131634	4.52E-11	1.04E-09	-0.4280018	6.61E-05	0	-0.5581825	2.49E-07	6.90E-06	-0.5826393	2.78E-07	5.52E-06	-0.8550161	1.61E-10	5.61E-09
Gsk3b	-0.3626213			-0.1242114			-0.0006434			-0.0191362			0.04370119		
Ikbkb	-0.3944253			-0.4117868			-0.5497125	0.006	0.06	-0.2987984			-0.277723		
Junb	2.10179447	5.39E-05	0	1.49297542			0.75966758			1.67224876			1.02101225		
Mstn	-0.9701743	0.03	0.08	-1.8641435	5.50E-05	0	-1.3631566	0.003	0.03	-1.4342014	0.003	0.03	-1.6709658	0.003	0.04
Mtor	-0.1856479			-0.4352534	0	0	-0.0765345			-0.0587486			0.07826		
Nfkbia	0.48953087			0.34088626			0.12397139			0.51776502			0.55216476		
Nol3	0.35462079			-0.1948529			0.27075141			0.13782787			0.21164634		
Prkaa1	-0.1250985			-0.0431805			0.16724791			0.06863348			-0.1507732		
Rheb	-0.536009	0	0.01	-0.5667091	0	0	-0.2793008			-0.2096313			-0.1158169		
Rps6ka1	0.84608062			1.45902051	0.004	0.01	0.48662641			1.18148563	0.02	0.1	1.07123279		
Rps6kb1	-0.7580955	0	0	-0.4958105	0.01	0.03	-0.4886425	0.01	0.09	-0.5827838	0.005	0.05	-0.6094505	0.01	0.1
Ccn4	1.66053332	0.01	0.04	1.66619993	0.01	0.03	0.28660856			-1.3366488			-1.4164371		
Trim63	-0.1194405			-0.6658114	0.01	0.03	-0.2713681			-0.0601036			0.27408859		

Table 4.4. Extracellular matrix related genes throughout the different time points after repeated simulated birth injuries.
P and q values are indicated for significantly differentially expressed genes compared to uninjured group. FC= Log2FC

	Days after 2nd Simulated Birth Injury														
Gene	3			7			21			35			63		
	FC	p	q	FC	p	q	FC	p	q	FC	p	q	FC	p	q
Mmp8	1			1.07			-0.71			0.21			-0.56		
Col1a1	0.98372203			1.2010992			-0.1228866			-0.8810262			-1.3146721		
Col3a1	1.21037758	0.01	0.05	1.49166045	0.004	0.1	0.43752722			-0.1674783			-0.7081826		
Itga1	0.04934163			0.59379572	0	0	0.33939788	0.03	0.15	0.43374693	0.009	0.05	0.26405894		
Itga2	0.02620677			0.09542747			0.06254833			-1.0862344	0.01	0.07	-0.7405512		
Itgb1	0.13898235			0.2707636			0.03145044			-0.0265108			-0.1522956		
Mmp1	0.45294773			0.17730176			-0.0517942			0.09056389			-1.709139		
Mmp2	0.27521354			1.09396247	0.008	0.02	0.49178323			0.24604027			-0.0758155		
Mmp9	1.08885893			1.65737323	0.01	0.03	0.393747			-0.1329704			-0.7321961		
Pdgfa	-0.6163226			-0.3086441			-0.3578908			-0.2329094			-0.8608714	5.00E-08	1.41E-06
Pdfgra	0.31025163			0.41523157			-0.0863701			0.08351219			-0.4507678		
Smad3	-0.9829924	0	0	-1.0431873	0	0	-0.7334231	0.01	0.08	-0.7788297	0.009	0.05	-0.9574591	0.005	0.05
Smad4	-0.2889801			-0.2002076			-0.0571093			-0.0338918			0.18623242		
Tgfb1	1.14273908	0.03	0.08	1.76862926	0	0	0.83367159			1.19081527	0.03	0.12	1.08073156		
Tgfbr1	0.19425668			0.22106398			0.11303336			0.22301536			0.20326674		
Timp1	2.84303327	3.95E-05	0	2.21586164	0	0	0.72818828			1.27942783	0.04	0.1	0.65999542		
Timp2	-0.1740448			0.36634178			0.23366219			0.19095401			-0.0442825		
Timp3	-0.2785393			-0.2382331			0.49908612			0.2056212			0.35892781		
Timp4	-0.3162146			-0.2132306			0.15182609			0.1179532			0.44529833		
Vwa1	0.61124212			0.99136444	0.01	0.03	0.18669157			0.20776831			0.01139593		

Table 4.5. Neuromuscular junctions related genes throughout the different time points after repeated simulated birth injuries.
P and q values are indicated for significantly differentially expressed genes compared to uninjured group. FC= Log2FC

	Days after 2nd Simulated Birth Injury														
Gene	3			7			21			35			63		
	FC	p	q	FC	p	q	FC	p	q	FC	p	q	FC	p	q
Dvl1	-0.85	8.92E-06	0	-0.58	0	0.01	-0.51	0.007	0.06	-0.53	0.007	0.05	-0.51	0.02	0.1
Agrn	0.07102083			0.42878044			0.03684727			-0.2860692			-0.265273		
App	0.1228353			0.47255595	0.03	0.06	0.02390995			0.16446805			-0.0030643		
Erbb2	1.04988573	0	0.03	0.78169282	0.04	0.08	0.41891115			0.28719009			0.53654034		
Gphn	-0.397876			-0.4483913			-0.1131154			-0.2095773			-0.0122485		
Musk	0.79191941			1.13027991	0.01	0.03	-0.0462679			-0.0948886			-0.2371049		
Nrg1	1.24181907	0	0.01	1.51925473	8.40E-05	0	0.1231052			1.12088398	0.02	0.1	0.811348		
Ptn	1.14273933	0.01	0.04	1.16021009	0.01	0.03	0.36964083			0.52350832			-0.16198		
Tnc	2.33961511	0	0.01	2.42767138	0	0.01	0.00639764			-0.0570216			-0.9897771		
Utrn	-0.3686152			-0.0802778			-0.1811844			-0.0649315			-0.2013801		

Table 4.6. Vascularization related genes throughout the different time points after repeated simulated birth injuries.
P and q values are indicated for significantly differentially expressed genes compared to uninjured group. FC= Log2FC

	Days after 2nd Simulated Birth Injury														
Gene	3			7			21			35			63		
	FC	p	q	FC	p	q	FC	p	q	FC	p	q	FC	p	q
Thsb1	1.7	0	0.02	1.81	0.004	0.01	0.5			0.57			0.03		
Angpt1	-0.562359	0.04	0.09	-0.4918092			0.44142617			-0.1530769			0.14926645		
Angpt2	-0.0535874			0.48069606	0.01	0.03	0.27448998			0.44452322	0.03	0.1	-0.1156		
Fgf2	-1.4901025	0.0001	0.001	-0.8692082	0.02	0.04	-1.0405345	0.007	0.06	-0.943594	0.02	0.1	-0.8296596		
Flt1	-0.0411508			-0.1269556			-0.0514609			0.02596042			-0.0590792		
Kdr	-0.8413409	0	0	0.16400614			-0.4384014			-0.6412035	0.02	0.1	-0.6169142		
Mmp14	0.65281754			1.58154279	0.002	0.01	0.47101963			0.63130721			-0.1493721		
Nrp1	-0.1903515			0.37244373			-0.0837235			-0.0273247			-0.2683051		
Tie1	0.27733478			0.4818113			0.23309979			0.19527437			0.11773356		
Vegfa	-1.0128641	0	0	-0.8615957	0	0	-0.6542518	0.01	0.09	-0.6074338	0.03	0.1	-0.7111762	0.03	0.18
Vegfb	-0.9132063	0	0	-0.6642029	0.006	0.01	-0.4725045			-0.6661703	0.008	0.05	-0.4278072		

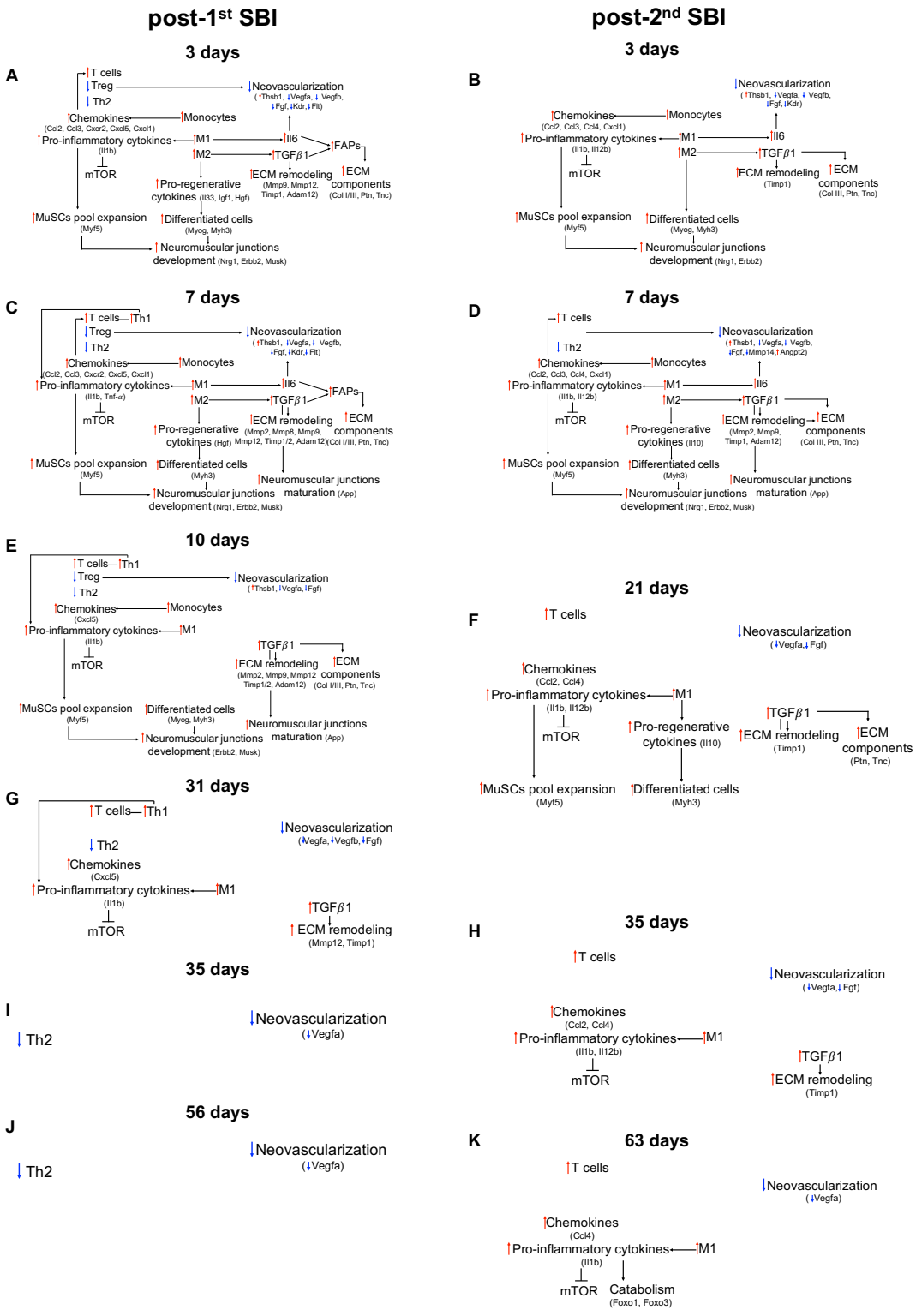

Figure 4.6 Schematic interpretation of the interplay between different pathways analyzed at several time points following single or repeated simulated birth injury.

4.2.4 Skeletal muscle ECM therapy improves pelvic floor muscle phenotype after repeated birth injuries

Chapter 3 investigated the efficacy of the SKM hydrogel at two therapeutic windows—either immediately after birth injury or at a delayed time point. These are clinically relevant time points for the prevention or treatment of PFM dysfunction, where the hydrogel can be administered on Labor and Delivery or on a routine post-partum visit. During the latter, PFM weakness—known to be a risk factor for the development of PFDs[18]—can be assessed by palpation or perineometer. Based on the findings from the rat pre-clinical model, the acellular biomaterial prevented and mitigated the pathological alterations at both time points, with parameters closer to the uninjured state after delayed injection. In addition, the gene expression indicated that, after hydrogel injection 4 weeks post-SBI, the SKM mostly clustered separately from saline and untreated SBI groups. Thus, since delayed administration of the hydrogel may be a more clinically relevant time point and we demonstrated efficacy of the biomaterial at this therapeutic window, we then investigated if delayed SKM injection will enhance muscle regeneration after repeated birth injuries (Fig. 4.7A).

At 4 weeks post-delayed injection (8 weeks post-2nd SBI), SKM administration increased fiber size in relation to saline ($P<0.001$) and to uninjured controls ($P<0.001$). Saline resulted in a substantial increase in fiber area compared to untreated SBI ($P<0.001$), but with fiber size lower than controls (Fig. 4.7B). SKM decreased the pathological increase in collagen observed in untreated SBI ($P<0.01$), restoring the content to the control levels ($P=0.64$). Saline injection had a similar response as SKM ($P=0.98$), with decreased collagen content in relation to untreated SBI ($P<0.01$) and analogous levels to controls ($P=0.45$, Fig. 4.7C).

As repeated birth injuries led to PFM dysfunction, our next step was to investigate the efficacy of SKM for the improvement of PCa function. In terms of active mechanical properties, SKM demonstrated a similar force-frequency curve compared to saline and untreated SBI (Fig.

4.7D) with analogous peak force values (saline; P=0.89, untreated SBI; P=0.99) and a trending decrease in relation to uninjured controls (P=0.1, Fig. 4.7E). For the passive mechanical properties, SKM injection resulted in a similar stress-strain pattern as uninjured controls, while the pattern after saline administration was similar to untreated SBI (Fig. 4.7F). However, due to the high variability, no differences were observed among the groups (Fig. 4.7G). Taken together, while SKM improved fiber size and decreased collagen content, these levels were not enough to detect differences in muscle function.

We then performed a gene expression study after the improvements in the histomorphological properties after SKM injection. Based on the peak cell infiltration of the hydrogel, PCa was harvested 7 days after biomaterial administration. Based on PC analysis (Fig. 4.7H), each group mostly clustered separately, with SKM and saline closer in relation to untreated SBI. Gene expression profiles for each time point are observed in Figure 4.8. Clustered heat maps indicating fold change of SKM and saline groups with respect to untreated SBI, and with differentially expressed genes between SKM and saline are demonstrated in Figure 4.7I. Pairwise comparisons are shown in Figure 4.9. SKM administration upregulated genes associated with the pro-regenerative phase, specifically macrophages (Adgre1, Arg1, Stat6) and T cells (Nkg7, Gata3) polarized towards the type 2 phenotype. Although increased expression of an inflammatory gene (Il1b) in relation to saline was observed, this gene was downregulated compared to untreated SBI for both injection groups. This same expression pattern was observed for genes related to myogenesis (Myh3, Adam12), cellular survival (Has1, Rps6ka1, Junb), ECM remodeling (Col1a1, Col3a1, Tgfb1, Mmp2, Mmp9, Timp1), neuromuscular junctions (Tnc, Agrn), and vascularization (Mmp14, Tie1); the genes were upregulated relative to saline but with decreased or unchanged expression compared to untreated SBI for both groups. Altogether, SKM mainly demonstrated an enhancement of the pro-regenerative phase. In addition, while increase

expression of genes associated with myogenesis, cellular survival, and ECM remodeling was identified, decreased or unchanged expression from untreated SBI was observed.

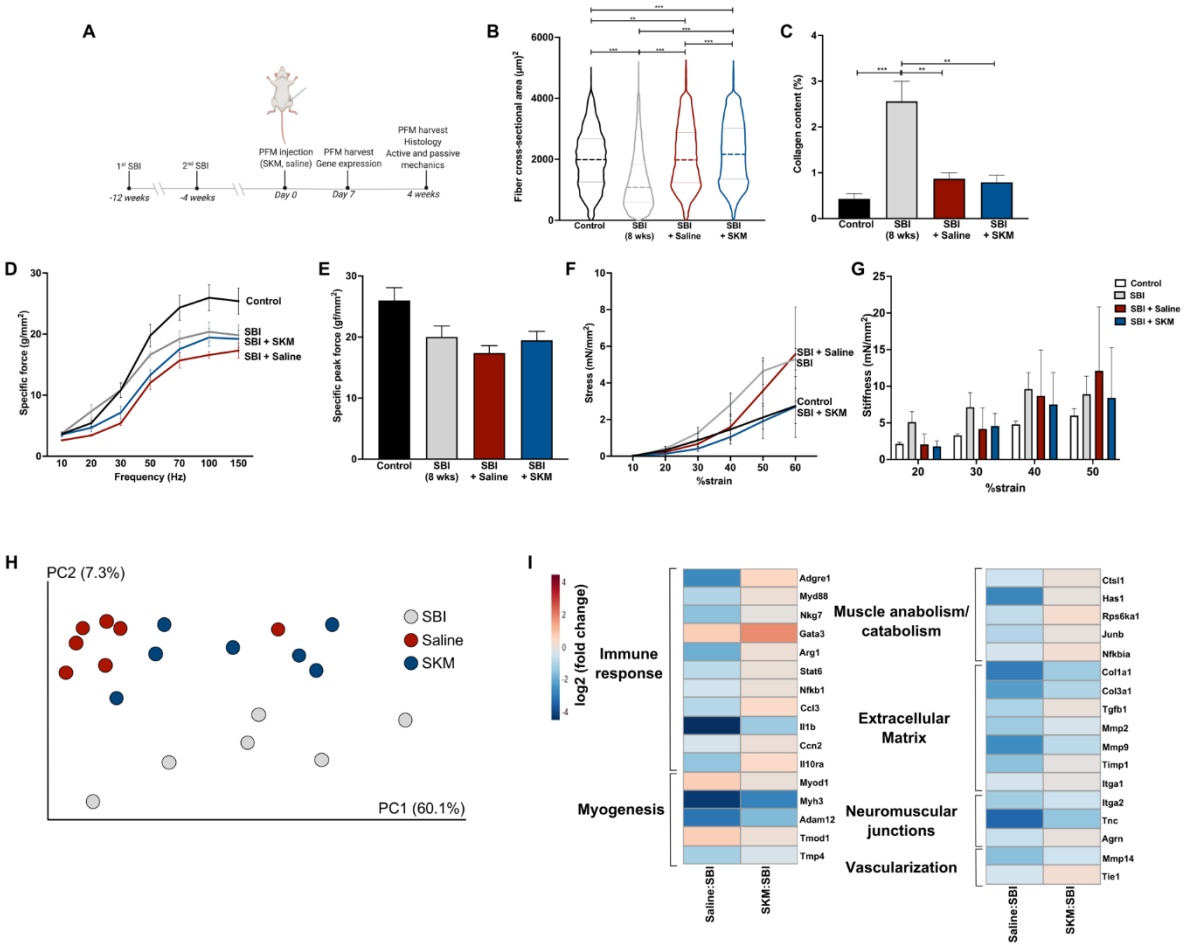

Figure 4.7 Delayed injection of skeletal muscle extracellular matrix hydrogel (SKM) after repeated birth injuries increased fiber size and mitigated collagen content.
(A) Study timeline. Quantification of fiber cross-sectional area (B) and collagen content (C) was compared across the four groups (uninjured controls, untreated simulated birth injury (SBI), SBI + saline, SBI + SKM). Active mechanical properties were analyzed across groups represented by force-frequency curves (D), and specific peak force (E). Passive mechanical properties were identified by stress-strain curves (F) and stiffness (G). (H) Principal components analysis of transcriptional signatures at 7 days post-injection. (I) Supervised heat map of fold changes for SKM and saline with respect to untreated SBI. Heat map includes significantly differentially expressed genes based on the pairwise comparison between SKM and saline groups. N=3-7/group for histological assessments, 4-3/group for mechanical assessment and 6-7/group for gene expression analyses. *P*-values derived from one-way ANOVA followed by pairwise comparisons with Tukey's range test for parametric data and Kruskal-Wallis followed by pairwise comparisons with Dun's test for non-parametrically distributed data. Gene expression analysis was analyzed based on NanoStringDiff package in R. *p<0.05, **p<0.01, ***p<0.001, mean±SEM.

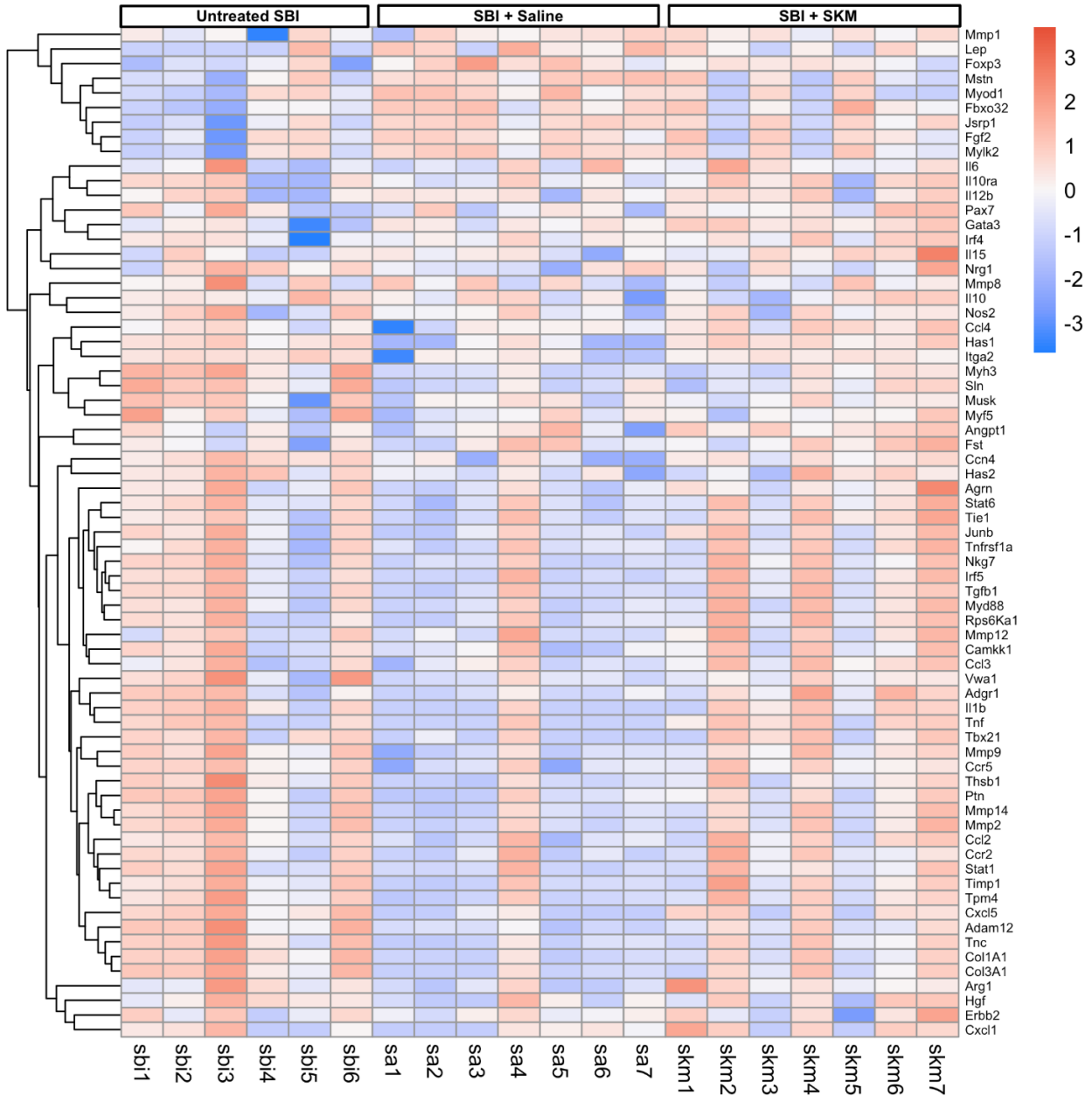

Figure 4.8 Gene expression profile across the replicates 7 days after delayed injection of skeletal muscle extracellular matrix (SKM) hydrogel.
Heat map of genes with the highest variation in the dataset. N=6-7/group.

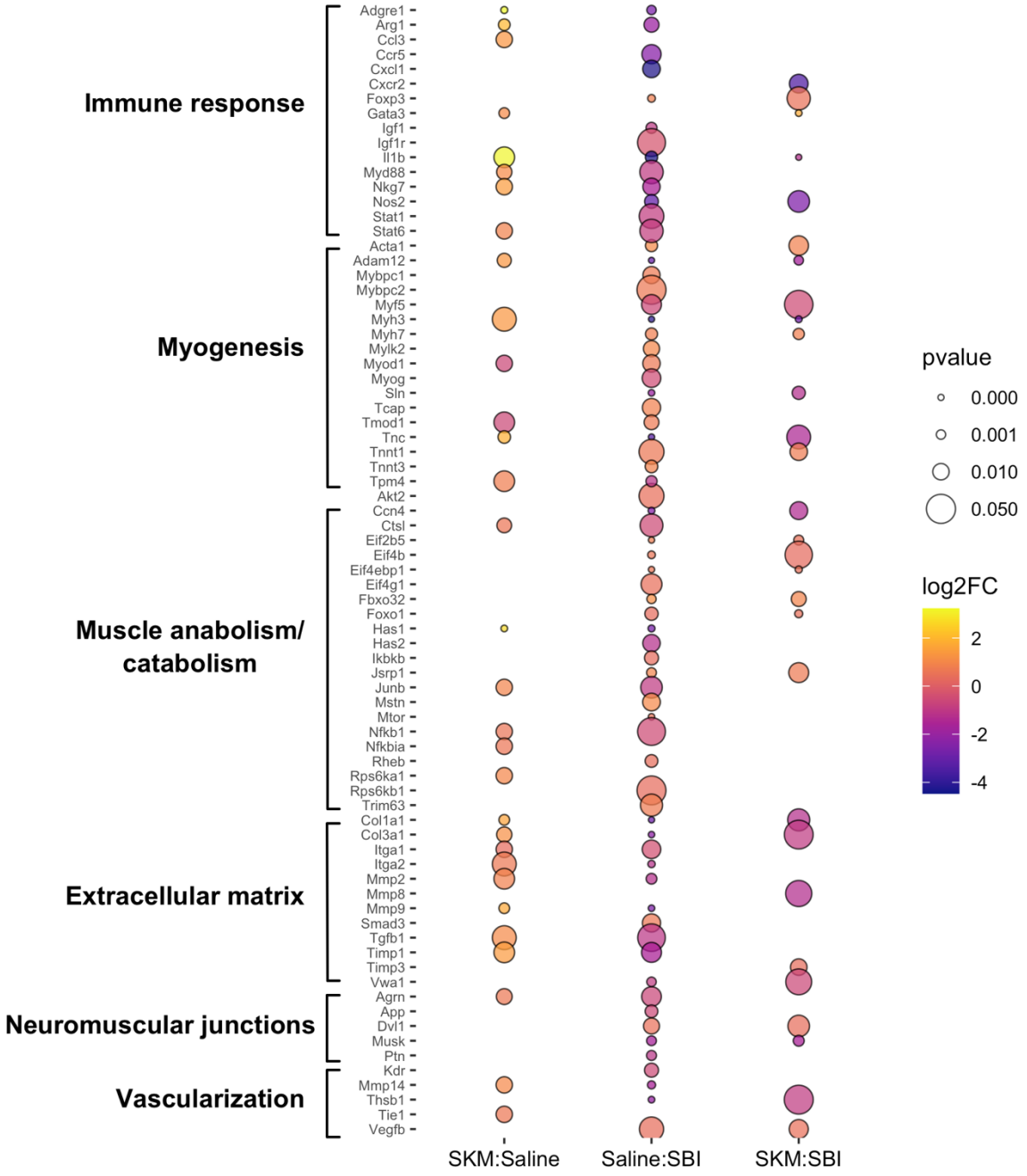

Figure 4.9 Pairwise comparisons after delayed injection of skeletal muscle extracellular matrix (SKM) hydrogel.
Significantly differentially expressed genes at 7 days post-injection.

4.3 Discussion

In the current study, we first wanted to assess if a single SBI impacts PCa force production since we have previously identified that in the rat model, validated for the studies of the human PFMs[6, 19], SBI leads to muscle atrophy and fibrosis. Despite these pathological alterations, PCa long-term active force generation recovered after a single SBI. However, passive mechanical properties were affected, as indicated by an increased stiffness. Published clinical studies demonstrate progressive worsening of PFM function after each subsequent vaginal delivery.[20] Thus, we assessed the effect of repeated birth injuries on PFM force production to determine if the rat model recapitulates this phenotype. In contrast to a single birth injury, repeated SBIs resulted in a 30% decrease in PFM contractile force production despite a 12-week recovery period, together with an increased passive stress. We next investigated changes in the morphometric properties after repeated birth injuries to begin to understand the mechanisms accounting for the observed decrease in PFM function. Our results demonstrate that relative to a single SBI, repeated birth injuries at the time of an atrophic and fibrotic PFM, lead to an impairment in muscle regeneration, reduced fiber size, increased collagen content, all which can negatively affect muscle function.[12] We then assessed changes in gene expression across physiological time points to further determine possible causes for the observed histological alterations. In relation to a single SBI, repeated birth injuries lead to a prolonged inflammatory response, upregulation of genes associated with catabolism, impairment in muscle anabolism and sustained expression of ECM remodeling genes. At last, delayed administration of SKM after repeated SBIs substantially increased fiber size and decreased collagen content, with no influence on muscle function. Gene expression analysis demonstrated an enhancement of genes associated with the pro-regenerative phase.

In our study, the reduced fiber size and increase in collagen content coincide with the decrease in active muscle force production and trending increase in passive stiffness at 12 weeks

post-2nd SBI. In our rat model, a substantial 150% increase in collagen content after the single injury was enough to increase stiffness. It is well established in the limb muscles that muscle force production has a direct relationship to myofiber cross-sectional area,[12] however the exact extent of alterations in fiber size that impact this functional parameter remains undetermined. We observed that a 15% decrease in fiber size at 8 weeks after single SBI was not enough to influence muscle active force production, while a 25% reduction after repeated birth injuries lead to decrease active force. Taken together, these data indicate a "dose-dependent" relationship between the number of birth injuries, the extent of the pathological alterations of the PFM morphometric properties, and the impact on active muscle function. The above provides a putative mechanistic link between multiparity and progressive worsening of the PFM function identified clinically.[20]

We performed a gene expression study to identify potential causes behind the histological alterations observed after 2nd SBI. With respect to a single SBI, a prolonged inflammatory response was observed after repeated injuries, which could also indicate such "dose-dependent" relationship between the number of birth injuries, and the presence of the altered immune response. As previously explained in chapter 2 (2.4), an inflammatory response negatively influences muscle anabolism, specifically the AkT/mTOR signaling, and also enhances muscle catabolism.[17] In our study, the persistent inflammatory response observed after repeated injuries (Fig. 4.6) could be associated with the profound reduction in fiber size, through impairment in muscle anabolism and upregulation of catabolism. In addition, a small fiber area could also be related to the observed increase in centralized nuclei. The genes associated with myogenesis pathway were upregulated at the expected time course as with a single SBI (Fig. 4.6), elucidating the investigation of other mechanisms behind the substantial increase in centralized nuclei identified at the long-term time points.

As with delayed injection after a single SBI, administration of SKM 4 weeks post-2nd SBI led to long-term improvements in tissue-level alterations. However, no differences in muscle function were detected across the groups. One possible reason behind this result is the small dynamic range between control and untreated SBI, which was only a 30% decrease in active force production. Another possible reason is that SKM might not be enough to influence muscle force, suggesting the co-delivery of the biomaterial with a bioactive molecule that will enhance muscle function. A potential candidate could be IGF-1 (insulin growth factor), which was not differentially expressed after repeated injuries and is known to stimulate the mTOR pathway, promoting protein synthesis with an overall improvement in force production,[21] as previously demonstrated in a skeletal muscle injury model.[22] The gene expression analysis 7 days after hydrogel injection mainly demonstrated upregulation of genes associated with the pro-regenerate phase of the immune response—correlating with the known effect of ECM hydrogels as immunomodulators.[23] To fully analyze pathways that could be involved in the improvement of PFM phenotype, other time points could be investigated, such as 3- or 21-days post-injection to cover the time point at which genes related to myogenesis begin to differentially express or the time frame around hydrogel degradation, respectively.

Due to significant technical constraints associated with dissecting the pubocaudalis branch of the levator ani nerve, we relied on the *ex vivo* mechanical testing. While the results could be potentially divergent from the *in vivo* mechanics, our protocol allowed us to uncouple potential neurogenic influence on the observed changes in muscle force and focus exclusively on the independent myogenic contributions to the observed phenotype.

In conclusion, our findings indicate that repeated birth injuries lead to increased pathological alterations, and prolonged inflammatory response compared to a single birth injury. The resultant impairment of PFM force production provides potential mechanistic link behind the

additive risk of multiparity for PFM dysfunction. In addition, biomaterial administration improved PFM phenotype, with potential influence on passive mechanical properties.

4.4 Materials and methods

4.4.1 Study design

The objectives of the current study were to: 1) assess PFM function after a single SBI to correlate with previously identified pathological alterations (Fig. 4.1A, 4.2A), 2) determine the impact of repeated birth injuries on PCa function, histological alterations (Fig. 4.3A), and gene expression profile (Fig. 4.4), 3) investigate the efficacy of the SKM hydrogel after repeated SBIs (Fig. 4.7A). A 2nd SBI (2.4.4) was performed 8 weeks after the 1st SBI, since muscle regeneration was completed at this time point (Fig. 2.3E). SKM injection was performed as previously described (3.4.2) 4 weeks after repeated birth injuries. The sample size, indicated in the figure legend, was calculated based on preliminary experiments. No outliers were excluded from the study. For the quantitative analyses, the investigators were blinded to the group identity.

4.4.2 Pelvic floor muscle mechanics

4.4.2.1 Active mechanical testing

Animals were anesthetized with 3% isoflurane @ 2 L/min; a midline incision was made at the level of the symphysis pubis, which was disarticulated, and PCa was identified and harvested for *ex vivo* mechanical testing. The PCa portion of the rat levator ani was again the focus of these experiments, as this muscle's stretch ratios are similar to pubococcygeus, which experiences the largest strains during human parturition.[19, 24] Immediately after dissection, animals were euthanized by CO_2 inhalation, followed by bilateral thoracotomy. The muscle was placed in an organ bath (805-A, Aurora Scientific, Aurora, Ontario) with aerated (95% O_2, 5% CO_2) mammalian Ringer's buffer (137 mN NaCl, 5mM KCl, 24 mM $NaHCO_3$, 1mM NaH_2PO_4, 11mM $C_6H_{12}O_6$, 1mM

$MgSO_4$, 2mM $CaCl_2$, pH 7.4) and platinum-based electrodes (Fig. 4.1B). Using 4.0 silk sutures, attached to the proximal enthesis and distal tendon, PCa was attached to the fixed post on one side and the lever arm of the force transducer (300C: Dual-Mode, 1.5 N, Aurora Scientific, Aurora, Ontario) on the other side (Fig. 4.11B). For all mechanical testing, electrical pulses were delivered to the platinum-based electrodes using PowerLab (4/35 Power Lab; ADI Instruments, Sydney, Australia) and an electrical stimulator (701C, Aurora Scientific, Aurora, Ontario). Force output was recorded from the force transducer with LabChart (v8.1.3; ADInstruments, Sydney, Australia).

To determine muscle length corresponding to the greatest force generation, known as the optimal muscle length (L_o), PCa was gradually stretched to achieve 0.05 V difference per increment, starting from the voltage at slack muscle length. PCa was stimulated with isolated 1 Hz electrical pulses at each muscle length until maximal force was determined.[25] Once L_o was identified, PCa was subjected to a range of stimulations to establish the force-frequency relationship in uninjured and injured animals. Electrical stimuli (0.2 ms, 1 A, 1200 ms trains) were applied with successive frequency increases (10, 20, 30, 50, 70, 100, 150 Hz). Each stimulus was interspersed by a two-minute rest interval. Maximum force at each frequency was normalized by physiological cross-sectional area, which was calculated using validated methods.[25, 26] Briefly, muscle mass was divided by the product of fiber length (L_f) and muscle density (1.06 mg/mm^3).[26] L_f was obtained by multiplying L_o by the previously determined PCa muscle length to fiber length ratio of 1.68.[6] After normalization, force-frequency curves and peak force were obtained.

4.4.2.2 Passive mechanical testing

After active mechanics experiments, the PCa was placed in a relaxing solution with leupeptin, a protease inhibitor, and stored at -20°C for at most 2 weeks.[27] The PFM was then micro-dissected to obtain small muscle fascicles—3 fascicles/muscle were analyzed. Laser

diffraction was used to measure the optimal sarcomere length (L_s) and calipers were used to measure the fascicle length at that L_s. Each fascicle was then attached to the force transducer and the fixed post at the previously measured fascicle length. Tissue was evaluated by stress-relaxation tests, where the muscle was stretched at a rate of 2 L_s/s in 10% increments until failure or to 60%, with 3-min relaxation period between increments.[28] Force values were divided by cross-sectional area—assuming cylindrical shape[27]—to obtain stress-strain curves. Sample stiffness was calculated by measuring the slope of the stress-strain curve at 20, 30, 40 and 50% stretch.

4.4.3 Immunohistochemical analyses

PCa was harvested, embedded in optimal cutting temperature media, and snap-frozen in isopentane chilled in liquid nitrogen. Samples were cryosectioned at 10 μm and prepared for immunohistochemical analyses. To assess fiber area and centralized nuclei, slides were fixed in 4% PFA, rinsed three times in 1x phosphate buffer saline (PBS) and incubated in blocking buffer for 1 hour (10% normal goat serum (Gemini Bio-products, Sacramento, CA) in PBS). Slides were then incubated overnight with anti-laminin antibody (Abcam, Cambridge, MA; 1:200), rinsed in PBS and incubated in Alexa Fluor 488 conjugated secondary antibody (Invitrogen, Carlsbad, CA; 1:500) for 30 minutes. After rinsing in PBS, nuclei were counterstained with Hoechst 33342 (1: 10000). Slides were mounted with Fluoromount (Sigma-Aldrich, St. Louis, MO) and scanned at 20X on the Ariol DM6000 B microscope (Leica, Wetzlar, Germany). Fiber area was quantified using a custom macro in ImageJ (NIH, Bethesda, MD) for a total of ~10,000 fibers per sample obtained from randomly selected 4-8 tissue sections. Centralized nuclei per total number of fibers were counted manually.

For the quantification of the intramuscular collagen content, slides were fixed in cold acetone, rinsed three times in 1xPBS and incubated in blocking buffer (10% normal goat serum (Gemini Bio-products, Sacramento, CA) + 0.3% Triton X-100 (Sigma-Aldrich, St. Louis, MO) +

1% bovine serum album (Sigma-Aldrich, St. Louis, MO) in PBS)) for 1 hour. Slides were then incubated overnight with collagen I primary antibody (Invitrogen, Carlsbad, CA, PA595137, 1:200), rinsed in PBS, and incubated with Alexa Fluor 488 conjugated secondary antibody (Invitrogen, Carlsbad, California; 1:500) for 2 hours. Slides were then rinsed in PBS and nuclei were counterstained with Hoechst 33342 (1:10000). Slides scanned at 20X (Ariol DM6000 B microscope, Leica, Wetzlar, Germany) were processed for quantification using freehand selection tool in ImageJ (NIH, Bethesda, MD). Collagen content was expressed as area fraction occupied by collagen staining.

4.4.4 Gene expression profile after repeated birth injuries

PCa was harvested at physiological relevant time points to assess potential causes behind the identified structural alterations at the tissue-level (i.e., profound reduction in fiber size, and increase collagen content). RNA isolation, and Nanotring nCounter analysis were done as previously described (2.4.7).

4.4.5 Statistical Analysis

For the primary mechanical outcome of interest, the specific peak force, sample size calculation (G*power software) yielded 7 animals/time point based on Cohen's d effect size of 1.7 obtained from the preliminary experiments, to achieve 80% power at a significance level of 0.05. For histological outcomes, Cohen's d effect size of 5.2, obtained from our previous study comparing morphological outcomes between animals subjected to a single SBI and unperturbed controls[29], was used to determine sample size. Power calculation yielded 3 animals/time point to achieve 80% power at a significance level of 0.05. Data with a parametric distribution were compared with a two-way ANOVA followed by Tukey's or Sidak's post hoc pairwise comparisons, when indicated. Fiber area, which followed a non-parametric distribution, was analyzed with

Krukal-Wallis test followed by Dunn's pairwise comparisons. Data were analyzed using GraphPad Prism v8.0, San Diego, CA. Gene expression normalization and differential expression was analyzed using the NanoStringDiff package in R, with a significance at a p value<0.05 and a fold change cutoff of 1 ± 0.25. [30]

4.5 Acknowledgements

Chapter 4 is currently being prepared for submission for publication of the material, Pamela Duran, Emma Zelus, Saya French, Lindsey Brunett, Karen L. Christman, and Marianna Alperin. "Repeated birth injuries lead to pelvic floor muscle dysfunction and impairment in regeneration". The dissertation author was the primary author of this paper.

4.6 References

1. Hallock, J.L. and V.L. Handa, The Epidemiology of Pelvic Floor Disorders and Childbirth: An Update. *Obstet Gynecol Clin North Am*. 2016; 43(1): p. 1-13.

2. Mant, J., Painter, R., Vessey, M., Epidemiology of genital prolapse: observations from the Oxford Family Planning Association study. *British Journal of Obstetrics and Gynecology*. 1997; 104: p. 579-585.

3. Palma, T., M. Raimondi, S. Souto, C. Fozzatti, P. Palma, and C. Riccetto, Prospective study of prevalence of overactive bladder symptoms and child-bearing in women of reproductive age. *J Obstet Gynaecol Res*. 2013; 39(8): p. 1324-9.

4. Rortveit, G., Hannestad, Y., Kjersti, A., Hunskaar, S., Age- and Type-Dependent Effects of parity on Urinary Incontinence: The Norwegian EPINCONT Study. *The American College of Obstetricians and Gynecologists*. 2001; 98(6): p. 1004-1010.

5. Chen, L., D. Luo, X. Chen, M. Jin, X. Yu, and W. Cai, Development of Predictive Risk Models of Postpartum Stress Urinary Incontinence for Primiparous and Multiparous Women. *Urol Int*. 2020; 104(9-10): p. 824-832.

6. Alperin, M., L.J. Tuttle, B.R. Conner, D.M. Dixon, M.A. Mathewson, S.R. Ward, and R.L. Lieber, Comparison of pelvic muscle architecture between humans and commonly used laboratory species. *Int Urogynecol J*. 2014; 25(11): p. 1507-15.

7. Kitamoto, T. and K. Hanaoka, Notch3 null mutation in mice causes muscle hyperplasia by repetitive muscle regeneration. *Stem Cells*. 2010; 28(12): p. 2205-16.

8. Pisconti, A., G.B. Banks, F. Babaeijandaghi, N.D. Betta, F.M. Rossi, J.S. Chamberlain, and B.B. Olwin, Loss of niche-satellite cell interactions in syndecan-3 null mice alters muscle progenitor cell homeostasis improving muscle regeneration. *Skelet Muscle*. 2016; 6: p. 34.

9. Yoshikawa, S., Y. Sumino, J. Kwon, T. Suzuki, T. Kitta, M. Miyazato, and N. Yoshimura, Effects of multiple simulated birth traumas on urethral continence function in rats. *Am J Physiol Renal Physiol*. 2017; 313(5): p. F1089-F1096.

10. Dessem, D. and R.M. Lovering, Repeated muscle injury as a presumptive trigger for chronic masticatory muscle pain. *Pain Res Treat*. 2011; 2011: p. 647967.

11. Lieber, R.L. and S.R. Ward, Cellular mechanisms of tissue fibrosis. 4. Structural and functional consequences of skeletal muscle fibrosis. *Am J Physiol Cell Physiol*. 2013; 305(3): p. C241-52.

12. Maughan, R.J., Watson, J., Weir, J., Strength and cross-sectional area of human skeletal muscle. *J. Physiol*. 1983; 338: p. 37-49.

13. Roman, W. and E.R. Gomes, Nuclear positioning in skeletal muscle. *Semin Cell Dev Biol*. 2018; 82: p. 51-56.

14. Mahdy, M.A.A., Skeletal muscle fibrosis: an overview. *Cell Tissue Res*. 2019; 375(3): p. 575-588.

15. Dumont, N.A., C.F. Bentzinger, M.C. Sincennes, and M.A. Rudnicki, Satellite Cells and Skeletal Muscle Regeneration. *Compr Physiol*. 2015; 5(3): p. 1027-59.

16. Tidball, J.G., Regulation of muscle growth and regeneration by the immune system. *Nat Rev Immunol*. 2017; 17(3): p. 165-178.

17. Costamagna, D., P. Costelli, M. Sampaolesi, and F. Penna, Role of Inflammation in Muscle Homeostasis and Myogenesis. *Mediators Inflamm*. 2015; 2015: p. 805172.

18. Blomquist, J.L., M. Carroll, A. Munoz, and V.L. Handa, Pelvic floor muscle strength and the incidence of pelvic floor disorders after vaginal and cesarean delivery. *Am J Obstet Gynecol*. 2020; 222(1): p. 62 e1-62 e8.

19. Catanzarite, T., S. Bremner, C.L. Barlow, L. Bou-Malham, S. O'Connor, and M. Alperin, Pelvic muscles' mechanical response to strains in the absence and presence of pregnancy-induced adaptations in a rat model. *Am J Obstet Gynecol*. 2018; 218(5): p. 512 e1-512 e9.

20. Shafik, A. and O. El-Sibai, Study of the levator ani muscle in the multipara: role of levator dysfunction in defecation disorders. *J Obstet Gynaecol*. 2002; 22(2): p. 187-92.

21. Barclay, R.D., N.A. Burd, C. Tyler, N.A. Tillin, and R.W. Mackenzie, The Role of the IGF-1 Signaling Cascade in Muscle Protein Synthesis and Anabolic Resistance in Aging Skeletal Muscle. *Front Nutr*. 2019; 6: p. 146.

22. Raimondo, T.M., H. Li, B.J. Kwee, S. Kinsley, E. Budina, E.M. Anderson, E.J. Doherty, S.G. Talbot, and D.J. Mooney, Combined delivery of VEGF and IGF-1 promotes functional innervation in mice and improves muscle transplantation in rabbits. *Biomaterials*. 2019; 216: p. 119246.

23. Dziki, J.L., L. Huleihel, M.E. Scarritt, and S.F. Badylak, Extracellular Matrix Bioscaffolds as Immunomodulatory Biomaterials<sup/>. *Tissue Eng Part A*. 2017; 23(19-20): p. 1152-1159.

24. Lein, K., Mooney, B., DeLancey, J., Ashton-Miller, J., Levator Ani Muscle Stretch Induced by Simulated Vaginal Birth. *Obstet Gynecol*. 2004; 103(1): p. 31-40.

25. Mendias, C.L., J.E. Marcin, D.R. Calerdon, and J.A. Faulkner, Contractile properties of EDL and soleus muscles of myostatin-deficient mice. *J Appl Physiol (1985)*. 2006; 101(3): p. 898-905.

26. Jannig, P.R., C.R.R. Alves, V.A. Voltarelli, L.H.M. Bozi, J.S. Vieira, P.C. Brum, and L.R.G. Bechara, Effects of N-acetylcysteine on isolated skeletal muscle contractile properties after an acute bout of aerobic exercise. *Life Sci*. 2017; 191: p. 46-51.

27. Burnett, L.A., M. Cook, S. Shah, M. Michelle Wong, D.M. Kado, and M. Alperin, Age-associated changes in the mechanical properties of human cadaveric pelvic floor muscles. *J Biomech*. 2020; 98: p. 109436.

28. Dunham, C.L., A.M. Chamberlain, G.A. Meyer, and S.P. Lake, Muscle does not drive persistent posttraumatic elbow contracture in a rat model. *Muscle Nerve*. 2018; 58(6): p. 843-851.

29. Duran, P., Sesillo, F., Burnett, L., Menefee, S., Cook, M., Zazueta-Damian, G., Dzieciatkowska, M., Do, E., French, S., Shah, M., Sanvictores, C., Hansen, K., Shtrahman, M., Christman, K., Alperin, M., Pro-regenerative Extracellular Matrix Hydrogel Prevents and Mitigates Pathological Alterations of Pelvic Muscles Following Birth Injury. *bioRxiv*. 2021.

30. Raman, A.T., A.E. Pohodich, Y.W. Wan, H.K. Yalamanchili, W.E. Lowry, H.Y. Zoghbi, and Z. Liu, Apparent bias toward long gene misregulation in MeCP2 syndromes disappears after controlling for baseline variations. *Nat Commun*. 2018; 9(1): p. 3225.

Chapter 5: Conclusions and future directions

5.1 Summary and Conclusions

This dissertation focused on two main goals that are highly needed for the advancement of female pelvic medicine: 1) understanding of the pathophysiology behind clinically observed pelvic floor muscle (PFM) weakness after childbirth, and 2) investigation of therapeutic approaches for prevention and treatment of PFM dysfunction. Little is known regarding changes in the intrinsic PFM components after childbirth, which could contribute to the development of PFDs. In addition, treatments for pelvic floor disorders (PFDs) are delayed and compensatory as they do not aim to restore tissue composition and function, prompting our investigation of biomaterials that will create an environment for healing at the time of administration.

The first chapter covered what is known about the PFMs and the current gap in knowledge in the pathophysiology behind PFMs dysfunction following birth injury. PFMs are essential for the proper function of the female pelvic floor, and their dysfunction is a major risk factor for the development of PFDs such as pelvic organ prolapse, and urinary and anal incontinence. Knowledge of the anatomy and physiology of the PFMs is one of the keys to understanding the pathogenesis of PFDs, which result in significant morbidity and substantially decreased quality of life for many women worldwide. Expanding the comprehension of the structure and function of PFMs is essential to enable the development of preventative and treatment strategies to counteract PFDs. Besides covering what is known about PFMs, this chapter also explained the endogenous skeletal muscle regeneration process, which is also crucial for the design of therapeutic approaches. Lastly, this portion of the thesis provided an extensive background related to the development of natural biomaterials, specifically decellularized extracellular matrix (ECM) hydrogels, together with applications focused on muscle-related conditions.

The second chapter explored the PFM response following birth injury, as a step towards the understanding of the pathophysiology behind PFM dysfunction after vaginal delivery. The first

portion of the chapter demonstrated that the pre-clinical rat model of simulated birth injury recapitulated the pathological alterations observed in women with symptomatic pelvic organ prolapse. Through histology and gene expression analyses, the early and delayed responses of pubocaudalis muscle—analogous to human pubovisceralis that is mostly stretched during delivery—were investigated. Histological assessment of myogenesis, by staining of quiescent or activated, as well as, differentiated muscle stem cells, indicated that this process followed the expected time-course based on limb skeletal muscle injuries. Gene expression analyses further demonstrated that the PFM undergoes a sustained inflammatory response, impairment in muscle anabolism and persistent ECM remodeling, which can potentially be associated with the observed muscle atrophy and fibrosis following birth injury.

The third chapter expanded from the understanding of PFM response identified in chapter 2. Beyond the lack of fundamental knowledge regarding tissue- and cell-level alterations after birth injury, development of preventative and therapeutic approaches is necessary for PFM dysfunction and associated PFDs. The chapter investigated the efficacy of a decellularized skeletal muscle ECM (SKM) hydrogel to prevent and treat the pathological alterations after birth injury with the goal of potentiating muscle recovery. Two clinically relevant time points were explored, either immediately after SBI or at a delayed time point. SKM could be administered on Labor and Delivery or at a post-partum visit. The animal studies demonstrated that, at both time points, the acellular biomaterial prevented PFM atrophy and mitigated fibrosis, potentially through the modulation of the immune response, native ECM remodeling and enhancement of myogenesis.

Lastly, the fourth chapter investigated the PFM response after repeated birth injuries, as multiparity further increases the risk for PFDs, especially for pelvic organ prolapse. The studies first evaluated PFM function through *ex vivo* assessment of active and passive force production. While a single injury led to a recovery in PFM active force, a subsequent SBI resulted in a

decrease in muscle force. In addition, a potential increase in stiffness was observed after both single and repeated injuries. Through histological analyses, it was further demonstrated that, after a 2nd SBI, PFM presented a reduction in fiber size, substantial increase in centralized nuclei and fibrosis. Gene expression analyses showed a prolonged inflammation in relation to a single SBI. Lastly, delayed administration of SKM post-2nd SBI led to long-term improvement of PFM phenotype, and modulation of immune response by upregulation of genes associated with pro-regenerative mediators.

All in all, these studies established the foundation for the understanding of PFM response following birth injuries—an area that is currently under investigated. In addition, efficacy was observed in the rat pre-clinical model. These novel results are promising and will motivate future studies for a deeper understanding of PFM phenotype and assessment of biomaterial response under the presence of other variables, such as changes in hormones during pregnancy.

5.2 Future directions

5.2.1 Deeper understanding of mechanisms behind pelvic floor muscle phenotype following birth injury

This thesis showed that a single birth injury leads to muscle atrophy, while repeated SBIs resulted in decrease fiber area but with significant increase in centralized nuclei even at a 12-week recovery period. Gene expression analyses demonstrated that myogenesis-related genes followed a similar pattern after 1st and 2nd injuries, indicating that the time course of regeneration might not be affected following repeated injuries. Besides being a hallmark of regeneration after an injury,[1] centralized nuclei are also identified in degenerative muscle in chronic conditions or muscle wasting. While muscle atrophy is identified by a decrease fiber size, muscle degeneration has unique features of accumulative muscle damage such as increased centralized nuclei, macrophage accumulation, altered vascularization, and reduced fiber size.[2] Thus, to have a better

understanding of the PFM phenotype after repeated birth injuries, characteristic features of muscle degeneration could be analyzed to evaluate if this is the reason behind the substantial increase in centralized nuclei—vessels and macrophage quantification could be performed at the long-term time point (i.e., 12 weeks).

Increased collagen content was classically identified as a predictor of increase passive stiffness. However, previous studies have investigated that the amount of fibrotic material (i.e., collagen) is not directly related to the stiffness in skeletal muscle.[3] Brashear, et al., recently found that the architecture of the ECM, analyzed by the alignment of collagen fibers, demonstrated a relationship with passive mechanical stiffness.[4] Thus, to further understand the reason behind the potential increase in stiffness after single and repeated birth injury, ECM alignment could be investigated through second harmonic generation which identifies non centrosymmetric structures like collagen.

Repeated birth injuries lead to a decrease in *ex vivo* active force production, focusing exclusively on the myogenic contributions. In addition, histological analyses focused on myofiber damage and regeneration following birth injuries with little investigation to other structures that affect overall muscle repair—the neuromuscular junctions (NMJs). Although we observed that genes associated with NMJs maturation and development followed the expected pattern based on acute limb skeletal muscle injury,[5] we did not analyze NMJs morphology. The evaluation of NMJs morphology by staining against the motor end plate (∝-bungarotoxin), and nerve terminal (neurofilament) will determine if simulated birth injury leads to a disruption of the NMJs, either at the muscle or nerve connection. On the assumption that NMJs are affected by the stretch-induced injury, *in vivo* experiments could be performed to investigate if such disruption affects muscle function, and to what extent, by performing nerve and muscle stimulation to obtain a neuromuscular transmission failure percent, as previously done.[6] Identification and dissection of levator ani nerve will need to be optimized and perfected before doing *in vivo* testing. A previous

study identified that birth injury via vaginal distention does not affect NMJs morphology in the external urethral sphincter.[7] However, the balloon inflation was done at 3 ml and we have shown previously that this distention volume does not induces a significant injury to the pubocaudalis muscle.[8]

As mentioned throughout the thesis, the studies were done in non-pregnant animals to investigate the impact of parturition-related strains and segregate any effect from the constant load of the pups and hormonal changes associated with pregnancy, which are known to affect mechanical properties and key pathways of muscle regeneration, respectively.[9, 10] Therefore, future studies with pregnant rats will need to be performed to evaluate the influence of those variables in PFM response following single and repeated birth injuries.

5.2.2 Future of biomaterial therapies for pelvic skeletal muscles

Hydrogels demonstrated efficiency in improving PFM phenotype either after 1st or 2nd SBIs based on the assessment of histological and gene expression analyses. However, SKM showed similar results compared to untreated SBI with *ex vivo* functional assessment following repeated injuries. One potential explanation for this result is the small dynamic range between control and SBI alone which was only a 30% decrease in active force production. To increase the range, vaginal distention in animal models could be combined with a nerve crush model, as it has been previously done for studies of the urethral sphincter.[7] Addition of direct nerve injury would not replicate the physiological conditions of childbirth, and studies will need to be performed to evaluate the PFM response with this combined model. Additionally, if SKM does not enhance muscle force production by increasing the dynamic range, the biomaterial could be delivered with a bioactive molecule. A potential candidate could be insulin growth factor (IGF-1), which is known to promote protein synthesis through the mTOR pathway,[11] leading to an overall improvement in force production, as previously demonstrated in a skeletal muscle injury model.[12] Although no

statistical significance was observed for the passive mechanical parameters, a potential decreased stiffness at low strains was identified, however, increase in sample size (n=15/group) would need to be performed to accurately conclude this result. In addition, second harmonic generation could be performed to evaluate the alignment of collagen fibers as proposed with the injury alone. Assessment of changes in ECM organization after hydrogel administration will aid in the understanding of the mechanism of action behind the decellularized biomaterial.

The next step in evaluating SKM administration for the prevention and treatment of PFM weakness after childbirth is to assess the efficacy of the biomaterial in pregnant animals, as previously mentioned. Besides investigating the effect of SKM in PFM, this therapy can also be applied to other pelvic skeletal muscles, which include the external urethral sphincter (EUS), and external anal sphincter (EAS). The dissertation author previously demonstrated that after SBI, the sphincters undergo sarcomere hyperelongation and myofibrillar disruption,[13] similar to the acute mechanism of injury of PFMs.[8] Future studies need to assess the response of EUS and EAS after the acute period, but based on the results obtained with PFMs, SKM seems a promising therapy to enhance the recovery of the sphincters following birth injury.

5.3 References

1. Dumont, N.A., C.F. Bentzinger, M.C. Sincennes, and M.A. Rudnicki, Satellite Cells and Skeletal Muscle Regeneration. *Compr Physiol*. 2015; 5(3): p. 1027-59.

2. Gibbons, M.C., A. Singh, O. Anakwenze, T. Cheng, M. Pomerantz, S. Schenk, A.J. Engler, and S.R. Ward, Histological Evidence of Muscle Degeneration in Advanced Human Rotator Cuff Disease. *J Bone Joint Surg Am*. 2017; 99(3): p. 190-199.

3. Smith, L.R. and E.R. Barton, Collagen content does not alter the passive mechanical properties of fibrotic skeletal muscle in mdx mice. *Am J Physiol Cell Physiol*. 2014; 306(10): p. C889-98.

4. Brashear, S.E., R.P. Wohlgemuth, G. Gonzalez, and L.R. Smith, Passive stiffness of fibrotic skeletal muscle in mdx mice relates to collagen architecture. *J Physiol*. 2021; 599(3): p. 943-962.

5. Liu, W. and J.V. Chakkalakal, The Composition, Development, and Regeneration of Neuromuscular Junctions. *Curr Top Dev Biol*. 2018; 126: p. 99-124.

6. Pratt, S.J.P., S.B. Shah, C.W. Ward, M.P. Inacio, J.P. Stains, and R.M. Lovering, Effects of in vivo injury on the neuromuscular junction in healthy and dystrophic muscles. *J Physiol*. 2013; 591(2): p. 559-70.

7. Song, Q.X., B.M. Balog, J. Kerns, D.L. Lin, Y. Sun, M.S. Damaser, and H.H. Jiang, Long-term effects of simulated childbirth injury on function and innervation of the urethra. *Neurourol Urodyn*. 2015; 34(4): p. 381-6.

8. Catanzarite, T., S. Bremner, C.L. Barlow, L. Bou-Malham, S. O'Connor, and M. Alperin, Pelvic muscles' mechanical response to strains in the absence and presence of pregnancy-induced adaptations in a rat model. *Am J Obstet Gynecol*. 2018; 218(5): p. 512 e1-512 e9.

9. Alperin, M., T. Kaddis, R. Pichika, M.C. Esparza, and R.L. Lieber, Pregnancy-induced adaptations in intramuscular extracellular matrix of rat pelvic floor muscles. *Am J Obstet Gynecol*. 2016; 215(2): p. 210 e1-7.

10. Liao, Z.H., T. Huang, J.W. Xiao, R.C. Gu, J. Ouyang, G. Wu, and H. Liao, Estrogen signaling effects on muscle-specific immune responses through controlling the recruitment and function of macrophages and T cells. *Skelet Muscle*. 2019; 9(1): p. 20.

11. Barclay, R.D., N.A. Burd, C. Tyler, N.A. Tillin, and R.W. Mackenzie, The Role of the IGF-1 Signaling Cascade in Muscle Protein Synthesis and Anabolic Resistance in Aging Skeletal Muscle. *Front Nutr*. 2019; 6: p. 146.

12. Raimondo, T.M., H. Li, B.J. Kwee, S. Kinsley, E. Budina, E.M. Anderson, E.J. Doherty, S.G. Talbot, and D.J. Mooney, Combined delivery of VEGF and IGF-1 promotes functional innervation in mice and improves muscle transplantation in rabbits. *Biomaterials*. 2019; 216: p. 119246.

13. Duran, P., S. Ward, K.L. Christman, and M. Alperin, Mechanical impact of parturition-related strains on rat pelvic striated sphincters. *Neurourol Urodyn*. 2019; 38(3): p. 912-919.